THE UNIVERSITY OF CHICAGO

PATHOGENIC PATHWAYS AND PRECLINCIAL TESTING IN MOUSE MODELS OF MUSCULAR DYSTROPHY

A DISSERTATION SUBMITTED TO

THE FACULTY OF THE DIVISION OF THE BIOLOGICAL SCIENCES

AND THE PRITZKER SCHOOL OF MEDICINE

IN CANDIDACY FOR THE DEGREE OF

DOCTOR OF PHILOSOPHY

DEPARTMENT OF PATHOLOGY

BY

BRANDON BARNETT GARDNER

CHICAGO, ILLINOIS

JUNE 2016

TABLE OF CONTENTS

LIST OF FIGURES

Chapter 1. Introduction

Chapter 2. Inhibition of TGFβ in a mouse model of muscular dystrophy

Chapter 5. Discussion

LIST OF TABLES

LIST OF COMMON ABBREVIATIONS

MD	Muscular Dystrophy
DMD	Duchenne Muscular Dystrophy
BMD	Becker Muscular Dystrophy
EDL	Extensor Digitorum Longus
DCM	Dilated cardiomyopathy
HCM	Hypertrophic cardiomyopathy
CK	Creatine Kinase
DGC	Dystrophin Glycoprotein Complex
LGMD	Limb Girdle Muscular Dystrophy
H & E	Hematoxylin & Eosin
MRI	Magnetic Resonance Imaging
DKO	Double Knockout
TGFβ	Transforming Growth Factor β
LAP	Latency Associated Peptide
MT	Mason's Trichrome
PBS	Phosphate Buffered Saline
SLC	Small Latent Complex
GDF	Growth and Differentiation Factor
BMP	Bone Morphogenic Protein
EGF	Epidermal-like Growth Factor
EBD	Evan's Blue Dye
HOP	Hydroxyproline

PFA	Parafromaldahyde
DMC	Dynamic Muscle Control
GLS	Global Longitudinal Strain
FS	Fractional Shortening
PEP	Peak Expiratory Pressure
PIP	Peak Inspiratory Pressure
MMP	Matrix Metaloprotease
RV	Right Ventricle
LV	Left Ventricle
EF	Ejection Fraction
RGD	Arginine Glycine Aspartic-Acid
WBP	Whole Body Plethtysmography
SNIP	Sniff Nasal Insipiratory Pressure
WGA	Wheat Germ Agglutinin
ECM	Extra Cellular Matrix
LVFS	Left Ventricular Fractional Shortening
LVID	Left Ventricular Internal Diameter
PAAT	Pulmonary Artery Acceleration Time
PA VTI	Pulmonary Artery Velocity Time Interval
BAC	Bacterial Artificial Chromosome

ABSTRACT

The muscular dystrophies are marked by progressive muscle degeneration and subsequent maladaptive repair. In the most common childhood form, Duchenne muscular dystrophy (DMD), patients develop weakness of skeletal muscles accompanied by cardiac and respiratory muscle dysfunction. Mouse models of muscular dystrophy replicate the pathological aspects of the human disease. Transforming growth factor beta (TGFβ) has been shown to be elevated in both human and animal models of MD, where it is associated with increased fibrosis and decreased muscle strength function and regeneration. Herein, a pre-clinical assessment of isoform specific anti-TGFβ antibodies was conducted in the *mdx/hLTBP4* model, which mirrors the regulation of TGFβ seen in human muscle. These antibodies elicited improved signs of regeneration on histopathology with reduction in fibrosis. A similar pre-clinical trial was also carried out using antibodies to latent transforming growth factor beta binding protein-4 (LTBP4). This approach yielded similar signs of decreased inflammation, increased regeneration and resistance to injury with anti-LTBP4 antibodies. In addition to testing novel approaches to ameliorate disease, I also helped characterize a large cohort of *Sgcg* null mice that serve as a model for Limb Girdle Muscular Dystrophy 2C. By analyzing echocardiographic data alongside histopathological quantitation, I found correlations between cardiac and muscle outcomes, providing new endpoints for preclinical analysis and identifying the abdominal muscles as important for cardiopulmonary outcomes.

Acknowledgements

I would like to thank my advisor Elizabeth McNally, MD, PhD for always being kind, brilliant and brave in her approach to research and commitment to training graduate students. I would also like to especially thank Alexis Demonbreuan, PhD for her patience and support throughout my PhD and thesis writing process. I am so grateful to have been able to work with such great mentors, and on a disease that means so much to me. I would finally like to thank my family, and Katie Smith for always supporting my goals and pushing me to be better every day. I hope to make them proud forever.

Chapter 1

MUSCULAR DYSTROPHY AND TGFβ

Introduction

Portions of this text and the figures derive from a Chapter entitled “Abnormal Muscle Physiology” appearing in Cardioskeletal Myopathies in Children and Young Adults by EM McNally, BB Gardner, S. Bogdanovich. (eds. Towbin, Jefferies, Blaxall, Robbins, Elsevier)

Introduction

The genetically mediated cardiac and skeletal myopathies often share a similar pathophysiology that adversely alters both normal cardiac and skeletal muscle function through cell intrinsic pathways. In these genetic disorders, myocyte functional defects arise from matrix, plasma membrane, sarcomeric, mitochondrial and nuclear perturbation that render dysfunction in both cardiac myocytes and in skeletal myofibers. Sarcomere structure is conserved between cardiomyocytes and skeletal myofibers, although the proteins that constitute the sarcomere may often differ in isoform or family

member. Mutations in genes that are expressed in both heart and muscle cause both cardiac and skeletal myopathy, although the pace at which disease manifests in heart or muscle may occur at strikingly different times in the course of disease.

Structural and functional differences between cardiac myocytes and skeletal myofibers may contribute to the distinct pathological manifestations in heart versus skeletal muscle, but often the physiological rationale for this may be unclear. One striking difference between heart and skeletal muscle is the capacity for regeneration. In skeletal myofibers, there is robust regeneration after injury (Carlson and Faulkner, 1983; Charge and Rudnicki, 2004). Skeletal muscle regeneration is mediated by satellite cells that, with injury, differentiate into committed myoblasts that first proliferate and then differentiate to repair and regrow muscle (Relaix and Zammit, 2012; Zammit et al., 2006). In contrast to skeletal muscle where the regenerative program has been comparably well outlined, regeneration in the heart and the degree to which it can repair ongoing injury from genetic defects remains controversial (Alexander and Bruneau, 2010; Jackson et al., 2001; Mercola et al., 2011). But what is known is that cardiac regeneration occurs at a vastly lower rate than skeletal muscle (Costamagna et al., 2014). In addition to the distinctly different regenerative potential of heart and skeletal muscle, the fundamental cell shape and elements of calcium handling and excitation-contraction coupling have differences adapted to the unique properties of both heart and skeletal muscle. In this chapter, I will review the muscular dystrophies and myopathies with specific focus on those that target both cardiac and skeletal muscle outlining the interaction and physiological consequences of concomitant heart failure and skeletal muscle weakness. The interrelationship between heart and muscle

dysfunction can exacerbate the disease course and represents an important area for therapeutic improvement.

The Muscular Dystrophies

The muscular dystrophies are a group of inherited neuromuscular disorders that may manifest in early childhood and progressively worsen throughout life. The most common subset of muscular dystrophies is caused by mutations that disrupt proteins localized to the sarcolemma. A genetic subset is typified by Duchenne Muscular Dystrophy (DMD), which occurs in 1:5000 males. Without cardiac and respiratory support, DMD patients will die of cardiopulmonary complications in the second or early third decade of life. Animal models have served as an invaluable tool in gaining insight into the pathophysiology of muscle loss and weakness in DMD, and studies in these models led to identification of the molecular mechanisms underlying force decrement in muscular dystrophy (Bogdanovich et al., 2002; Bogdanovich et al., 2008; Petrof et al., 1993; Stedman et al., 1991). The physiological properties of dystrophic muscle were discovered with methods to elucidate the ex vivo muscle mechanics, commonly using the *extensor digitorum longus* (EDL). Related ex vivo mechanical studies have also been adapted for examining the *tibialis anterior* and diaphragm mouse muscle.

Ex vivo muscle studies employ standardized electrical stimulation protocols of an entire muscle or muscle group while suspended between force transducers to permit measurement of force. There are multiple muscle parameters that can be measured on explanted muscle in order to characterize the origins of force decrement in normal and dystrophic muscle. Major measurements revolve around determining force generation

in twitch or tetanus. These measurements correlate with in vivo muscle function and can be used as major indicators of myofiber health. Beyond standard measurements of force production, methods have been devised to elicit more intense and damaging conditions in the form of eccentric contraction and fatigue models in order to represent physiological stressors that occur to muscle in vivo (McCully and Faulkner, 1986; Sacco and Jones, 1992). These “fiber damaging” protocols have also been vital to provide a better perspective on how and why a weakened sarcolemma leads to tissue damage and necrosis (Lieber et al., 2002). The abnormal muscle physiology in dystrophic muscle can be characterized by a constant decrease in force response to isometric twitch, tetanus and eccentric contraction over time. Indeed, many animal studies use such *ex vivo* physiologic testing in evaluating potential therapeutics.

Cardiac involvement in DMD is common and a leading cause of morbidity and mortality. Nearly all patients with DMD will develop cardiac manifestations of their disease, either cardiomyopathy or changes in cardiac rhythm and conduction (arrhythmias) (Fayssoil et al., 2010; Finsterer and Stollberger, 2008). Cardiomyopathy is seen histologically as myocardial fibrosis and early clinical signs of cardiomyopathy correlate with sinus tachycardia (Finsterer and Stollberger, 2003; Thomas et al., 2012). Progressive cardiac degeneration can be monitored using cardiac MRI and/or echocardiography and typically progresses to dilated cardiomyopathy.

Duchenne Muscular Dystrophy (DMD)

DMD and the milder allelic variant Becker muscular dystrophy (BMD) are X-linked recessive diseases caused by loss of function mutations in the *DMD* gene encoding

dystrophin (Hoffman et al., 1987). The *DMD* gene is located on chromosome Xp21 and spans 2.5 MB (Coffey et al., 1992; Monaco et al., 1986), consisting of 79 exons (Brown, 1997; Khurana et al., 1990). Mutations in *DMD* produce diverse outcomes, and the severity of disease is linked to the type of mutation and degree of residual dystrophin protein produced (Bladen et al., 2015; Flanigan et al., 2009; Koenig et al., 1988). Deletions and duplications spanning multiple exons account for nearly two-thirds of DMD. Premature stop codons and single (or small) nucleotide changes account for the remaining one-third of DMD cases. Premature truncation of dystrophin commonly results in loss of dystrophin protein likely through nonsense-mediated decay reducing mRNA levels and what little protein is produced is unstable. An intact carboxy-terminus is needed to stabilize dystrophin through its protein-protein interactions that link to the transmembrane dystrophin protein complex (Flanigan et al., 2011). In contrast, BMD mutations leave some dystrophin protein present. BMD mutations reduce the amount of dystrophin protein and/or arise from internal truncations that maintain the reading frame and keep an intact carboxy-terminus (Bies et al., 1992; Monaco et al., 1988; Vulin et al., 2014). Mutations that target a small highly conserved domain near the carboxy terminus render a more severe phenotype indicating the importance of this domain (Beggs et al., 1991; Koenig et al., 1989). In the case of premature truncations due to stop codons or splice site variants, alternative splicing to the next available exon that maintains a reading frame can produce a subset of myofibers that express dystrophin, referred to as revertant fibers. The presence of these missplicing events was the impetus for strategies that promote these events as a therapeutic effort, referred to as exon skipping (Mitrpant et al., 2009).

Dystrophin is a major link between the extracellular matrix and intracellular structural elements. In the absence of dystrophin, the sarcolemma cannot sustain its integrity and ruptures easily with contraction. Sarcolemmal rupture, whether occurring in a skeletal myofiber or a cardiomyocyte, is accompanied by an increase in cytosolic Ca^{2+}, triggering a cascade of intracellular events including proteolysis and mitochondrial dysfunction. The cell membrane is very susceptible to Ca^{2+} changes, as Ca^{2+}-dependent proteases become constitutively activated, leading to necrosis. These proteolytic activities and necrosis are accompanied by a primarily mononuclear inflammatory response and macrophage infiltrate that is thought to further weaken muscle performance (Tidball and Villalta, 2010). The basic process of cellular disruption and repetitive injury is also seen in dystrophin-deficient cardiomyocytes. Adding additional stressors to the myocardium such as pressure overload via transverse aortic constriction, or adrenergic stimulation via dobutamine infusion further enhances myocyte breakdown, leading to cardiac dysfunction (Jung et al., 2008; Kamogawa et al., 2001; Yasuda et al., 2005).

Morphologically, dystrophic muscles consist of myofibers that vary in size and shape, foci of necrosis, and fibrofatty infiltration (**Figure 1.1**). Not all muscles are equally damaged in DMD; this is also true for relevant animal models. In this thesis, I will present data on the abdominal muscles as correlative of cardiopulmonary outcomes a mouse model of Limb Girdle Muscular Dystrophy type 2, which arises from mutations in the dystrophin-associated protein γ-sarcoglycan.

Clinical symptoms in DMD begin in early childhood with delayed motor milestones such as walking. Diagnosis is usually made by age five with proximal

muscle weakness seen as difficulty rising from the floor, running and climbing stairs (Dubowitz, 1975; Jennekens et al., 1991). Muscle weakness is progressive and, in DMD, the average age at which ambulation is lost is around 11 years. The mainstay of treatment currently relies on glucocorticoid steroids use, either prednisone or deflazacort. ith steroid treatment, ambulation is maintained on average approximately two years longer (McAdam et al., 2012; Moxley et al., 2010). Dystrophin is normally present in all skeletal muscles including the heart. Lack of dystrophin in DMD muscle directly correlates to cardiac involvement and susceptibility of the cardiomyocyte sarcolemma to stressful contractions, which leads to Ca^{2+} overload and activation of a deadly cascade. This results in protein degradation and finally cardiomyocyte death. Cardiac dysfunction can be detected by approximately age ten

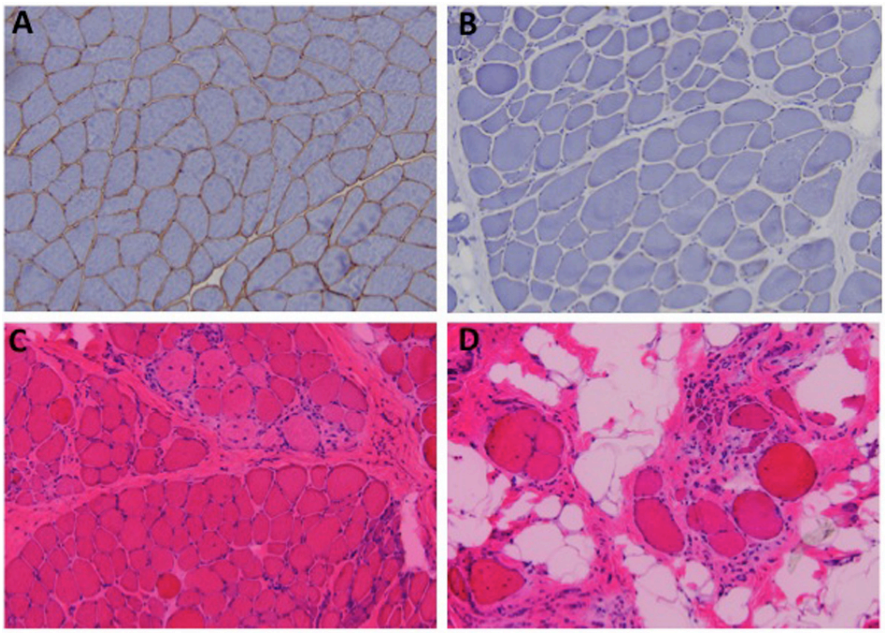

Figure 1.1 Histological findings from pediatric DMD muscle demonstrating the characteristic fiber size variation, centrally placed nuclei and fibrofatty infiltration. A. Normal muscle stained for dystrophin (brown). B. Mild dystrophic phenotype and absent dystrophin (no brown staining). C. Hematoxylin and eosin (H&E) staining showing moderate dystrophic phenotype with an increase in fibrous tissue deposition. D. H&E staining showing a severe dystrophic phenotype with fibrous and fatty replacement of muscle. Images courtesy of Dr. Peter Pytel, Dept. of Pathology, University of Chicago.

using cardiac magnetic resonance imaging (MRI) (Hor et al., 2009). With cardiac MRI, abnormalities of ventricular strain and volume can be quantitated even before reduced ventricular function is detected.

Cardiomyocyte loss in DMD results in a unique pattern of fibrotic area localized first in the epicardium and later spreading through the myocardium; cardiac MRI is well suited to identifying fibrosis in DMD-associated cardiomyopathy (Tandon et al., 2015a). These fibrotic changes can be detected using gadolinium or other contrast agents that produce delayed enhancement. MRI findings are thought to correlate with histological findings such as inflammatory response and macrophage infiltration as well as the formation of scar tissue. Over time, interstitial fibrosis may progress and correlate with regional wall motion abnormalities, which can also be seen on echocardiography (Ameen and Robson, 2010). With progressive fibrosis, dilated cardiomyopathy (DCM) develops in DMD and BMD (Tandon et al., 2015b). In addition to changes in ventricular morphology and function, EKG changes are present in DMD. By age ten, sinus tachycardia is often evident, and notably this same finding is replicated in mouse models (Bostick et al., 2008; Thomas et al., 2012).

Serum biomarkers of disease progression, including those that reflect skeletal and/or cardiac muscle disease, are of considerable interest for their use in clinical trials and to provide information regarding disease prognosis. The mainstay of serum testing in DMD has been to monitor serum creatine kinase (CK), as this is highly elevated in DMD and BMD, and is thought to reflect sarcolemmal disruption (Allen and Whitehead, 2011). In DMD, the CK-MB isozyme fraction of total serum CK may be elevated, reflecting regenerating skeletal muscle. Cardiac biomarkers are variably elevated in

DMD and can include troponin subunits (Matsumura et al., 2007). Newer biomarkers for DMD are emerging from research studies of both animal models and humans; these include titin subfragments, myosin light chain and carbonic anhydrase among others (Dahlqvist et al., 2014; Hathout et al., 2014; Rouillon et al., 2014).

Limb-Girdle Muscular Dystrophy (LGMD)

The LGMD family of muscular dystrophies is a diverse group of muscle disorders defined by the pattern of muscles afflicted, which include mainly the hips, shoulders and proximal limb musculature. Distal muscles are affected less and later in the course of disease. LGMD is caused by mutations in more than 15 autosomal genes. Some of the genes mutated in LGMDs encode protein products that are components of the sarcomere, the nuclear lamina, the sarcolemma or the cytoplasm.

Cardiomyopathies have been described in LGMDs type 2C, 2D, 2E, 2F, 2I, and LGMD1B. The timing of cardiomyopathy onset and associated pathology in LGMD is variable and can manifest in unique combinations in each individual patient, including hypertrophic versus dilated myopathy, with or without arrhythmias. The sarcoglycanopathies arise from loss of function mutations in the genes encoding the sarcoglycan subunits including α-, β-, γ- and δ-sarcoglycan. These subunits are each single-pass transmembrane proteins and four together form the sarcoglycan complex in both skeletal and cardiac striated muscle. The sarcoglycans are a subunit within the dystrophin glycoprotein complex, where they contribute to binding dystroglycan and reinforcing the transmembrane linkages between the cytoplasm and matrix. The sarcoglycans associate with the extracellular matrix on their extracellular side, while

maintaining cytoskeletal anchoring on its cytoplasmic domain (Crosbie et al., 2000; Holt and Campbell, 1998). For reasons that are still poorly understood, loss of function mutations in the sarcoglycans result in an inability of myofibers to protect themselves against contraction-induced damage, despite leaving dystrophin at its usual position at the sarcolemma (Heydemann and McNally, 2007). It is important to note that, EKG and/or echocardiographic abnormalities are common in the sarcoglycanopathies and should be monitored, with a high percentage of patients developing cardiac dysfunction at some point in life, especially for β-, γ- and δ-sarcoglycan (Melacini et al., 1999; Politano et al., 2001).

Animal Models

Animals have been used to model MD since the discovery of dystrophin in 1984. Evolutionarily, dystrophin and its associated protein complex evolved early in the phylogenetic lineage of striated muscle, and there does not seem to be sarcomeric muscle without some form of dystrophin complex (DGC) in the animal kingdom. Although the DGC varies greatly between species, almost all forms have a large dystrophin-like protein linking its many components to cytoskeletal filamentous (F)-actin. As a result, dystrophin null models have been generated and also characterized from naturally occurring models in *Drosophila*, mice, zebrafish, dogs and hamsters among others. Of these, murine models have arguably provided the most invaluable and robust insights into the pathophysiology of muscular dystrophy.

The best characterized mouse model is the *mdx* mouse, a model of DMD (Partridge, 2013). *The mdx* mouse has a naturally occurring nonsense mutation early

on in the *Dmd* gene. Loss of dystrophin is not a mortal lesion in mice, and *mdx* mice remain ambulatory with a modestly shortened lifespan. The murine histopathology has many of the same features of human DMD but is less severe, especially when comparing older animals with older DMD humans (**Figure 1.2**). One muscle that displays histopathology close to what is seen in human DMD is the diaphragm. The *mdx* diaphragm develops pathology seen as early as a few weeks post-birth. This is also seen in other MD models (**Figure 1.3**) (Stedman et al., 1991). The early dystrophic morphology of *mdx* diaphragm is thought to derive from a failure in muscle regeneration. In Chapter 4, I will present data on the histopathology of the abdominal muscles (Gardner et al., 2015). Serum CK levels in DMD patients and *mdx* mice are elevated as an early biomarker of disease. In human DMD with progressive loss of muscle mass and replacement by fibrosis, the serum CK decreases in end stage disease. However, in the *mdx* mouse, where muscle mass is maintained along with ambulatory capacity, serum CK levels remain elevated. *Ex vivo* muscle mechanics performed on *mdx* muscle demonstrates that, in the absence of dystrophin, the muscle is weaker with reduced force production per stimulation. In addition to being weaker, dystrophin null muscle is highly susceptible to damage during lengthening contractions, a property not seen in normal muscle (Bulfield et al., 1984; Moens et al., 1993).

Unlike humans with DMD who lose ambulation, *mdx* mice remain ambulatory. However, *ad libitum* exercise in *mdx* mice is reduced compared to wildtype controls (Carter et al., 1995). *mdx* mice can also be induced to exercise with forced treadmill

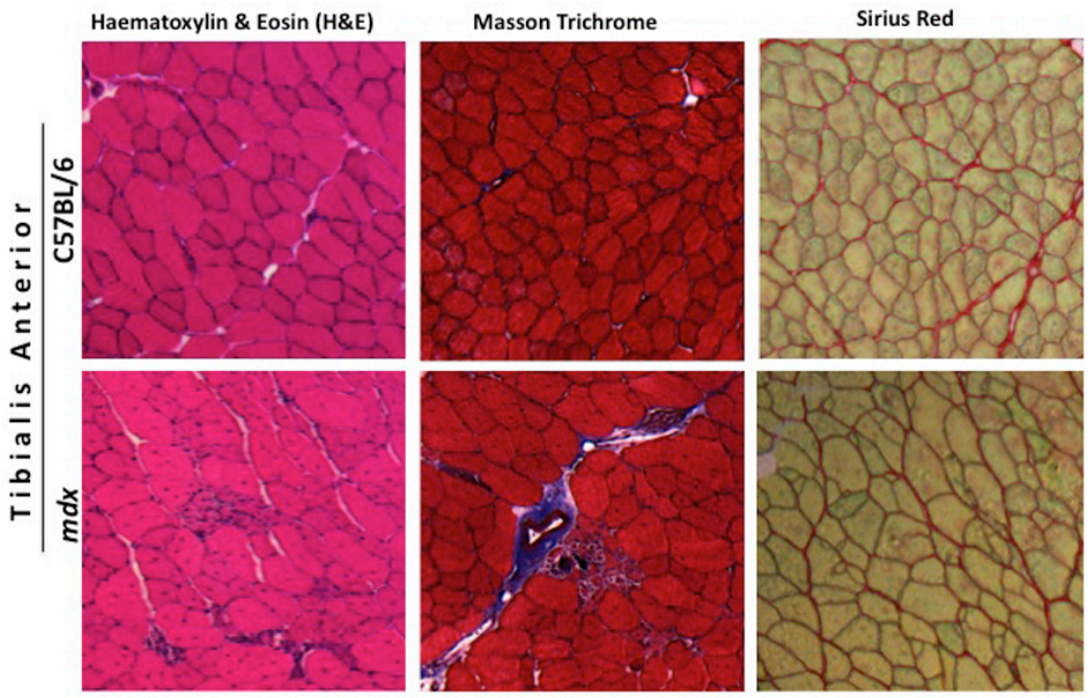

Figure 1.2 The *mdx* model of muscular dystrophy demonstrating a similar pathology to human DMD. H&E staining highlights fiber size variation, centrally placed nuclei and mononuclear cell infiltrate. Masson's Trichrome and Sirius Red staining demonstrate the increase in fibrosis that typifies muscular dystrophy and documenting replacement of muscle by fibrosis in the tibialis anterior muscle.

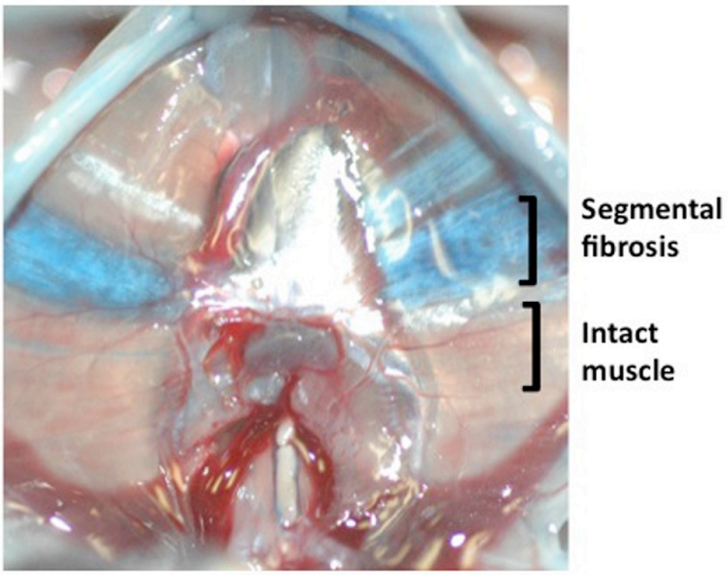

Figure 1.3 Diaphragm muscle pathology in an animal model of muscular dystrophy. The diaphragm muscle is shown from an 8 week *Sgcg* null mouse model and represents the mild end of the phenotypic spectrum at this age. The animal was injected with Evans blue dye, a vital tracer that marks sarcolemmal disruption. White areas, which overlap with blue areas, represent segmental fibrotic replacement of the diaphragm muscle. An area of intact muscle is indicated for comparison.

running being a common method used to monitor exercise tolerance; forced exercise can be used to exacerbate *mdx* muscle pathology and their overall dystrophic phenotype (De Luca et al., 2003; Fraysse et al., 2004). In addition to the *mdx* mouse with a natural occurring exon 23 premature stop codon, there are four other artificially created dystrophin null mouse models and the degree to which dystrophin positive revertant fibers occur varies from model to model (Chapman et al., 1989; Cox et al., 1993; Im et al., 1996; Rafael et al., 2000). Due to the relatively mild disease course *mdx* mice experience compared to humans, a more severe double knock out (DKO) model lacking both dystrophin and utrophin was generated. The dystrophin/utrophin (*mdx/utrn*$^{-/-}$) DKO mouse model has reduced lifespan and cardiopulmonary dysfunction (Deconinck et al., 1997; Deconinck et al., 1998; Grady et al., 1997). Utrophin is similar in structure to dystrophin and its overexpression seems to be a robust compensatory mechanism in mice, one that humans have not retained (Amenta et al., 2011; Krag et al., 2004). Recently, a new severe mouse model of *mdx* muscular dystrophy was created by bacterial artificial chromosome mediated-transgenic expression of the large extracellular scaffolding protein LTBP4, because this TGF-β scaffolding moiety modifies muscular dystrophy in mice and humans (Ceco et al., 2014). Specifically, the LTBP4 transgene exacerbates the dystrophic phenotype via increasing local TGF-β activation. Consequently, these mice have weaker muscles and display an increased inflammatory infiltrate compared to the *mdx* mouse without the transgene. This model was used for preclinical testing of biological reagents in Chapters 2 and 3.

Beyond rodent models, there are large animal species that have naturally-occurring mutations in the dystrophin gene. Large animal DMD models include the

canine golden retriever and German shorthaired pointer (Cooper et al., 1988; Schatzberg et al., 1999). The canine models have a closer resemblance to human pathology than the rodent animal models, but the breeding costs and individual variation between the groups forces judicious use of these models for experimentation.

Anatomy of Breathing in Muscular Dystrophy

The muscles of respiration are some of the earliest and most severely afflicted in the muscular dystrophies, and for reasons that are still poorly understood, fail at different rates. This differential rate of decline leads to an imbalance between expiratory and inspiratory strength, often changing thoraco-abdominal anatomy and mechanics (D'Angelo et al., 2011; Sawnani et al., 2015). Understanding how this imbalance changes the mechanics of breathing is a relatively new area of study, and is one of importance for developing new therapies to support the individual anatomy of each patient. In healthy/normal subjects, the rib cage expands but does not significantly distort in shape during respiration due to equal and opposite expanding pressures applied between the diaphragm, abdominal muscles and intercostal muscles that stabilize this compartment. This interrelationship is perturbed in muscular dystrophy, and the rib cage distorts unevenly due to an imbalance in muscle strength and/or scoliosis. As a result, patients may develop unique compensatory mechanisms to adjust for their challenges.

Although some generalizations can be made about respiratory failure in muscular dystrophy, it is important to note that, ultimately, no two patients are the same and a

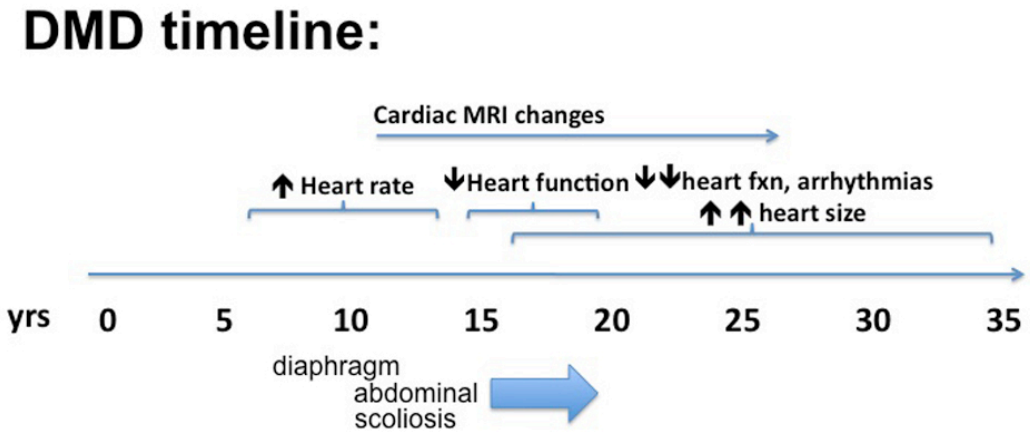

Figure 1.4 DMD timeline. The earliest cardiac finding in DMD is often sinus tachycardia which can be detected often before age 10. With the sensitivity of cardiac MRI, strain and delayed enhancement can be detected usually between ages 10 and 15. Around this same time, there is weakening of the diaphragm muscle, accompanied by weakness of the accessory muscles of respiration including the abdominal muscles. Scoliosis may also occur during this time. With progression, the heart becomes enlarged, taking on the course of DCM.

wide range of phenotypes can be seen between and within diagnostic subtypes of muscular dystrophy. For instance, some individuals with LGMD show primary weakness in expiratory muscles compared to inspiratory muscles with little diaphragm involvement, while others show the opposite trend (Romei et al., 2012). Additionally, some patients will develop kyphoscoliosis while others will develop little to no deformation of spine, leading to different compensatory mechanics between these groups as well (**Figure 1.4**).

Transforming growth factor beta (TGFβ) in the muscular dystrophies

The transforming growth factor beta (TGFβ) super-family of proteins are a highly conserved set of cytokines broadly expressed throughout development and adult life where they serve functions in orchestrating differentiation and also recovery from injury, respectively (Goumans et al., 2009; ten Dijke and Arthur, 2007; Zavadil and Böttinger, 2005). TGFβ family members are processed intracellular to form a dimerized ligand and this dimerization requires the prodomain, also known as the latency associated peptide (LAP), which is non-covalently linked to the C-terminal active domain (Schmierer and Hill, 2007) (**Figure 1.5**). This aggregate of the prodomain with active domain is referred to as the small latent complex, and is one means by which TGFβ is regulated in an inactive form. The LAP domain sterically inhibits the binding of TGFβ ligand to its receptor until chemical, physical or enzymatic events unseat the ligand from its LAP position (Fontana et al., 2005; Koli et al., 2001; Saharinen et al., 1999). In this way, TGFβ and its LAP are thought to serve as a signal of ECM degradation and weakness when localized to ECM as a latent element.

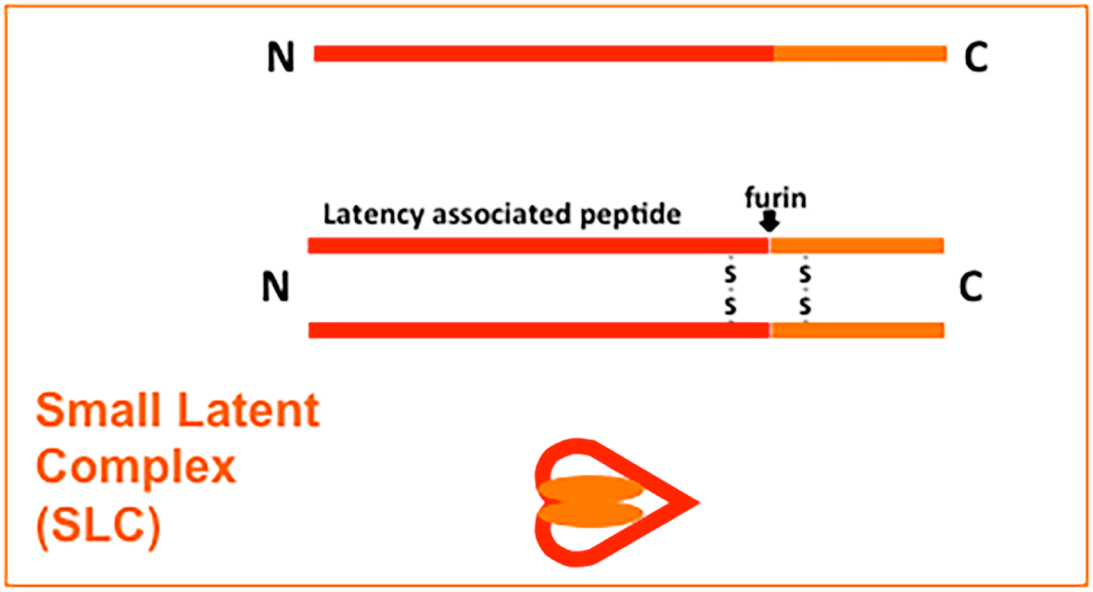

Figure 1.5. Schematic of TGFβ processing. TGFβ is produced as a single peptide that is cleaved by furins and then dimerized covalently by disulfide bonds. The final small latent complex consists of the latency associated peptide or prodomain non-covalently linked to the carboxy-terminal active domain (orange).

There are ~50 TGFβ family members but TGFβ 1, 2, and 3 constitute the key proteins that contribute to the TGFβ performing roles while other protein members of this family are in the Growth and Differentiation Factors (GDFs), Bone Morophogenetic Proteins (BMPs) and Activins (Schmierer and Hill, 2007). TGFβ overexpression has been implicated in promoting many disease processes including epithelial-mesenchymal transition in certain cancers, fibrotic scarring and reduced muscle regeneration and wasting (Border and Noble, 1994; Burks and Cohn, 2011; Feng and Derynck, 2005; Kalluri and Neilson, 2003). Most muscular dystrophies are characterized by increased tissue fibrosis, especially DMD where it has been best studied. Indeed TGFβ and its receptors are upregulated in the *mdx* mouse and in human DMD muscle (Bernasconi et al., 1995; Chen et al., 2005; Iannaccone et al., 1995). These and other studies have focused extensively on the upregulation of TGFβ-1 without as much attention to TGFβ-2 and TGFβ-3 (Dadgar et al., 2014; Nelson et al., 2011a).

Inhibition of TGFβ forms was examined using antibodies that neutralize TGFβ and prevent interaction with its ligands (Dasch et al., 1989). Specifically, the 1D11 antibody, a monoclonal antibody that recognizes TGF-β1 and TGFβ-2, was shown to improve respiratory function, grip strength and reduce fibrosis in a 9 month study in the *mdx* mouse (Nelson et al., 2011a). In another study, losartan, an angiotensin receptor blocker thought to be a downstream consequence of TGFβ activation was also shown to reduce fibrosis and markers of fibrosis (Cohn et al., 2007a). This study also examined the effect of losartan or TGFβ neutralization on acute recovery from injury including effects on regeneration, finding that both promoted regenerative potential

(Cohn et al., 2007a). Interestingly, in the study led by Nelson, 1D11 showed little improvement in reducing inflammation or other long-term histologic markers of disease noting that markers of disease were not so dramatically elevated in the *mdx* mouse model of DMD.

Latent transforming growth factor beta (LTBP) in muscular dystrophy

The small latent complex, consisting of dimerized TGFβ active domain coupled to its latency associated peptide, is secreted to the ECM covalently linked to latent TGFβ binding proteins, known as LTBPs. The link between the small latent complex and an LTBP is covalent through two disulfide bridges. LTBPs are members of the fibrillin superfamily and incorporate into the ECM like fibrillin (Robertson et al., 2015). Both fibrillins and LTBPs contain more than 15 epidermal like growth factor (EGF) domains, and fibrillins contain more than LTBPs since they are larger in size. In addition, these proteins contain "8-cys" repeats, some of which are specialized to bind directly to TGFβ (Yuan et al., 1997). The TGFβ binding domain relies on the presence of conserved cysteine residues, which form four disulfide bonds; disrupting these cysteine residues disrupts TGFβ binding. Therefore, the LTBP family has both structural and regulatory roles in homeostasis that may be interdependent.

A genome-wide search for modifiers of muscular dystrophy in mice identified *Ltbp4* (Heydemann et al., 2009). This approach relied on using an intercross of the *Sgcg* null mouse that lacks the dystrophin associated protein γ-sarcoglycan and shares similar histopathological defects as the *mdx* mouse model. The *Ltbp4* locus was found to strongly influence sarcolemmal leakiness, a reflection of membrane stability, as well

as fibrosis. An insertion/deletion polymorphism was found in *Ltbp4* that changes the proline-rich "hinge" region of LTBP4 protein resulting in either deletion of 12 amino acids or insertion of 12 amino acids. Mice with the deleterious "deleted" *Ltbp4* allele have elevated SMAD signaling, while strains with the protective "insertion" *Ltbp4* allele have reduced SMAD signaling. This hinge region can be proteolyzed and undergo a conformation change that is coupled to TGFβ release (Saharinen et al., 1999). Stabilizing the hinge region using an antibody or small molecular therapy may prove to be an effective way to reduce TGFβ activation. Mice with a hypomorphic *Ltbp4* allele develop cardiomyopathy and pulmonary defects and do not survive into adulthood, limiting studying this gene in mature tissues (Sterner-Kock et al., 2002).

In humans, there are two common alleles of the *LTBP4* gene found at high frequency in the population (**Figure 1.6**). These two alleles differ from each other at four amino acid positions spread along the length of the LTBP4 protein. The LTBP4 "risk" allele is associated with increased SMAD signaling while the LTBP4 "protective" allele is associated with reduced SMAD signaling. In DMD, boys with the protective *LTBP4* allele lose ambulation at age 12.5 ± 3.3 years of age while those with the deleterious risk allele lose ambulation at 10.7 ± 2.1 years of age (Flanigan et al., 2013). Two other groups replicated this same finding demonstrating that the LTBP4 allele is protective (Bello et al., 2015; van den Bergen et al., 2015). None of the four amino acid substitutions fall within the hinge region of LTBP4 but one does fall near the the "8-cys" region implicated in TGFβ binding. Because LTBP4 binds all three isoforms of TGFβ, therapeutic approaches directed at LTBP4 are expected would likely reduce cellular availability of all three isoforms and act as a pan-TGFβ suppressor.

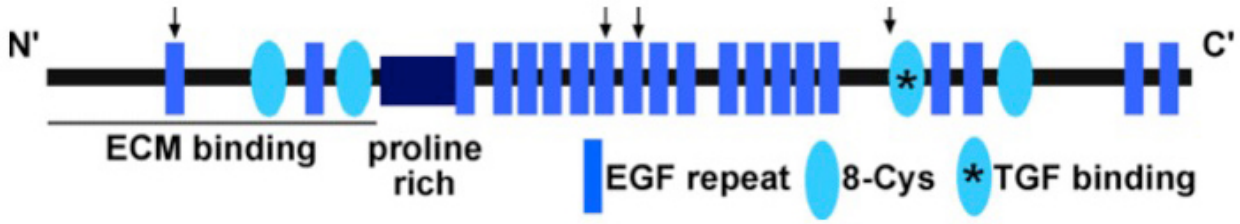

Figure 1.6. Latent TGFβ protein 4 (LTBP4) domains. The largest form of LTBP4 includes multiple epidermal growth factor (EGF) domains, interspersed with 8-cysteine containing repeat regions. There is a proline rich hinge region (dark blue) that separates the amino-terminus that binds to the extracellular matrix. The 8-cys domain marked with an asterisk binds TGFβ. The arrows indicate the position of non-synonymous single nucleotide polymorphisms in human *LTBP4* that correlate with muscular dystrophy outcomes.

OVERVIEW OF THESIS

The chapters in this thesis focus on two areas: 1) Exploring the efficacy of anti-TGFβ antibody and anti-LTBP4 antibodies in a pre-clinical short-term trial conducted in a mouse model of DMD, and 2) Characterizing the inter-relationships among muscle groups in mice with muscular dystrophy.

Chapter 2 describes studies conducting a 30-day preclincial examination of two humanized monoclonal antibodies against TGFβ-2 or TGFβ-3 in the *mdx* mouse, a model of Duchenne muscular dystrophy (DMD). To determine outcomes, mice were tested for grip-strength, cardiac function and respiratory function at three separate time-points prior to sacrifice at which time muscles were excised and processed for measures of fibrosis, membrane-leak, and inflammation. Both antibodies had some effect on reducing inflammation, membrane leak and fibrosis although not always in the same muscle groups. These studies are considered preclinical in nature since these antibodies could be transitioned into the clinical setting as a biological therapy for DMD. These studies were undertaken based on the rationale that while TGFβ-1 increases in dystrophic muscle, TGFβ-2 and TGFβ-3 comprise the majority of the TGFβ within a muscle.

Chapter 3 is a summary of a preclinical study conducted similarly to chapter 2 using polyclonal antibodies generated against LTBP4 protein. These two antibodies were designated 28199 and 28200 and generated against the “hinge-like” proline-rich region of LTBP4 that is highly conserved and integral to the binding and latent nature of TGFβ family members. The rationale for pursuing LTBP4 as the target was based on the concept that LTBP4 binds all three TGFβ isoforms and as such this may provide a

means to target all the TGFβ in muscle without completely ablating TGFβ availability. This strategy may provide greater tissue specificity and therefore have a more favorable side effect profile when used long term.

In Chapter 4, I will summarize findings from a study of over 200 twelve-week old *Sgcg* mice. *Sgcg* mice lack the dystrophin-associated protein γ-sarcoglycan. *Sgcg* mice have a phenotype very similar to *mdx* mice. However, these mice have a more severe cardiac phenotype that allows better integration of cardiac and pulmonary findings (Roberts et al., 2015). This cohort of mice was used for mapping genetic modifiers of mice (Swaggart et al., 2014; Swaggart et al., 2011) and provided a unique cohort that allowed us to make comparisons among muscle groups. Importantly, these data allowed us to make correlations between muscle groups. These data were the first to suggest that the abdominal "core" muscles may contribute to cardiopulmonary health in mouse models of muscular dystrophy, and suggest that the abdominal muscle group may be similarly important in human muscular dystrophy.

In Chapter 5, I provide a contextual analysis of these data and how these findings can be interpreted based on our current knowledge and trends of literature in both murine and human muscular dystrophy fields. TGFβ has been implicated in many disease processes, including muscular dystrophy and may provide an approach to therapy especially in reducing inflammatory infiltrate and fibrosis. Mechanical support of the abdominal muscles, especially in response to respiratory decline, may be beneficial in muscular dystrophy and is worth exploration. Together these findings provide approaches and outcomes for treating and monitoring muscular dystrophy progression.

Chapter 2

Evaluation of targeted TGFβ isoform inhibition in a mouse model of muscular dystrophy

ABSTRACT

TGFβ is a key cytokine that regulates growth and development as well as response to injury. Muscular dystrophy is a chronic degenerative disease of muscle characterized by elevated TGFβ. Previous studies examined the role of neutralizing TGFβ using a well-characterized antibody that reacts with multiple TGFβ isoforms, albeit with varying sensitivity among the isoforms. To assess the degree to which TGFβ-2 and TGFβ-3 contribute to muscular dystrophy progression, we assessed individually TGFβ-2 and TGFβ-3 antibodies for their ability to modulate features of muscular dystrophy. We conducted a short term four week study of TGFβ antibody injections and assessed histological and functional readouts of muscle disease and function. We found that anti-TGFβ-3 neutralizing antibody improved several readouts of muscle membrane stability and function, while TGFβ-2 neutralizing antibody may improve muscle regenerative capacity. Both antibodies reduced macrophage infiltration in muscle. Together these data identify that TGFβ specific antibodies target unique aspects of the muscular dystrophy disease process.

RESPECTIVE CONTRIBUTIONS

This work was conducted with the generous collaboration and mentorship of Dr. Alexis Demonbreun. Two technicians, Mr. James Warner and Patrick Page, also contributed significantly to the execution of these experiments. They are responsible for some or all of the data associated with measuring dye uptake, muscle mass, serum creatine kinase levels, internal nuclei number, fiber cross-sectional area and immunohistochemical quantification data. Patrick Page additionally assisted me with the collection of grip strength, preparation of antibody injections, organization of notes and records. Mr. Andy Vo analyzed the RNA sequencing data. Dr. Sasha Bogdanovich and I together acquired ex-vivo muscle mechanical data, and Dr. Bogdanovich analyzed the Sirius Red staining. Dr. Bogdanovich helped edit related sections of this Chapter. Ms. Judy Early prepared paraffin-embedded histologic sections while James Warner and I acquired the microscopic images. Mrs. Michelle Hadhazy conducted whole-body plethysmography, general animal care, serum collection and administered the majority of intraperitoneal injections of antibody preparations. I conducted and collected echocardiography, fiber cross-sectional area, determined hydroxyproline content in addition to analyzing these data and editing the manuscript. Dr. Alexis Demonbreun generated figures and edited the Chapter. Dr. Elizabeth McNally conceived the experiments, contributed to data analysis and edited this Chapter.

INTRODUCTION

TGFβ in Muscular Dystrophy.

TGFβ is a dimerized cytokine essential to normal mammalian growth and development where it regulates septation events in the developing lungs, heart and peripheral vasculature (Gaengel et al., 2009; Guo and Wang, 2009). In addition to its role in development, TGFβ and its family members have critical roles in response to tissue and organ injury, most notably in the mediation of fibrotic response (Border and Noble, 1994; Kalluri and Neilson, 2003; Leask and Abraham, 2004; Penn et al., 2012). Duchenne Muscular Dystrophy (DMD) is the most common cause of X-linked recessive disease in humans and is characterized with excessive fibrosis in muscle in humans and its primary animal model, the *mdx* mouse. Along with this increase in fibrosis is a concomitant increase in TGFβ and its receptors (Bernasconi et al., 1995; Iannaccone et al., 1995). Unbiased gene expression profiling of DMD muscle at early and later stages of disease identified the TGFβ pathway as markedly elevated in the later symptomatic stages of disease (Chen et al., 2005).

Targeting intracellular TGFβ signaling pathway reduces dystrophic phenotype and restores function in the mdx model of DMD.

TGFβ is represented by a set of three family members, TGFβ-1, TGFβ-2 and TGF-β3. These proteins activate transcriptional events via tyrosine-kinase receptor mediated activation of the intracellular canonical SMAD pathway, and inhibition of this pathway at varying levels has been the focus of pre-clinical studies in the *mdx* mouse model of DMD (Burks and Cohn, 2011; De Luca, 2012; MacDonald and Cohn, 2012). FDA

approved angiotensin II receptor antagonists such as losartan reduce SMAD signaling indirectly by reducing TGFβ transcriptional levels. Losartan was found to reduce features of cardiomyopathy and improve respiratory function in independent pre-clinical trials of the *mdx* mouse model of DMD (Cohn et al., 2007a; Nelson et al., 2011a). In humans with DMD, losartan or the angiotensin converting enzyme inhibitor lisinopril have been equally successful in treating cardiomyopathy but with limited effect on reducing skeletal muscle dysfunction (Allen et al., 2013). In other studies, this same limited effect on skeletal muscle targeting of TGFβ by losartan was seen (Bish et al., 2011). Together, these data suggest that more potent blockers of TGFβ may be needed to see a skeletal muscle effect in DMD.

Blockade of TGFβ improves regeneration and respiratory function in the *mdx* mouse

The 1D11 antibody is a monoclonal antibody that recognizes TGFβ1 and TGFβ2 (Dasch et al., 1989). 1D11 also recognizes TGFβ3, and when compared, 1D11's affinity for TGFβ-2 was much less than for TGFβ-3 (Zwaagstra et al., 2012). Thus while many investigators consider 1D11 a "pan-TGFβ" antibody, it does not react to TGFβ isoforms equally and only poorly recognizes TGFβ-2 (Zwaagstra et al., 2012). The 1D11 antibody was shown to improve the *mdx* muscle's response to acute cardiotoxin injury (Cohn et al., 2007a). In a 9 month study, the 1D11 antibody was shown to improve respiratory function, grip strength and features of fibrosis (Nelson et al., 2011a). However, despite this improvement many features of muscular dystrophy were still

present in the 1D11-treated *mdx* mice, suggesting that additional or potent therapies would be needed.

Isoform specific antibodies for TGFβ-2 or TGFβ-3 may be useful for treating muscular dystrophy.

Although TGFβ1 is induced in muscular dystrophy (Nelson et al., 2011a), we identified that TGFβ3 is also induced at the mRNA level. When compared, TGFβ2 and TGFβ3 mRNA contributed significantly to the TGFβ pool in muscle. Therefore, we hypothesized that TGFβ isoform-specific neutralizing antibodies may be beneficial in muscular dystrophy. Through a collaborative effort with Novartis Institutes of Biomedical Research, humanized TGFβ2 and TGFβ3 specific antibodies were made available for testing in a mouse model of muscular dystrophy. Antibodies were administered via intraperitoneal injection over a 30-day trial period with intermittent *in vivo* phenotyping over time. Interestingly, anti-TGFβ2 and anti-TGFβ3 antibody therapy both reduced some histologic aspects of dystrophy, while only the group that received anti-TGFβ3 demonstrated improved muscle strength and performance.

MATERIALS AND METHODS

Animal use and care

mdx/hLTBP4 BAC mice were generated as described previously (Ceco et al., 2014) *hLTBP4 BAC* mice were engineered to carry two copies of the human LTBP4 locus, including its regulatory regions, on a bacterial artificial chromosome (BAC). *hLTBP4 BAC* transgene positive mice were then crossed to *mdx* mice (Jackson Laboratories) to generate *mdx/hLTBP4 BAC* mice. Only male mice were used for the study. Animals were housed in a pathogen-free barrier facility at Northwestern University. Care and handling was always conducted with personal protective equipment in a manner consistent with standards approved by Northwestern's Institutional Animal Care and Use Committee (IACUC).

Intraperitoneal injection and antibody preparation

Humanized murine monoclonal antibodies specific to TGFβ-2 or to TGFβ-3 were generated by Novartis and provided at a stock concentration of 7.55 mg/ml and 5.45 mg/ml respectively and stored at -80°C (Novartis, Basel, Switzerland). Mice were injected once a week via intraperitoneal injection for a total of four doses prior to sacrifice. On injection days, stock solutions stored at -20°C were diluted into sterile Eppendorf tubes containing sterile phosphate buffered saline (PBS) (Invitrogen, 14-829-1A) at a concentration of 5mg/kg the morning of each injection date. The total volume injected did not exceed 190µl per individual injection. Individualized aliquots were prepared by a non-blinded technician in a sterile laboratory hood and kept covered on ice for injection by a different, blinded technician. Sterile BD Micro-Fine IV Insulin

Syringes (Fisher Scientific, 14-829-1A) were used to inject the intraperitoneal cavity of unanesthetized animals.

Body weight and muscle analysis

Mice were weighed weekly over the course of thirty days with body mass recorded on Days 0, 7,14, 21, and 28. Upon sacrifice tibia lengths were measured using digital calipers. Raw body mass was normalized to the average tibia length and expressed as fold change from Day 0. Muscle were removed and immediately weighed. Muscle mass was normalized to tibia length. The left and right tibialis anterior, quadriceps, gluteus/hamstring, gastrocnemius/soleus, kidneys and abdominal muscles were excised and weighed prior to Evans blue dye (EBD) uptake analyses. The left and right extensor digitorum longus (EDL) muscles were excised for *in vitro* electrophysiologic study. Both tibialis anterior muscles and the left and right heart ventricles were collected for histologic analyses. The diaphragm, abdominal muscles and quadriceps were hemisected, and one portion was used for hydroxyproline (HOP) quantification while the other portion was used for histologic analyses. The quadriceps muscle was large enough to be used for histology, EBD and HOP analysis. The midportion of the quadriceps muscle was used for histological analysis while the remaining portion was minced and used for EBD and HOP quantitation.

Excised muscles were immediately frozen in liquid nitrogen, placed in pre-cooled Nalgene cryovials and stored at -80^{o}C or placed in 10% formaldehyde for processing. Seven μm sections from the center of the quadriceps muscle and triceps muscle were stained with hematoxylin and eosin (H&E). The percentage of myofibers with internal

nuclei was calculated from the number of myofibers containing internal nuclei / total number of myofibers counted per field, standardized as a percentage (approximately n ≥ 150 fibers per animal from at least n ≥ 3 animals per condition). Mean fiber size and fiber variation was calculated using the cross-sectional area of individual myofibers (n ≥ 150 fibers per animal, from at least n ≥ 3 animals per condition). Imaging was performed using a Zeiss Axio Imager.M2 microscope using a 10X or 20X objective. Statistics analysis used Prism (Graphpad, La Jolla, CA) using a one-way ANOVA.

Immunofluorescence microscopy

Seven µm sections from the triceps muscle were fixed in 4% cold paraformaldehyde (PFA) for 10 minutes, rinsed in PBS (Gibco, 14190-144) and blocked in PBS with 0.1% Triton and 10% fetal bovine serum (FBS) for 1 hour at room temperature. The sections were incubated with either anti–pSmad2/3 antibodies (pSMAD2/3, Abcam, ab51451) or anti- F4/80 conjugated to Alexa-488 (ab6640, Abcam, Cambridge, MA) at a dilution of 1:100 overnight at 4°C. Donkey anti-rabbit 488 (1:2500, Thermo Fisher Scientific, A-21206) and WGA-594 (W11262, 1:100, Thermo Fisher Scientific) were incubated for 1 hour at room temperature. One PhosStop™ Phosphatase inhibitor tablet (Sigma-Aldrich, 04906837001) was added to 10ml of PBS and used for all incubations with the anti-pSMAD antibody. Nuclei were visualized with Vectashield with DAPI (Vector Laboratories). Imaging was performed using a Zeiss Axio Imager.M2 microscope using a 20 X objective. F4/80 positive cells were quantified from at least 3 fields per mouse and 3 animals per genotype (Ceco et al., 2014). Statistical analysis was performed with Prism (Graphpad, La Jolla, CA) using a one-way ANOVA.

Fibrosis quantification and analysis

Picrosirius red staining was performed on the center core taken from the midsection of the quadriceps muscles fixed in 10% formalin. Representative images (n ≥ 5 animals per condition) of stained whole muscle sections were taken at 10x magnification on a Zeiss Axio Imager.M2. The images were adjusted for brightness and contrast and converted to black and white images. Whole muscles were outlined (with exclusion of external fascia) using ImageJ software (NIH). Contours of picrosirius red positive staining inside previously outlined muscle were optimized by threshold and converted to binary images. Area fraction (% area) of picrosirius red stained muscle was calculated compared to whole muscle area. Statistical analysis was performed with Prism (Graphpad, La Jolla, CA) using a one-way ANOVA.

Hydroxyproline (HOP) content was measured (Ceco et al., 2014; Flesch et al., 1997; Swaggart et al., 2011) on the diaphragm and abdominal muscles. The quadriceps muscles, minus the core taken for H&E staining, was minced and divided; half was used for HOP determination. Muscles were excised, minced, weighed, and flash frozen in liquid nitrogen. Tissue was stored at -80°C until the HOP assay was performed. The assay was performed on frozen muscle that was kept on ice until added to sterile glass culture tubes (Corning, 9826-13). Muscle was hydrolyzed overnight in 2 ml of 6 M hydrochloric acid at 115°C. Once hydrolyzed, 10 µl of hydrosylate was mixed with 150 µl isopropanol, then 75 µl of 1.4% chloramine-T (Sigma-Aldrich) in citrate buffer and incubated at room temperature for 10 minutes. After 10 minutes, one milliliter of Ehrlich's reagent [3 g of 4-(dimethylamino) benzaldehyde (Sigma-Aldrich), 10 ml ethanol, 675 µl sulfuric acid] was added, vortexed,

and incubated for 30 minutes in a water bath at 55°C. Hydroxyproline content was quantified via absorbance at 558 nm using the Synergy HTX multi-mode 96-well plate reader (BioTek®, Winooski, VT) plate reader. A standard curve (0–4,000 nM, trans-4-hydroxy-l-proline; Sigma-Aldrich) was included in each assay results are reported as nM HOP/mg tissue. Statistical analysis was performed with Prism (Graphpad, La Jolla, CA) using a one-way ANOVA.

Evans blue dye analysis

Evans blue dye (EBD) uptake into muscle was quantified as described previously (Ceco et al., 2014; Heydemann et al., 2005; Swaggart et al., 2014). Approximately forty hours prior to sacrifice, animals were injected intraperitoneally with 5 μl/g body mass EBD (Sigma, E-2129) dissolved in phosphate-buffered saline at 10 mg/ml. The entire gastrocnemius/soleus and gluteus/hamstrings muscles, the remaining portion of quadriceps muscle, and both kidneys were harvested for the dye uptake assay. Muscles were removed, minced, weighed and incubated in 1 ml of formamide for 2 h at 55°C with shaking. Spectrophotometric absorbance was measured at 620 nm using the Synergy|HTX Multi-mode plate reader (BioTek, Winooski, VT). Results were reported as the absorbance per milligram of tissue.

For section-based analysis of dye uptake, the triceps muscle were sectioned and fixed with ice-cold acetone. Sections were stained with WGA-488 (W11261, Thermo-Fisher Scientific) and mounted in Vectashield with DAPI. Representative images of stained muscle sections were taken at 5x magnification on a Zeiss Axio Imager.M2. The percentage of EBD-positive muscle was calculated in Image J from the area of

EBD-positive muscle divided by the total muscle area. Statistical analysis was performed with Prism (Graphpad, La Jolla, CA) using a t-test.

Serum Creatine Kinase Measurement

Serum creatine kinase was quantified as described previously (Demonbreun et al., 2015). Approximately 20 µl of blood collected was collected from individual mice through serial retro-orbital bleeds on the day prior to the first antibody injection, day 20 and day 30. Heparinized capillary tubes (Fisher, Pittsburgh, PA) were used to collect blood into separator tubes (Becton Dickinson, Franklin Lakes, NJ) followed by a 5-minute incubation and then centrifuged for 10 minutes at 8000 X g. The separated plasma fractions were immediately placed on ice, stored at -80C, and then assayed later using the Enzy-Chrom CK Assay kit (ECPK-100; BioAssay Systems, Hayward, CA). Serum creatine kinase activity was measured in the Synergy|HTX Multi-mode plate reader (BioTek, Winooski, VT). Statistical analysis was performed with Prism (Graphpad, La Jolla, CA) using a one-way ANOVA. Mice that were injected with cardiotoxin were excluded from the day 30 analysis.

Grip strength Measurement

Grip strength was conducted in a pathogen-free procedure room using a grip strength meter (Columbus Instruments, 1027SM) consisting of a metal horizontal bar attached to a force meter according to standardized operating procedures described by the Treat-NMD working group (DMD_M.2.2.001) (http://www.treat-nmd.eu/downloads/file/sops/dmd/MDX/DMD_M.2.2.001.pdf). Mice were tested every

seven days, beginning at day zero, for a total of five time-points for each subject. Each time-point consisted of four trials consisting of three forelimb challenges, with at least one minute of rest between trials. During one challenge, the animal grips the bar with forelimbs downward facing while the operator uses the animal's tail to pull it in a plane horizontal to the bar. The force was recorded at the time just before the animal's grip released. Mean, maximum, minimum values, and statistical analysis was performed with Prism (Graphpad, La Jolla, CA) using a t-test at each time point.

In Vitro electrophysiology and mechanics

Contractile and physiological parameters (n= 6 mice per group) were performed in the EDL muscle. The Aurora Scientific 1200A intact (*in vitro*) muscle test system was used (Aurora Scientific, Inc, Aurora, Ontario, Canada). The system consisted of vertically placed muscle bath filled with oxygenated (gas mixture: 5%$C0_2$, 95%O_2) Ringer solution (120mM NaCl, 4.7mM KCl, 1.2mM $MgSO_4$; 1.2mM KH_2PO_4; 1.75mM $CaCl_2$; 0.05mM EDTA; 25mM $NaHCo_3$; 15mM glucose), maintained at 24°C by circulating water. Briefly, EDL muscle was dissected and weighted, tendon tied using 5-0 sutures and transferred to the previously described muscle bath, where it was attached to Aurora Scientific dual force transducer, between two platinum electrodes placed longitudinally alongside the muscle. The muscle was stimulated using Aurora Scientific high power follow stimulator (Aurora Scientific, Inc, Aurora, Ontario, Canada). The protocol consisted of 3 twitches, 3 tetanii, and 5 lengthening (eccentric: ECC) contractions, each separated by 2 minutes (Bogdanovich et al., 2002; Bogdanovich et al., 2008). EDL length was adjusted to produce optimal twitch and tetanus at 500ms duration, and this

length was measured (L_0). For ECCs muscle was stimulated with 5 tetanic stimuli; duration of 700ms (500ms isometric phase and 200 ms eccentric phase), and it was lengthened by 10% L_0 at velocity of 0.5 L_0/s during the contraction. The percentage of force decrement between first and fifth ECCs was obtained from isometric phase of ECC. Parameters analyzed from isometric contractions were: isometric max twitch force, time to max twitch force, ½ relaxation time, and isometric max tetanic force. Data acquisition Dynamic Muscle Control (DMC) software v.5.294 from Aurora Scientific, Inc. was used to obtain and analyze force recordings of twitch, tetanic and ECC parameters. EDL's cross sectional area (CSA) was calculated by dividing muscle mass by the muscle density coefficient (1.06g*cm^3), muscle L_0 and the EDL length coefficient of 0.45. This CSA was used to calculate specific force of twitch and tetanii. Right EDL muscle was flash-frozen in liquid nitrogen and left EDL fixed in paraformaldehyde, frozen in liquid nitrogene and both were stored at -80°C.

Cardiotoxin injection

Ten days prior to sacrifice, on day 20 of the protocol, the right tibialis anterior (TA) muscle was injected with ten microliters of 10 μM cardiotoxin (Sigma, C9759) in sterile PBS (Gibco, 14190-144) using a insulin syringe (Fisher Scientific, 14-829-1A), while the left tibialis anterior muscle was mock injected with PBS alone (n=6 of each condition). Specifically, the needle of an insulin syringe was inserted near the distal tendon of the TA and directed down the midline of the muscle proximally towards the knee. The cardiotoxin solution was slowly released as the needle was retracted. Both TA muscles were excised, flash frozen in liquid nitrogen then stored at -80°C. Muscle was sectioned

and stained with hematoxylin and eosin for analysis. Images were acquired on the Zeiss Axio Imager.M2using a 10x objective.

Echocardiography

Echocardiographic studies were conducted in a sterile animal facility procedure room according to standard protocols (Spurney et al., 2008), and as described previously (Gardner et al., 2015). Animals were imaged at day 0, day 14 and day 28 of the protocol. Animals were anesthetized using isoflurane, 2% in O_2, and then placed on a heated platform for imaging. Time on isoflurane was recorded for each animal, and all studies were completed in less than 15 minutes. During imaging, isoflurane was titrated to avoid heart rates below 350bpm and averaged ~450bpm. Mice with heart rates below 350bpm were excluded from analysis. Imaging utilized a Vevo 2100 (Visualsonics, Toronto, Ontario, Canada) ultrasound machine with 40Mhz probe to acquire all measurements and images. Left- ventricular fractional shortening was acquired by collecting M-mode images in both the parasternal long-axis and parasternal short-axis views while global longitudinal strain (GLS) was derived from the parasternal long-axis view only. Imaging was conducted on n=12 animals per condition.

Whole Body Plethysmography

Unanesthetized whole-body plethysmography was used to measure respiratory function using a Data Sciences International, Buxco® Finepointe® 4-site WBP. Individual mice were placed in a calibrated cylindrical chamber. Each mouse was allowed to acclimate to the plethysmography chamber for 120 minutes before recording was initiated. Data

was recorded for a total of 15 minutes broken into 3 consecutive 5-minute periods. Tidal volume (ml), frequency (breaths/minute), minute volume (tidal volume multiplied by respiratory rate, ml/minute), Ti (Time inspiration), and Te (Time expiration), and PENH (pause = Te-Tr/Tr, penH ((PEP/PIP) X pause) were evaluated using Finepoint software (DSI). Studies were performed at room temperature. Statistical analysis was performed using Finepoint software (DSI, St. Paul Minnesota).

RESULTS

TGFβ isoforms are expressed differentially in muscle.

RNA sequencing of the abdominal muscles and quadriceps from wildtype 129Sv/EmsJ mice showed differential expression of *Tgfb1*, *Tgfb2* and *Tgfb3* (Table 1.1). Specifically, we found *Tgfb3* mRNA to be expressed at ~ 6 times the levels of *Tgfb1*, and *Tgfb2* was expressed at ~2-3 X the level of *Tgfb1* in these muscles. Together these data suggest that *Tgfb2* and *Tgfb3* constitute far more of the TGFβ encoding mRNA pool in skeletal muscle compared to *Tgfb1*.

Table 2.1. Relative mRNA expression levels as determined by RNA sequencing.

Gene Name	Gene Description	FPKM value Abdominal	FPKM value Quadriceps
Tgfb1	transforming growth factor, beta 1	2.6389	2.7175
Tgfb2	transforming growth factor, beta 2	7.4401	5.7572
Tgfb3	transforming growth factor, beta 3	19.0089	10.0939

FPKM (fragment per kilobase of exon per million fragments mapped) X10.

Pre-clinical trial protocol

LTBP4 was identified as a modifier of muscular dystrophy in both mice and humans and is associated with increased membrane fragility and fibrosis (Flanigan et al., 2013; Heydemann et al., 2005). A mouse model containing a human LTBP4 BAC was generated and crossed with the *mdx* mouse model of DMD to generate the *mdx/h*LTBP4 mouse, that was recently characterized and shown to have increased TGFβ signaling, sarcolemmal leak, fibrosis, inflammation and muscle weakness compared to *mdx* controls (Ceco et al., 2014). Together, these qualities made the m*dx/h*LTBP4 mouse a useful model in which to test the effect of α-TGFβ therapy on muscular dystrophy.

Thirty-six male *mdx/hLTBP4* BAC mice were divided into three groups of 12 and distributed into the three groups to minimize differences in both body mass and age among groups (**Table 2.1**). At day 0, body mass ranged from 21.6-31.8 grams among animals with group means of 28.1±0.7 g, 28.3±0.6 g and 25.4±0.5 g for the groups designated to receive PBS, α-TGFβ-2 and α-TGFβ-3, respectively. The mean age for these 3 groups at day zero was 70.5, 72.5 and 71.4 days respectively, with no significant difference found between groups based on mass or birthdate via ordinary one-way ANOVA. Although all groups began with twelve animals, premature death of three mice during the trial period lead to modified group n values of 12, 10, and 10 for PBS, α-TGFβ2 and αTGFβ3, respectively. Two deaths were related to complications with intraperitoneal injection, while two deaths were related to isoflurane exposure during echocardiography. The outline of the antibody injection protocol is shown in **Figure 2.1**.

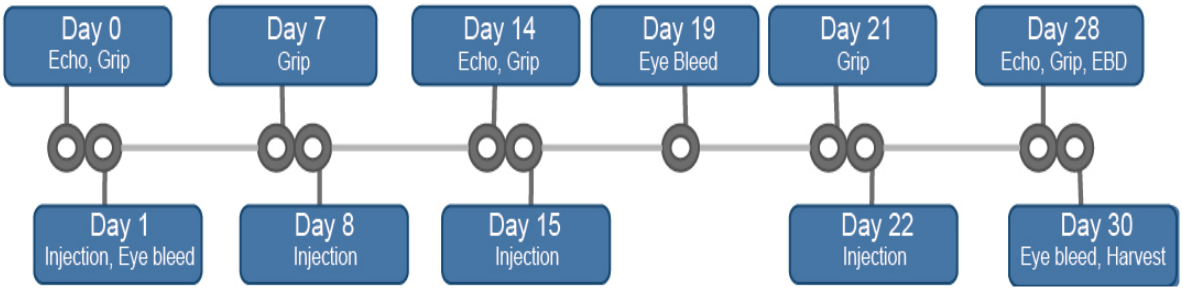

Figure 2.1 Pre-clinical trial design and timeline for α-TGFβ antibody testing
Above is a time-line representing the *in vivo* phenotyping and injection schedule of the 30-day pre-clinical protocol. Twelve mice per condition received pre-injection baseline phenotyping. No differences were found between groups at baseline for these measures.

TGFβ antibody injections did not affect growth over 4 weeks in mdx/hLTBP4 BAC mice.

To investigate changes in growth, body mass was measured at days 0, 7, 14, 21, and 28. Body mass increased in each groups over time at a similar rate to recently published studies of similar time-period (Latres et al., 2015). The average increase in body mass for PBS, anti-TGFβ2 and anti-TGFβ3 injected groups over the 30-day protocol was 2.5g, 1.6g, and 2.3g, respectively. This translated to an average increase of 9.4±1.7%, 6.5±2.0 %, and 10.2±1.5% over baseline for PBS, α-TGFβ2 and α-TGFβ3 injected groups respectively (n≥10 mice per group at each time point). No differences were seen between any conditions in body mass **(Figure 2.2A)** or body mass/tibia length **(Figure 2.2B)** at any time point when groups were compared via ordinary one-way ANOVA within each time point. A matched repeated-measures 2-way ANOVA to investigate differences over time did not reveal any significant difference between groups.

Differences in whole muscle mass have been shown to be indicative of therapeutic response and are useful for normalization (Bogdanovich et al., 2002; Wagner et al., 2002). All muscles were excised and weighed prior to processing and compared via ordinary one-way ANOVA. Mean gluteus/hamstring muscle mass normalized to tibia length was reduced in the anti-TGFβ-3 group (0.016±0.006 g/mm) compared to PBS group (0.02±0.0008 g/mm) (**Figure 2.2C,** n≥13 muscles per condition, $P<0.05$). No significant differences were seen between the masses of any muscle group normalized to tibia length, including quadriceps **(Figure 2.2D)**. These data suggest anti-TGFβ therapy does not hinder normal growth and maturation.

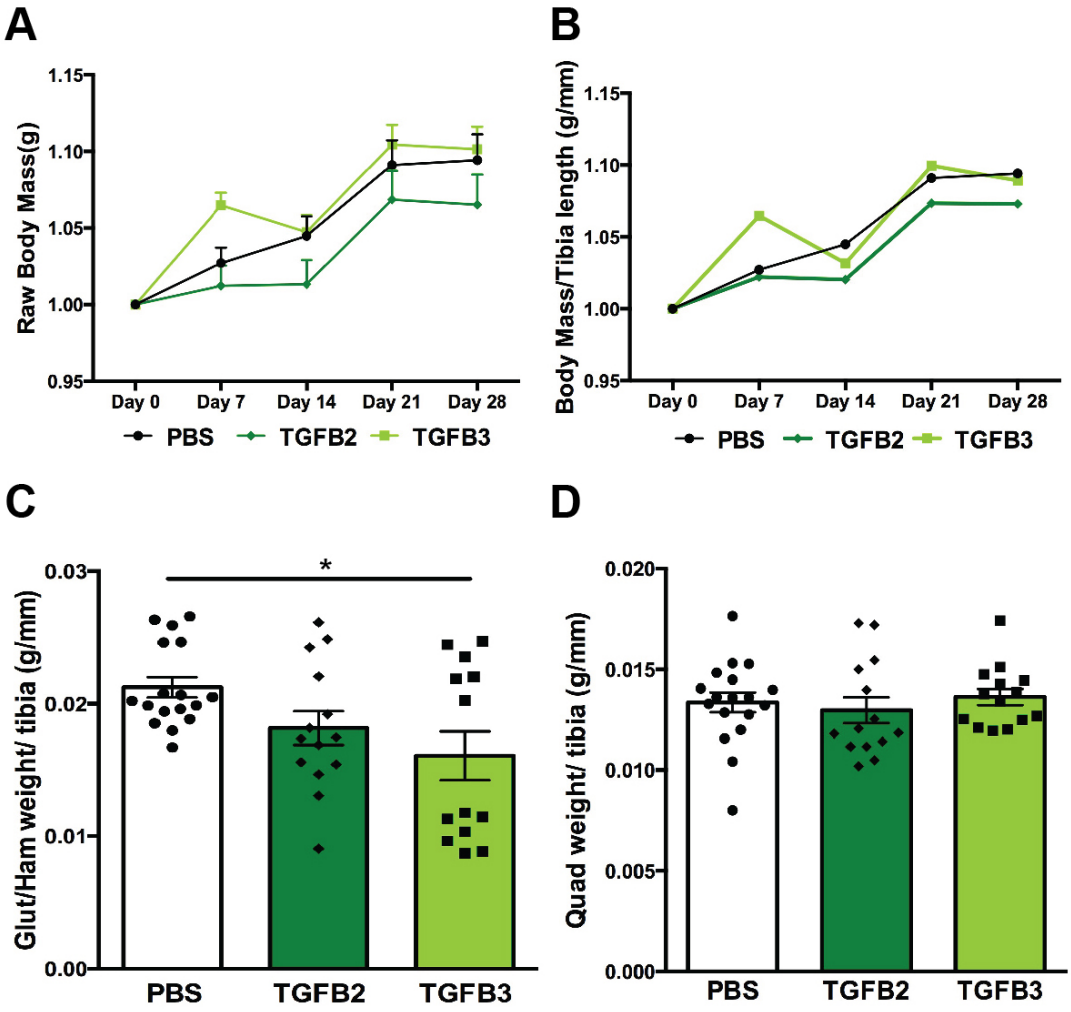

Figure 2.2 Body mass was unaffected by TGFβ antibody injection. Body mass was collected the day prior to initial injection (day 0) and at four subsequent time-points prior to sacrifice. **A)** Mean raw body mass did not differ between groups at baseline, nor at any time point thereafter when compared by ordinary one-way ANOVA (n≥ 0 mice per group at each time point). **B)** Body mass normalized to tibia length was analyzed similarly to raw body mass in 2.2A and no differences found between groups at baseline, nor any time point thereafter. **C)** anti-TGFβ3 injected gluteus/hamstring muscle weight was found be significantly decreased compared to PBS-injected muscle weight via ordinary one way ANOVA (n≥13 muscles per group, $P<0.05$) when all excised muscle mass was analyzed for differences in raw mass and raw mass/tibia length. **D)** anti-TGFβ2 or anti-TGFβ3 injections did not result in changes in quadriceps mass when compared against PBS via one-way ANOVA.

Anti-TGFβ antibody injections reduced macrophage infiltration.

To determine if isoform specific TGFβ neutralization modifies muscle histopathology, muscle from *mdx/h*LTBP4 mice injected with anti-TGFβ2, anti-TGFβ3, or PBS was analyzed via light microscopy. Quadriceps and triceps muscle were harvested at day 30 and analyzed. These muscles displayed characteristic features of muscle disease including fibrosis, internalized nuclei, and immune infiltrate (**Figure 2.3A, triceps)**. The mean cross-sectional area of individual myofibers was not significantly different between anti-TGFβ2 (926±55 μm2), anti-TGFβ3 (756±46 μm2) and PBS (814±49 μm2) injected controls via a one-way ANOVA or simple t-test (**Figure 2.3B,** n≥3 mice per condition, n~ 150 myofibers per animal). However, anti-TGFβ2 and anti-TGFβ3 injections resulted in an increase in larger sized myofibers and a reduction in medium sized myofibers compared to PBS (**Figure 2.3C)**. Additionally, triceps and quadriceps muscle had an increased percentage of myofibers containing internalized nuclei with anti-TGFβ-2 injection compared to PBS (60.2±1.9% compared to 47.4±2.3 %) via a one-way ANOVA (**Figure 2.3D,** n≥3 mice per condition**,** $P<0.05$), while anti-TGFβ3 (47.6±3.5%) was not different from PBS. These data suggest that anti-TGFβ2 injections may promote myofiber regeneration.

Inflammation is a prominent feature in many forms of muscle disease and can be assayed by documenting macrophages infiltration (Kronqvist et al., 2002). Activated macrophages, marked by F4/80 conjugated to Alexa-488, were decreased after injection of either anti-TGFβ-2 (7.7±1.3 cells) or anti-TGFβ-3 (10.5±3.5 cells) antibodies compared to PBS (33±5.7 cells) using a one-way ANOVA **(Figure 2.3E,** n≥3 mice per

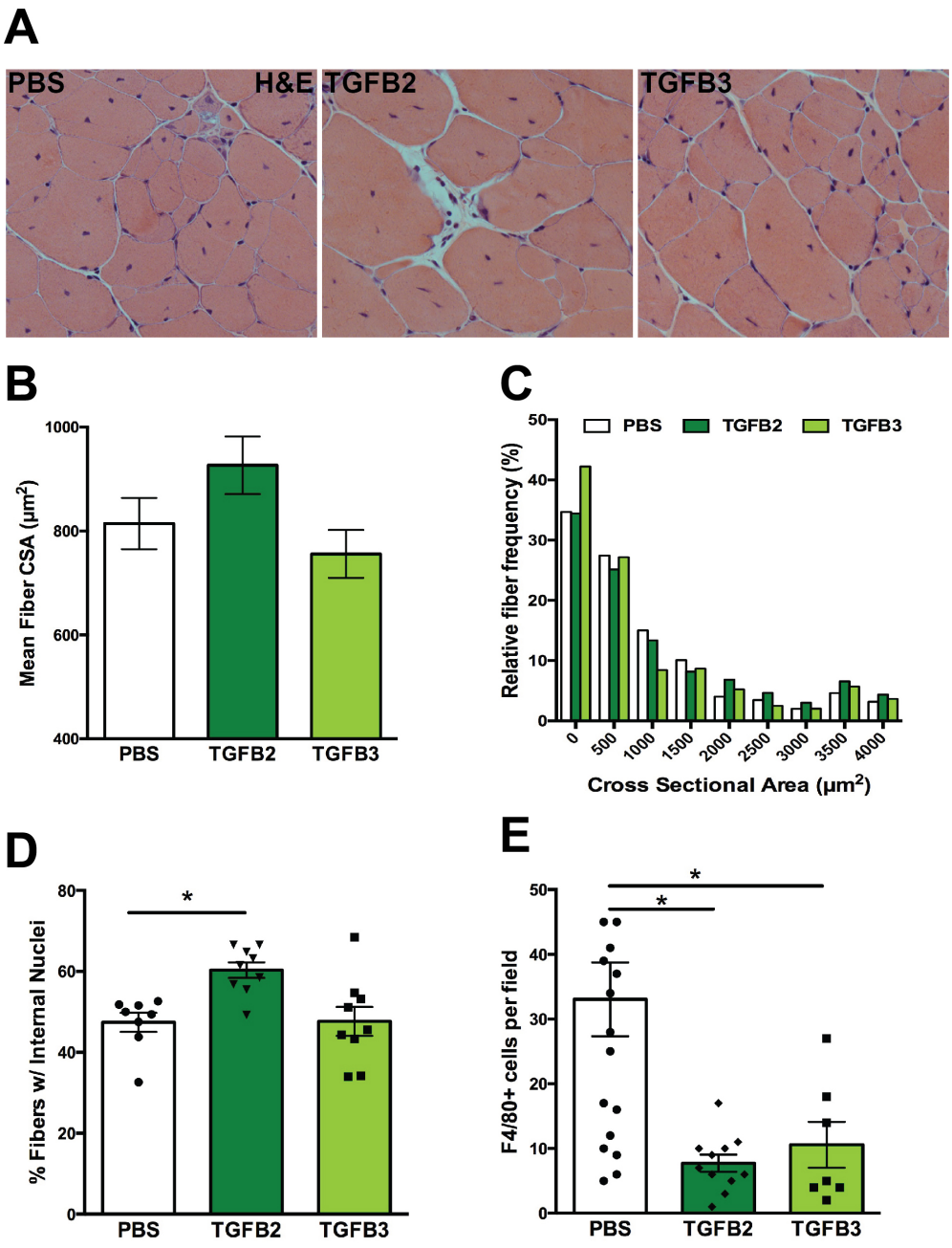

Figure 2.3 Anti-TGFβ antibodies reduce macrophage infiltration. A) Representative histology was used to visualize the inflammatory infiltrate, centralized nuclei, and mean myofiber cross-sectional area. **B)** Mean cross-sectional area (CSA) of triceps showed no difference between groups (n≥3 mice per group). **C)** anti-TGFβ2 and anti-TGFβ3 injections increased number of large myofibers and reduced medium sized myofibers compared to PBS. **D)** Triceps histology of anti-TGFβ2 injected mice had significantly more centralized nuclei compared to PBS via a one-way ANOVA (n≥3 per group, $P<0.02$). **E)** Both anti-TGFβ2 and anti-TGFβ3 injections both reduced F4/80 labeled macrophages when compared via a one-way ANOVA (n≥3 per group, $P<0.05$ for both).

condition, P<0.05). This is consistent with the improved pathological features noted with anti-TGFβ condition.

Dye uptake is influenced by TGFB neutralization.

Evans blue dye (EBD) is a vital tracer that is normally excluded from healthy myofibers (Heydemann et al., 2009). In many forms of muscular dystrophy, sarcolemmal defects allow for uptake of this dye into muscle reflecting a decrease in sarcolemmal integrity (Swaggart et al., 2014). **Figure 2.4A** shows representative images of dye uptake (red) into the triceps muscle where myofibers were outlined with Alexa-488 conjugated wheat germ agglutinin (WGA) (green). Both anti-TGFβ2 and anti-TGFβ3 injected muscles trended towards a reduction in dye uptake compared to PBS controls (**Figure 2.4B,** n≥4 mice per group). EBD can also be measured in the entire muscle using spectrophotometric methods. Anti-TGFβ3 was found to decrease gluteus/hamstring dye uptake significantly over PBS controls (0.32±0.6 abs/g compared to 0.47±0.2 abs/g) as measured by t-test **(Figure 2.4C,** P<0.05, n≥8 mice per condition).

Elevated serum creatine kinase (CK) is a hallmark of muscle injury in both mice and humans (De Luca, 2012). Raw and baseline normalized CK was analyzed at three time points for which serum was collected, day 0, day 20, and day 30. No significant differences in serum CK levels were found between groups at any time point. However, anti-TGFβ3 injected mice trended towards a reduction in serum CK levels after 30 days when normalized to CK levels present at day 0 (**Figure 2.4D,** n≥5 mice per condition). These data suggest that anti-TGFβ injection improved sarcolemma integrity resulting in reduced leak.

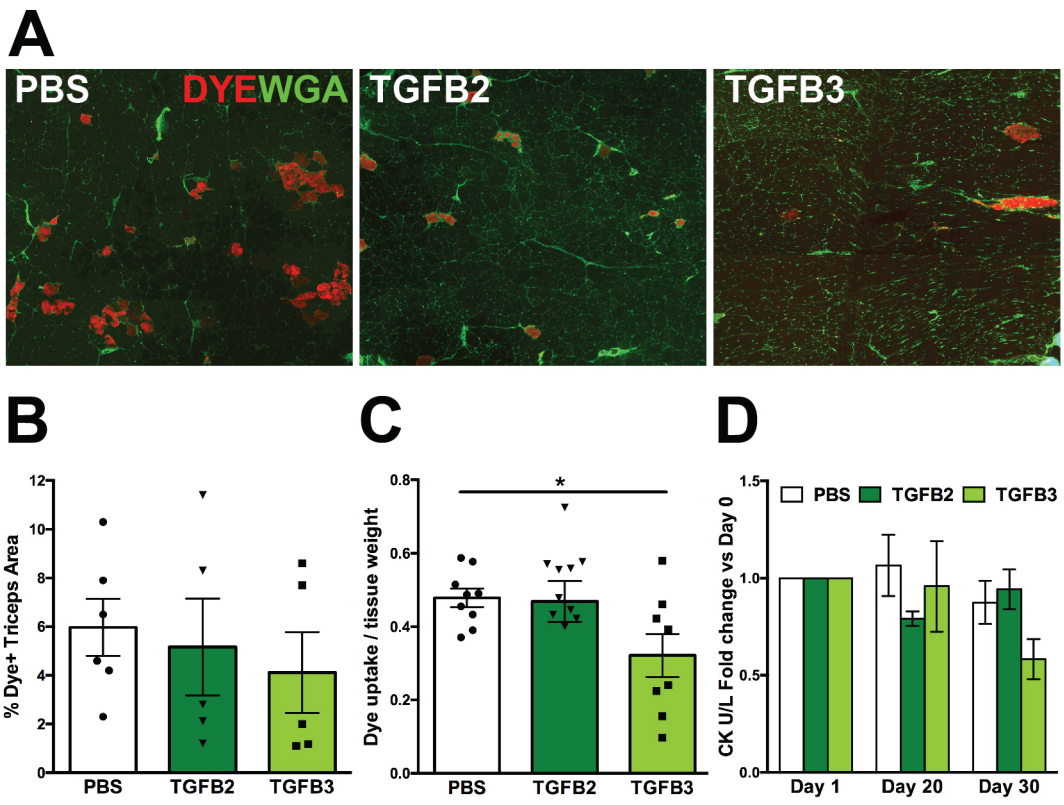

Figure 2.4 Improved sarcolemmal integrity after anti-TGFβ antibody injections. **A)** Immunofluorescence microscopy of representative images of triceps muscle from animals that were injected with Evans blue dye prior to sacrifice. Alexa-488 conjugated wheat germ agglutinin (WGA) was used to outline the boundaries of myofibers (green) while naturally fluorescent dye can be visualized as red cytoplasmic staining. **B)** Quantification of triceps dye shows a trend towards reduced dye uptake for both α-anti-TGFβ2 and anti-TGFβ3 injection when compared to PBS injection (n≥4 per condition). **C)** Colorimetric measurement of dye uptake in whole Gluteus/Hamstring muscle is significantly lower in the anti-TGFβ3 injected group ($P<0.05$, n≥8 mice per condition). **D)** All three groups show a non-significant decline in serum creatine kinase (CK) over the 30-day trial period with the largest reduction seen with anti-TGFβ3 injection.

Reduction in fibrosis with Anti-TGFβ2 and α-TGFβ3 injections.

Picrosirius red is a polyazo dye with high affinity for collagen used in histologic staining to highlight regions of extra-cellular matrix (ECM) connective tissue and fibrosis. In healthy muscle, the ECM is relatively thin and therefore contains low levels of picrosirius red on histology. Mid-belly muscle sections of quadriceps muscle were stained with picrosirius red and imaged to determine the fibrosis composition within the muscle **Figure 2.5A**. Significantly decreased levels of fibrosis occurred after anti-TGFβ2 injection, while anti-TGFβ3 injection resulted in a trend towards reduction when compared to PBS controls (9.1±1.9%, 12.8±1.0%, and 15.5± 3.0% respectively) (**Figure 2.5B,** $P<0.05$, $n\geq6$ mice per condition).

Hydroxyproline (HOP) is a modified amino acid found in collagen, and elevated HOP concentration is seen in dystrophic skeletal muscle (Heydemann et al., 2009). HOP content was quantified in the quadriceps, diaphragm and abdominal muscle groups. Anti-TGFβ3 injection reduced HOP content when compared to PBS (8097±1711 mM HOP/g versus 30532±5906 mM HOP/g, respectively) via a one-way ANOVA in the diaphragm muscle only (**Figure 2.5C,** $P<0.05$, $n\geq8$ mice per condition). In muscular dystrophy models, diaphragm muscle typically has markedly elevated levels of fibrosis compared to other muscle groups. HOP content in anti-TGFβ2 injected quadriceps muscle did not replicate the picrosirius red data when compared via simple t-test and ordinary one-way ANOVA likely due to increased sensitivity of the picrosirius red imaging assay (**Figure 2.5C**) (Lohcharoenkal et al., 2014; Smith and Barton, 2014). These data combined suggest that anti-TGFβ injections reduce fibrosis within skeletal muscle.

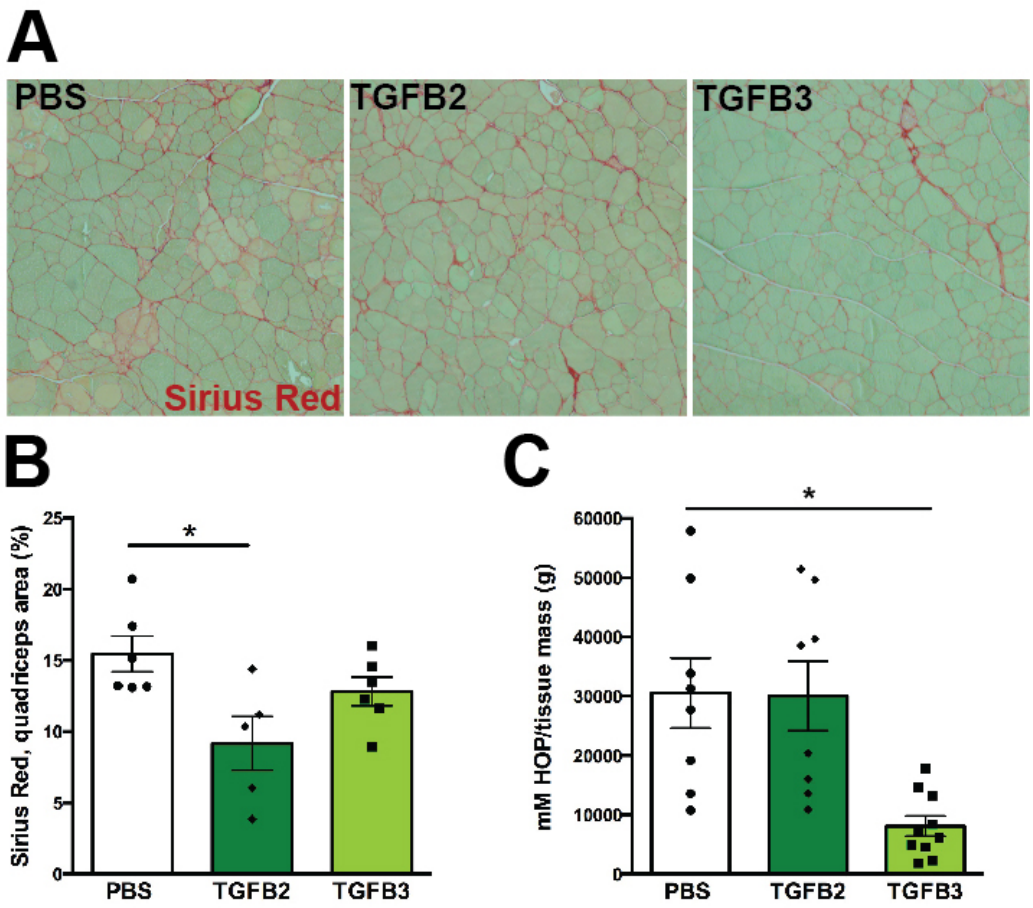

Figure 2.5 Anti-TGFβ2 antibody therapy reduced fibrosis in the quadriceps and diaphragm muscles. A) Representative images of picrosirius red stained quadriceps muscle. **B)** Whole mid-belly quadriceps images were analyzed for percent area of picrosirius red staining per total quadriceps area. Anti-TGFβ2 injection significantly reduced the amount of picrosirius red compared to PBS when analyzed via t-test ($n \geq 6$ for each condition, $P<0.05$). **C)** Diaphragm fibrosis measured by the less sensitive HOP quantitation assay showed that anti-TGFβ3 injection reduced HOP content compared to PBS via t-test ($n \geq 8$ per group, $P<0.05$).

Muscle strength and performance in α-TGFβ injected mice

To investigate the effect anti-TGFβ injections on muscle strength over time, *in vivo* grip strength was examined. Grip strength was measured on days 0, 7, 14, 21 and 28 of therapy and was observed to increase in all groups over time with respect to baseline (**Figure 2.6A**). The anti-TGFβ3 injected group showed the largest increase in strength normalized to body mass, while anti-TGFβ2 injection was not different from PBS injected controls at all time points analyzed. Despite this trend, there were no significant differences observed between any groups when raw values and baseline adjust values are analyzed via matched repeated measures two-way ANOVA. When baseline adjusted data is subjected to t-test between groups and PBS, the anti-TGFβ3 group showed significantly increased grip strength at day 7 and day 14 ($P<0.05$). This improvement was not significance at the subsequent time points ($P=0.27$ and $P=0.94$ respectively).

Ex vivo muscle mechanics of the EDL muscle showed that anti-TGFβ-3 injections improved the percentage force decrease during eccentric contraction compared to PBS injection using a simple t-test (39.4±5.9% compared to 64.0±5.1%, respectively) (**Figure 2.6B,** $P<0.05$, $n\geq4$ mice per condition). Anti-TGFβ-3 injections trended towards improved percentage force decrease while undergoing eccentric contraction compared to PBS (50.4±3.9, $P<0.07$). Other measures of muscle force, including twitch and tetanic specific force, were not significantly improved compared to PBS control with either anti-TGFβ injections (**Figure 2.6C and 2.6D,** $n\geq7$ muscles per condition). These data suggest that anti-TGFβ-3 injection protected myofibers against contraction-induced injury.

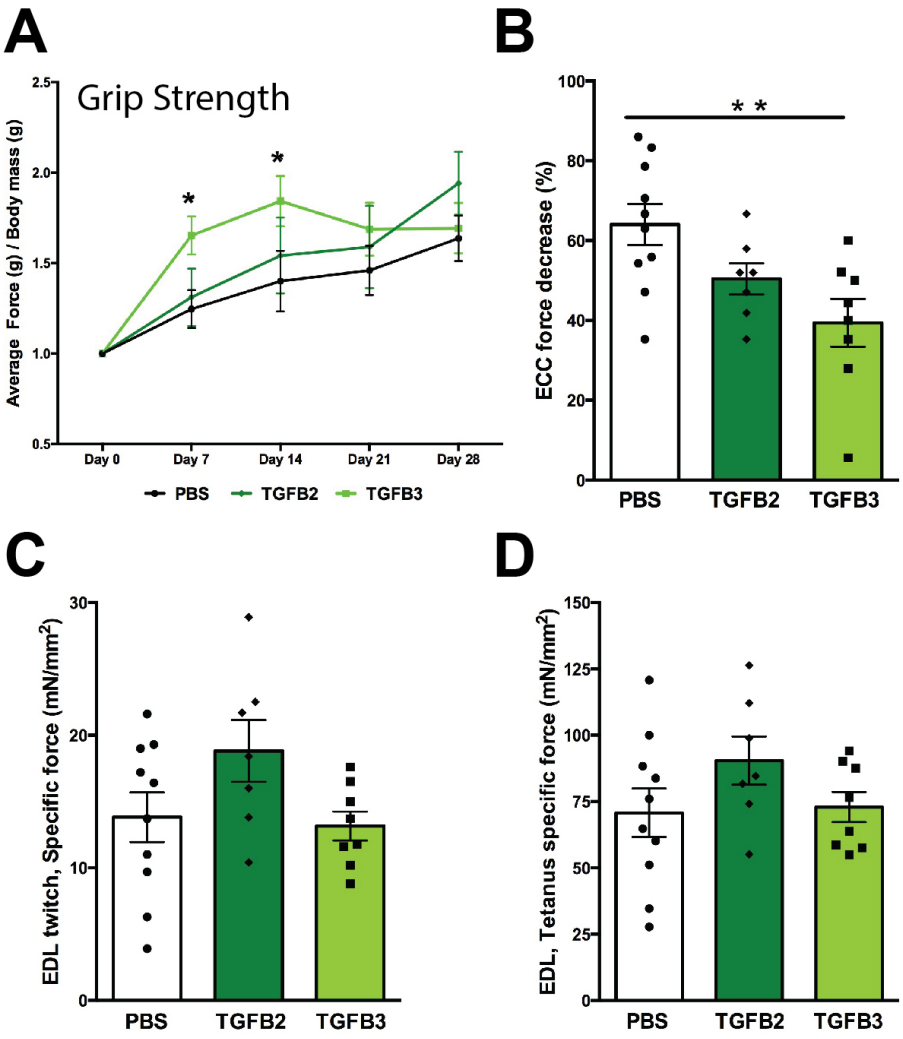

Figure 2.6 Anti-TGFβ3 antibodies preserve muscle function in response to eccentric contraction. A) Mean grip strength normalized to body mass over time reveals a general increase in strength over time across all conditions although the protocol. There were no significant differences via repeated measures 2-way ANOVA. When baseline normalized and raw values are analyzed via one-way ANOVA per each time point, only the anti-TGFβ3 group showed a significant difference compared to PBS and only at day 7 and 14 ($n \geq 10$ per group at each time-point, Day 7 $P<0.05$, Day 14 $P<0.05$). **B)** Anti-TGFβ3 injected EDL muscle has a significantly smaller reduction in force than PBS injected controls in response to repeated eccentric contractile injury ($n \geq 7$ muscles per group, $P<0.05$). **C and D)** Anti-TGFβ2 injected mice trended towards higher twitch (left) and tetanic (right) force than PBS injected animals, but this result was not significantly higher via ordinary one-way ANOVA or t-test.

Effect of α-TGFβ injection on cardiac function

Cardiac decline in muscular dystrophy has been characterized in both human disease and mouse models using imaging modalities (De Luca, 2012; Gardner et al., 2015). Echocardiography was performed at days 0 and 28 and analyzed for measures of left ventricular fractional shortening (LVFS), pulmonary artery flow, mitral valve function and quality of flow through the pulmonary artery. Only the anti-TGFβ3 injection group (26.1±1.0%) showed improved LVFS when compared to the PBS injected group (22.6±1.05%) at day 28 (**Figure 2.7A,** n≥11 mice per condition). No significant differences in LVFS were found between any groups at day 0 using a one-way ANOVA or over time with a repeated measures two-way ANOVA (**Table 2.2**).

The anti-TGFβ-3 injected group trended towards a reduction in left ventricular internal dimensions in diastole (LVIDd) on day 28 compared to the PBS injected group, with a mean value of 3.9 ± 0.05 mm compared to a 4.05±0.05mm (**Figure 2.7B,** n≥9 mice per condition). There was no significant difference in LVIDs (systole) with anti-TGFβ2 (3.04±0.08 mm) or anti-TGFβ3 (2.97±0.06mm) injection compared to the PBS (3.14±0.08mm) injected group (**Figure 2.7C,** n≥11 mice per condition). No significant differences in LVIDd or LVIDs were found between any groups at day 0 via a one-way ANOVA nor between any groups over time with repeated measures two-way ANOVA.

Pulmonary artery velocity time integral (PA VTI) is a Doppler interrogation of blood flow in the pulmonary artery (PA) and is an indirect measure of right ventricular function (RV) and stroke volume. The anti-TGFβ3 injected group showed increased PA VTI on day 28 compared to the PBS injected group, with a mean value of 25.4±1.0cm^2 compared to a 20.7±1.2cm^2 (**Figure 2.7C,** n≥9 mice per condition). Pulmonary artery

acceleration time (PAAT) measures the time for flow to reach its maximum velocity in the PA. Decreased PAAT values have been positively correlated with higher PA pressures in mice as both values are affected by the compliance of the PA and its distal pulmonary circuitry (Thibault et al., 2010). No significant differences were seen between groups at day 28 via a one-way ANOVA or over time when compared via repeated measures 2-way ANOVA.

Flow through the mitral valve (MV) was measured and the ratio between maximum velocity during early passive ventricular filling (E) and maximum velocity during atrial kick (A) was calculated and analyzed for as many mice as time would permit ($n \geq 5$ for each group and time-point). A higher MV E/A is indicative of healthy passive ventricular diastolic filling (Jearawiriyapaisarn et al., 2010). Only the anti-TGFβ3 injected group trended towards improvement of MV E/A at day 28 with a 1.9±0.2 increase compared to 1.4±0.2 and 1.3±0.25 seen with anti-TGFβ2 and PBS injections, respectively (**Figure 2.7F**). Despite the improvement seen with anti-TGFβ3 injection, there was no significant difference compared to PBS injected animals when measured via repeated measures 2-way ANOVA. This lack of significance can be attributed to the large standard deviation and n seen in both groups. Additionally, no group was significantly different than PBS at day 0 when measured via a one-way ANOVA. Combined, the echocardiography data suggest that anti-TGFβ2 injection performed similarly to PBS while anti-TGFβ3 injections showed improved flow patterns for both left and right ventricular function.

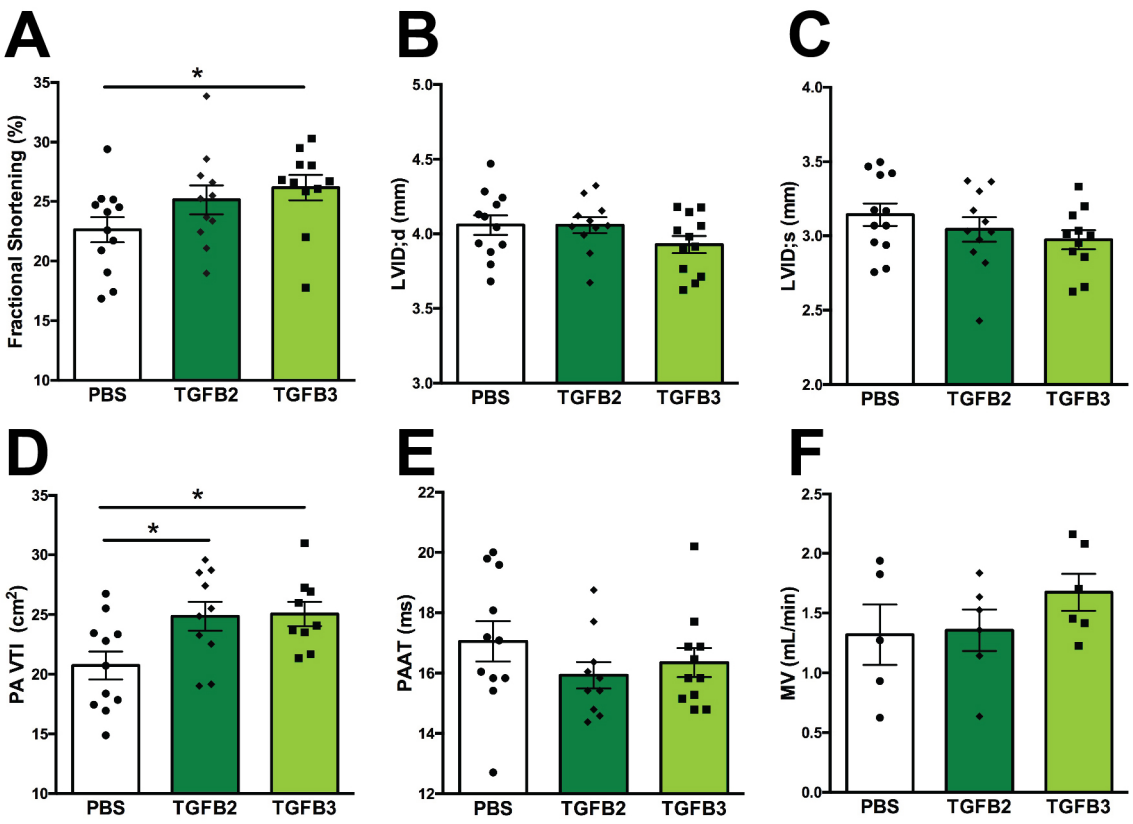

Figure 2.6 Anti-TGFβ antibody effect on cardiac function. A) Mean fractional shortening (FS) was increased in the anti-TGFβ3 injected group after 28-days compared to the PBS group (P<0.05). **B & C)** LVIDd and LVIDs trended towards reduction in the anti-TGFβ3 injected group compared to PBS injected group, although this was not signficant. **D)** Pulmonary artery velocity time integral (PA VTI) increased in both the anti-TGFβ2 and anti-TGFβ3 injected groups when compared to PBS injection via t-test on day 28 (both P<0.05). **E)** Pulmonary artery acceleration time (PAAT) was not significant between groups at day 28. **F)** Mitral valve E/A ratio shows a non-significant increase in anti-TGFβ3 injected animals compared to PBS injected animals.

Table 2.7. Anti-TGFB effects on cardiac function.

	PBS		TGFB2		TGFB3	
Echo parameter	Day 0	Day 28	Day 0	Day 28	Day 0	Day 28
FS (%)						
Mean ± SEM	26.7 ± 1.45	22.6 ± 1.05	28.3 ± 1.6	25.1 ± 1.2	24.7 ± 0.6	**26.1 ± 1.0***
N=	9	12	9	11	10	11
LVID;d						
Mean ± SEM	3.98 ± 0.1	4.1 ± 0.06	4.03 ± 0.05	4.05 ± 0.05	3.9 ± 0.06	3.9 ± 0.05
N=	9	12	9	11	11	12
LVID;s						
Mean ± SEM	2.91 ± 0.1	3.14 ± 0.08	2.94 ± 0.1	3.04 ± 0.08	2.99 ± 0.06	2.97 ± 0.06
N=	9	12	9	11	11	11
PA VTI (cm^2)						
Mean ± SEM	25.6 ± 1.6	20.7 ± 1.2	27.6 ± 1.4	**24.9 ± 1.2***	20.2 ± 0.7	**25.4 ± 1.0***
N=	6	11	9	10	10	9
PAAT (ms)						
Mean ± SEM	18.5 ± 1.6	17.1 ± 0.7	17.44 ± 0.9	15.9 ± 0.4	16.9 ± 1.1	16.3 ± 0.5
N=	6	11	9	10	9	11
M/V (cm^2/cm^2)						
Mean ± SEM	2.0 ± 0.22	1.3 ± 0.25	1.9 ± 0.2	1.4 ± 0.2	1.5 ± 0.3	1.9 ± 0.2
N=	8	5	8	6	6	8

DISCUSSION

Differential expression of TGFβ isoforms in muscle.

Dysregulation of TGFβ is a feature of DMD, first observed in human and mouse muscles (Bernasconi et al., 1995; Chen et al., 2005). These early studies focused heavily on *TGFB1*, noting its upregulation in dystrophic muscle and specifically correlating the increase of *TGFB1* with fibrosis. In a larger study of many different types of muscular dystrophy, a TGFβ centered network was a common "node" of gene dysregulation in multiple forms of muscle disease (Dadgar et al., 2014). In this light, it is interesting to note that in normal mouse muscle that *Tgfb1* contributes relatively little to the total TGFβ pool. In wildtype mouse muscle, we observed that *Tgfb3* is expressed at higher levels than *Tgfb2* and especially *Tgfb1*, which contribute relatively little to the total TGFβ pool. While numerous groups have reported the increase of TGFβ1 in dystrophic muscle, including the Nelson study that used quantitative PCR to measure a 3-4 fold upregulation of *Tgfb1* mRNA in quadriceps, gastrocnemius and triceps (Nelson et al., 2011a). This group also noted an induction of *Tgfb3*. Whether this relative increase of TGFβ in muscular dystrophy is compensatory to, or causative of dysfunction is still unknown. However, each of these studies focused on that upregulation rather than total TGFβ pool, which contains significant amounts of TGFβ-2 and TGFβ-3. It was because of the contribution of TGFβ-2 and TGFβ-3 that we elected to test TGFβ isoform specific neutralizing antibodies in a murine model of muscular dystrophy.

Anti-TGFβ3 antibody injection improved inflammation and sarcolemmal leak.

Neutralizing antibodies to TGFβ3 were found to reduce macrophage inflammation, reduce Evans blue dye uptake and diaphragm muscle collagen content and protect against eccentric contraction. These data suggest an effect on stabilizing the sarcolemma, and this was also reflected in the trend towards a reduction in serum CK. Importantly, anti-TGFβ3 antibody replicated two specific findings seen previously in the study that used the pan-TGFβ 1D11 antibody in the *mdx* mouse model (Nelson et al., 2011a). Both 1D11 and anti-TGFβ-3 showed significantly reduced fibrosis in the diaphragm muscle as measured by HOP content, a reflection of collagen content. The diaphragm muscle is known to be one of the most severely affected muscles in the *mdx* model, and is often considered more reflective of what is seen in human DMD (Stedman et al., 1991). It is possible that a significant fibrosis burden must be present in order to see a decrease, and this burden may only be adequately present in the diaphragm muscle in this model of muscular dystrophy. Additionally, both antibodies produced significant increases in grip strength over time, although the anti-TGFβ3 antibody did so only transiently. We did not assess whether any neutralization of the antibodies occurred over time, and this could account for loss of activity of the non-species matched antibody. Longer term studies with species specific antibodies would help resolve this question.

Anti-TGFβ2 antibodies reduced inflammation and increased central nuclei, a marker of regeneration.

Overall, the anti-TGFβ2 antibody showed few differences in many assays of muscle degeneration and muscle function. Both the anti-TGFβ2 and anti-TGFβ3 injected groups shared a significantly reduced activated macrophage content compared to PBS, suggesting a role for both isoforms in the recruitment of inflammatory infiltrate. Macrophage infiltration in muscle has a complex role in muscular dystrophy and many injury states since macrophages can be both beneficial and deleterious depending on subtype (Kharraz et al., 2013). Further subtyping macrophages could shed more light on the function of macrophage reduction after TGFβ inhibition. The anti-TGFβ2 antibody significantly reduced fibrosis in the quadriceps muscle as measured by picrosirius red staining on histology, but was not shown to increase fibrosis in the quadriceps based on HOP assay. This discrepancy is likely due to increased sensitivity of the sirius red assay, but could also be due to a different fibrotic makeup between muscles.

These data combined suggest that TGFβ2 and TGFβ3 play different roles with TGFβ3 perhaps playing a more essential role in the stability of muscle membranes and TGFβ2 being more important for regeneration. Muscle regenerates from an endogenous stem cell pool, referred to as the satellite cells (Chang and Rudnicki, 2014; Cheung and Rando, 2013). In muscular dystrophy, satellite cells are redirected by a Wnt3A and TGFβ2 pathway into fibrogenesis (Biressi et al., 2014). This redirection of myogenesis is thought to amplify the fibrotic response and explain the exhaustion of the stem cell pool in muscular dystrophy.

Limitations and future directions

Most parameters measured after four weeks of antibody injections showed relatively few deleterious outcomes, indicating that neutralizing TGFβ2 or TGFβ3, did not dramatically adversely affect muscle function. Although four mice died during the course of the study, all deaths were due to traumatic procedures and not the antibody content as PBS injected animals died similarly. Despite being well tolerated, the overall effect of isoform specific TGFβ neutralization was relatively modest for most parameters measured. The relatively minimal effect could be anticipated since the study used a short term dosing design. Muscular dystrophy is a chronic disease and longer term exposure is needed. Additionally, these studies were carried out in animals with established disease and it may be necessary to start TGFβ neutralization earlier in the course of disease similar to what was done in the Nelson study (Nelson et al., 2011a). The Nelson study importantly showed benefit on a number of functional and histological measures, and the degree to which this effect was due to specific TGFβ isoforms is not known. The 1D11 antibody does not react equally to TGFβ isoforms (Zwaagstra et al., 2012). Our study lacked an anti-TGFβ1 antibody arm, whereas the 1D11 antibody neutralizes TGFβ1 in addition to its effects on TGFβ2 and TGFβ3. Thus, while a number of outcomes were suggestive of improvement in this short-term study, and anti-TGFβ3 antibodies showed more benefit than anti-TGFβ2 antibodies, longer term studies with species-matched antibodies are needed.

Chapter 3

Anti-LTBP4 antibody injection and its effect on muscular dystrophy

ABSTRACT

Muscular dystrophy is a chronic degenerative disease of muscle characterized by elevated TGFβ levels. Genetic variants in *LTBP4*, a TGFβ binding protein that confers its latency and localization to the extra-cellular matrix, modifies muscular dystrophy and other disease processes. Specifically, mice and humans with muscular dystrophy with the protective LTBP4 alleles display decreased TGFβ activation and improved outcomes. Previous studies examined the role of a neutralizing TGFβ antibody in the *mdx* model of Duchenne Muscular Dystrophy. The neutralizing TGFβ antibody reacts variably with multiple TGFβ isoforms. To assess the degree to which TGFβ can be limited at an earlier upstream point, we administered two different rabbit polyclonal antibodies raised against the same region of LTBP4 important in TGFβ activation. We conducted a short-term four-week study of once weekly intraperitoneal anti-LTBP4 antibody injections and assessed histological and functional readouts of muscle disease and function. We found that even short-term exposure to anti-LTBP4 neutralizing antibody improved measures of regenerative capacity and reduced features of muscle membrane instability and dysfunction. Reduced macrophage infiltration in muscle was observed after LTBP4 antibody exposure and one antibody trended towards improved

cardiac function. Together these data identify that LTBP4 specific antibodies may be useful to mitigate TGFβ hyperactivation in muscular dystrophy.

RESPECTIVE CONTRIBUTIONS

This work was conducted with the generous collaboration and mentorship of Dr. Alexis Demonbreun. Two technicians, Mr. James Warner and Patrick Page, also contributed significantly to the execution of these experiments. They are responsible for some or all of the data associated with measuring dye uptake, muscle mass, serum creatine kinase levels, internal nuclei number, fiber cross-sectional area and immunohistochemical quantification data. Patrick Page additionally assisted me with the collection of grip strength, preparation of antibody injections, organization of notes and records. Mr. Andy Vo analyzed the RNA sequencing data. Dr. Sasha Bogdanovich and I together acquired ex-vivo muscle mechanical data, and Dr. Bogdanovich analyzed the Sirius Red staining. Dr. Bogdanovich helped edit related sections of this Chapter. Ms. Judy Early prepared paraffin-embedded histologic sections while James Warner and I acquired the microscopic images. Mrs. Michelle Hadhazy conducted whole-body plethysmography, general animal care, serum collection and administered the majority of intraperitoneal injections of antibody preparations. I conducted and collected echocardiography, fiber cross-sectional area, determined hydroxyproline content in addition to analyzing these data and editing the manuscript. Dr. Alexis Demonbreun generated figures and edited the Chapter. Dr. Elizabeth McNally conceived the experiments, contributed to data analysis and edited this Chapter. Figure 3.1 is reproduced from Ceco E, Bodganovich S, Gardner BB, Miller T, DeJesus A, Earley JU,

Hadhazy M, Smith LR, Barton ER, Molkentin JD, McNally EM. Targeting latent TGFβ release in muscular dystrophy. (2014) Science Translational Medicine 6(259):259ra144. PMCID 4337885. I conducted the experiments in Figure 3.1A.

INTRODUCTION

In Duchenne muscular dystrophy (DMD), the loss of dystrophin weakens the sarcolemma of muscles rendering them susceptible to contraction-induced damage. Mutations in the dystrophin-associated proteins, the sarcoglycans, lead to a similar weakened sarcolemma and myofiber injury. A genomewide scan for modifiers of muscular dystrophy in mice identified the *Ltbp4* gene, encoding latent TGFβ binding protein 4, as an important determinant of sarcolemma fragility and fibrosis (Heydemann et al., 2009). In humans with DMD, polymorphisms in the *LTBP4* gene were shown to correlate with extended ambulation in DMD patients and reduced TGFβ signaling (Bello et al., 2015; Flanigan et al., 2013; van den Bergen et al., 2015).

LTBP4 encodes an extracellular matrix-associated protein and is highly expressed in skeletal muscle. LTBPs are anchored to extracellular matrix fibrils through the N-terminus, whereas the C-terminus binds to latent TGFβ to form a large latent complex (Chen et al., 2005; Saharinen and Keski-Oja, 2000; Sinha et al., 1998). A proline-rich hinge domain separating the N- and C-terminal domains is the target of proteolysis, and this cleavage is associated with latent TGFβ release and activation (Dallas et al., 2002; Ge and Greenspan, 2006; Hyytiainen et al., 1998; Taipale et al., 1992). TGFβ activity regulates injury and repair in muscle, kidney, lung, heart and brain (Chin et al., 2001; Kane et al., 1991; Karonen et al., 1997; Lin et al., 1995; Schiller et al.,

2004). TGFβ activity is triggered in both chronic and acute muscle injury (Kane et al., 1991; Leask and Abraham, 2004). TGFβ1 mRNA levels are elevated in human DMD (Bernasconi et al., 1995; Chen et al., 2005; Gosselin et al., 2004), and systemic administration of neutralizing TGFβ antibody or the angiotensin II type 1 receptor blocker losartan helps to normalize muscle architecture, repair and function in the mdx mouse model of DMD, suggesting a direct role for excessive TGFβ signaling in muscle disease (Cohn et al., 2007a; Nelson et al., 2011a).

The modifier polymorphism in murine *Ltbp4* encodes a deletion or insertion of 12 amino acids within LTBP4's hinge region (Heydemann et al., 2009). The *Ltbp4* allele with the smaller hinge is more susceptible to proteolysis and is associated with increased release of latent TGFβ and TGFβ signaling (Heydemann et al., 2009). Because human LTBP4 has an even smaller hinge, human LTBP4 is predicted to release more latent TGFβ. We found that the human LTBP4 hinge was more readily proteolyzed than the murine LTBP4 hinge (Ceco et al., 2014). Further, an antibody that blocked proteolytic cleavage of LTBP4 demonstrated that the proline-rich hinge is the site of proteolysis. The human *LTBP4* gene was inserted into *mdx* mice using a bacterial artificial chromosome (BAC). *Mdx* mice with the human *LTBP4* BAC showed increased muscle membrane leakage and fibrosis. Furthermore, the presence of the human *LTBP4* gene was associated with weaker muscles, greater infiltration of muscles by macrophages and increased TGFβ signaling.

Because these data identify cleavage of LTBP4 as a potential target for treating muscular dystrophy and provide a biological strategy for regulating TGFβ release, we

now conducted a four-week study using the anti-LTBP4 antibodies in the hLTBP4/mdx model of muscular dystrophy.

MATERIALS AND METHODS

Animal use and care

The *mdx/hLTBP4* BAC mice used in these experiments were generated as previously described (Ceco et al., 2014). Mice were cared for and housed as described in Chapter 2 in a manner consistent with standards approved by Northwestern's Institutional Animal Care and Use Committee (IACUC).

Antibody generation

The proline-rich 19 amino acid sequences EPRPEPRPDPRPGPELPLPC and EPRPEPRPDPRPGPELPC were conjugated to KLH and used as antigens in rabbits (Pocono Animal Farms). Two different antibodies were raised to the same LTBP4 sequence, designated 28199 and 28200. Affinity purification was carried out against the peptide antigen by Pocono Rabbit Farms.

Intraperitoneal injection and antibody preparation

Mice were injected once a week via intraperitoneal injection in a similar regimen and protocol as chapter 2 with the exception of dosing. On injection days, stock solutions stored at -80°C were diluted into sterile Eppendorf tubes containing sterile phosphate buffered saline (PBS) (Invitrogen, 14-829-1A) at a concentration of 5mg/kg according to the mass of each mouse the previous morning. The total volume injected did not exceed 190μl per individual injection.

Immunofluorescence microscopy

Seven µm sections from the triceps muscle were fixed and processed as previously described in chapter 2 methods prior to incubation with either anti–pSmad2/3 antibodies (pSMAD2/3, Abcam, ab51451) or anti- F4/80 conjugated to Alexa-488 (ab6640, Abcam, Cambridge, MA). Imaging was performed using a Zeiss Axio Imager.M2 microscope using a 20 X objective.

All other analyses were carried out identically to that described in Chapter 2.

LTBP4 isoforms are expressed differentially in striated muscle.

LTBP4 was identified as a modifier of limb girdle muscular dystrophy in both mice and humans and is associated with decreased membrane stability and increased pathology (Flanigan et al., 2013; Heydemann et al., 2005). RNA sequencing of wildtype DBA/2J (WT^{D2}) and dystrophic ($Sgcg^{D2}$) abdominal and quadriceps muscle and left ventricle revealed varied expression levels of *Ltbp* isoforms 1 through 4 **(Table 3.1)**. *Ltbp2 and Ltbp4* were induced in dystrophic muscle. *Ltbp4* expression comprises the majority of the *Ltbp* pool present in skeletal muscle.

Table 3.1 Relative level of expression of *Ltbp4* isoforms in normal and dystrophic muscle and heart as determine by RNA sequencing.

	Abdominal muscles		***Quadriceps muscles***		***Left ventricle***	
	WT^{D2}	***$Sgcg^{D2}$***	***WT^{D2}***	***$Sgcg^{D2}$***	***WT^{D2}***	***$Sgcg^{D2}$***
Ltbp1	32.62	54.27	36.84	50.07	112.33	108.85
Ltbp2	4.54	36.69	2.89	93.02	11.45	10.36
Ltbp3	155.32	173.94	148.46	291.56	102.97	113.16
Ltbp4	509.13	735.59	445.61	803.60	1256.11	1427.72

RNA sequencing was performed from DBA/2J (WT^{D2}) wildtype mice and *Sgcg* null mice in the DBA/2J background ($Sgcg^{D2}$). Values are expressed as FKPM (fragment per kilobase per million X10).

LTBP4 is organized in a striated pattern around muscle fibers.

Ltbp4 was identified as a modifier of muscular dystrophy in mice from an unbiased genomewide screen where it strongly associated with increased membrane fragility and fibrosis (Heydemann et al., 2009). We examined LTBP4's pattern of protein expression using anti-LTBP4 antibodies and confocal microscopy. Two distinct extracellular pools of LTBP4 were seen using four different anti-LTBP4 antibodies. One pool of LTBP4 protein was parallel to the long axis of myofibers, and a second pool was observed closely apposed to the sarcolemma in a striated pattern in muscle (**Figure 3.1A**). The LTBP4 localized near the sarcolemma was in a striated pattern. This pattern reflected an organized matrix immediately surrounding muscle fibers and suggested that LTBP4 is positioned to stabilize the myofiber**.**

The hinge region of human LTBP4 is a target of serine proteases.

The insertion/deletion polymorphism that modifies muscular dystrophy in mice alters the proline rich region (PRR) of LTBP4 by 12 amino acids. The shorter PRR hinge was associated with greater LTBP4 proteolytic susceptibility, increased TGFβ signaling, and worsening of muscular dystrophy (Heydemann et al., 2009). The exacerbated muscle membrane fragility and muscle fibrosis seen with a shorter PRR hinge was associated with decreased grip strength (Heydemann et al., 2009). Human LTBP4 has a smaller LTBP4 hinge region compared to the murine LTBP4 sequence (**Figure 3.1B**). The canine LTBP4 hinge is also small, and it is notable that DMD mutations in these two

species cause severe disease that is associated with accelerated loss of ambulation (Sharp et al., 1992; Vainzof et al., 2008; Worton et al., 1988).

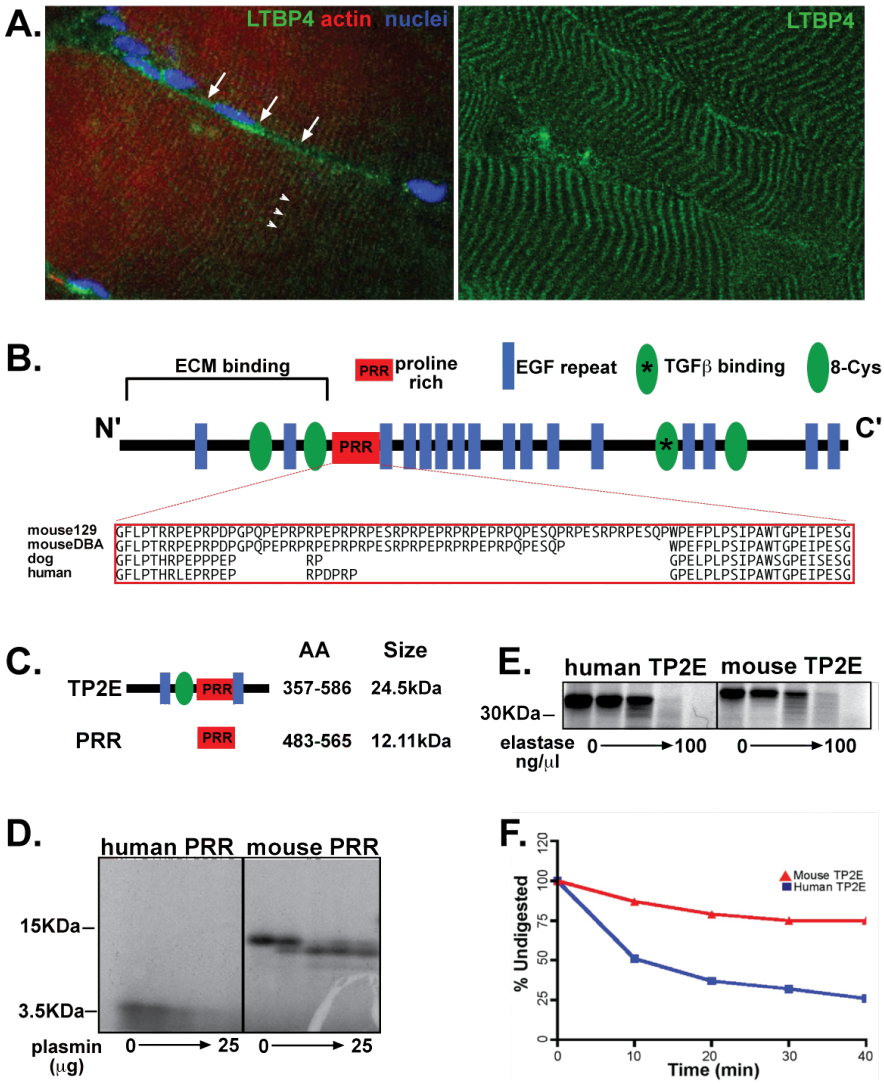

Figure 3.1 LTBP4 has a striated pattern in muscle. A) Individual muscle fibers were isolated from murine muscle and stained with multiple antibodies to LTBP4. Longitudinal muscle fibers have two pools of LTBP4 protein, which run parallel (white arrows) and perpendicular (white arrow heads) to the long axis of the muscle. The perpendicular or costameric LTBP4 is closely apposed to the muscle membrane (white arrows). The right panel shows the costameric LTBP4 pattern in striated muscle. **B)** Mice have an insertion/deletion polymorphism that alters the proline-rich region (PRR) of LTBP4. The majority of mouse strains carries the insertion allele shared by the 129T2/SvEmsJ strain (129), while a minority of mouse strains shares the deletion seen in the DBA/2J strain (D2). This polymorphism regulates the severity of muscular dystrophy in mice and alters proteolytic cleavage of LTBP4, a process that is linked to TGFβ release and signaling. Human LTBP4 has a smaller PRR hinge compared to murine LTBP4. **C)** Fragments containing either human or murine LTBP4 PRR hinge were expressed in vitro and digested with either plasmin (**D**) or elastase (**E**), two serine proteases know to cleave LTBPs. Human LTBP4 was more readily digested compared to murine PRR (**F**).

RESULTS

To test whether human LTBP4 protein was more susceptible to proteolytic cleavage than murine LTBP4, the PRR hinge from LTBP4 was expressed in vitro and digested with serine proteases. With increasing concentrations of plasmin, the human LTBP4 PRR hinge was rapidly digested whereas the murine PRR hinge was comparatively resistant to plasmin treatment (**Figure 3.1D**). A larger fragment of LTBP4 containing the PRR and flanked by an 8 cysteine repeat and two EGF motifs was similarly rapidly digested compared to the comparable murine LTBP4 sequence and results were similar for plasmin and elastase (**Figure 3.1D, E**) (Ceco et al., 2014), two serine protease family members that have been shown to cleave LTBPs in vitro (Flaumenhaft et al., 1993; Koli et al., 2001; Saharinen et al., 1998).

Pre-clinical trial protocol

The *mdx/h*LTBP4 mouse, which carries the human LTBP4 gene was used in these studies (Ceco et al., 2014). Thirty-six male *mdx/hLTBP4* BAC mice were divided into three groups of 12 to minimize differences in both body mass and age among groups (**Table 3.2**). At day 0, body mass was 28.1±0.7 g, 25.9±0.7 g and 26.5±0.7 g for the groups designated to receive PBS, 28199 and 28200, respectively. The mean age for all groups at day 0 was 70.5, 61.0 and 71.4 days respectively, with no significant difference found between groups based on mass or birthdate via ordinary one-way ANOVA. Although all groups began with twelve animals, premature death of three mice during the initial trial period lead to final n values of 12, 10, and 11 for PBS, 28199 and 28200 respectively. Additional mice were added to augment the loss of animals due to death in each cohort.

Table 3.2 Cohorts for preclinical assessment of anti-LTBP4 antibodies.

	Day1		Day 30	
	body mass (g)	**age (Days)**	**body mass (g)**	**age (Days)**
PBS	28.1	70.5	30.7	100.3
28199	25.9	61	29.9	92
28200	26.5	71.4	28.3	103.8

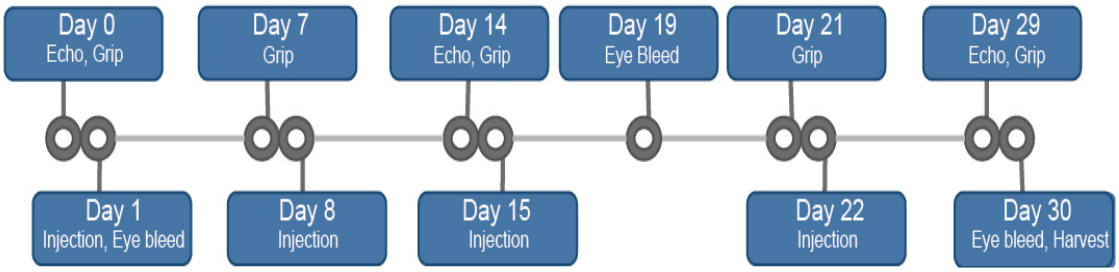

Figure 3.2 Pre-clinical trial design and timeline for α-LTBP4 antibody testing. Above is a time-line representing the *in vivo* phenotyping and injection schedule of the 30-day pre-clinical protocol.

Anti-LTBP4 antibody injections did not affect overall body mass but increased lower body hind limb mass in mdx/hLTBP4 BAC mice.

To investigate changes in growth, body mass was measured at days 0, 7, 14, 21, and 28. The average increase in body mass for PBS, 28199, and 28200 injected groups was 2.5g, 3.9g, and 1.8g over the 30-day protocol for an average increase of 9.4±1.7%, 13.8±1.2%, and 6.0±1.4% over baseline, respectively (n≥10 mice per condition). This increase was slightly higher than the 3-6% mean increase seen for *mdx* mice increase (Latres et al., 2015). No differences were seen between any conditions in body mass **(Figure 3.3A)** or body mass/tibia length **(Figure 3.3B)** at any time point when groups were compared via ordinary one-way ANOVA within each time point. A matched repeated-measures 2-way ANOVA to investigate group effect over time did not reveal any significant affect of α-LTBP4 therapy over time.

Differences in whole muscle mass have been shown to be indicative of therapeutic response in muscular dystrophy models (Bogdanovich et al., 2002; Wagner et al., 2002). All muscles were excised and weighed prior to processing and compared for differences. The 28200 antibody group did not show any difference compared to PBS in any muscle group for raw or tibia-length normalized muscle mass. In contrast, the 28199 antibody group increased mass in both the quadriceps and gluteus/hamstring muscles normalized to tibia length (quadriceps, 0.015±0.002 g/mm, glut/ham=0.026±0.001) compared to PBS group (quadriceps 0.013±0.0005 g/mm, glut/ham=0.021±0.001) (**Figures 3.3C and 3.3D,** n≥9 muscles per condition, $P<0.05$ for both muscle groups, one-way ANOVA). These data suggest α-LTBP4 antibody

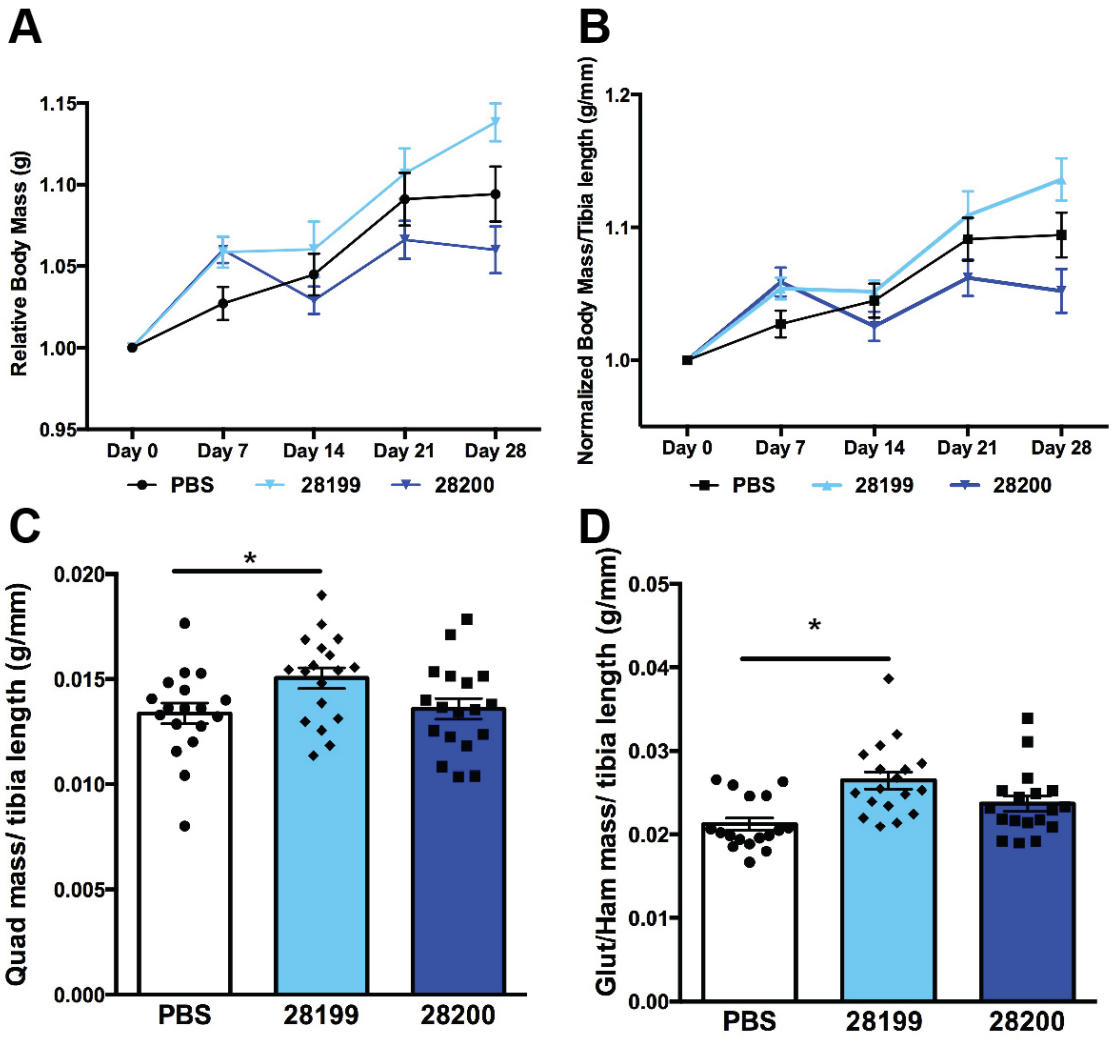

Figure 3.3 Body mass was unaffected by LTBP4 antibody injection and may additionally preserve hind-limb muscle mass. Body mass was collected the day prior to initial injection (day 0) and at four subsequent time-points prior to sacrifice. **A)** Mean raw body mass did not differ between groups at baseline, nor at any time point thereafter when compared by ordinary one-way ANOVA (n≥10 mice per group at each time point). **B)** Body mass normalized to tibia length was analyzed similarly to raw body mass in 3.3A and no differences were found between groups at baseline, nor any time point thereafter. **C)** The 28199 antibody injected quadriceps muscle weight was found to be significantly higher compared to PBS-injected muscle weight via ordinary one-way ANOVA (n≥17 muscles per group, $P<0.05$) when all excised muscle mass was analyzed for differences in raw mass and raw mass/tibia length. **D)** The 28199 antibody injections resulted in mice with significantly increased glut/ham mass normalized to tibia length when compared to PBS via one-way ANOVA (n≥17 per condition, $P<0.05$).

injections did not affect normal growth and development, and in the case of 28199, may increase hindlimb muscle mass compared to PBS.

Both anti-LTBP-4 antibodies reduced macrophage infiltration and increased measures of regeneration in quadriceps muscle.

To determine if α-LTBP4 antibodies modified muscle histopathology, muscle from *mdx*/hLTBP4 mice injected with 28199, 28200, or PBS was analyzed via light microscopy. The quadriceps muscles were harvested at day 30 and analyzed for characteristic features of muscle disease including fibrosis, internalized nuclei, myofiber cross-sectional area and immune infiltrate (**Figure 3.4A, triceps)**. The mean cross-sectional area (CSA) of individual myofibers varies greatly in dystrophic muscle, and its variance is a hallmark of disease. Mean CSA was significantly higher in 28199 treated triceps (975.8±53.3 μm2) when compared to PBS (821.6±49.6 μm2) injected controls via a one-way ANOVA and simple t-test. (**Figure 3.4B,** n≥3 mice per condition, $P<0.05$, n~ 150 myofibers per animal). When these data are plotted as a histogram binned according to relative CSA frequency, the higher frequency of very small (CSA<1000 μm2) fibers in the PBS group can be more readily appreciated compared to either α-LTBP4 antibody (**Figure 3.4C**, n≥3 mice per condition).

Nuclei in healthy muscle reside at the periphery of the cell, adjacent to the sarcolemma. Non-adjacent "internal nuclei" located on the interior of myofibers is an indication of active regeneration (Coulton et al., 1988). Both the 28199 and 28200 antibody injected groups had significantly more myofibers containing one or more internalized nuclei in triceps (60.5±4.8% and 62.8±5.1%, respectively) compared to PBS

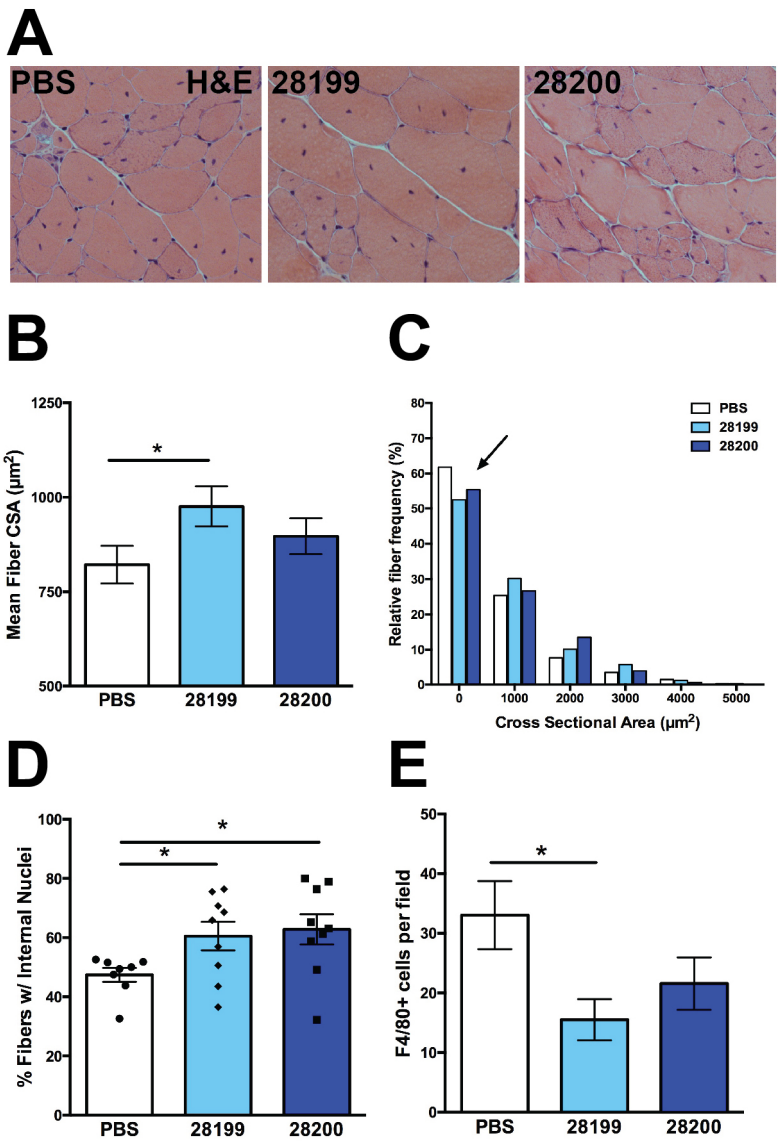

Figure 3.4 Anti-LTBP4 antibody injection increased markers of active regeneration and reduced macrophage infiltration. A) Representative histology was used to visualize the inflammatory infiltrate, centralized nuclei, and mean myofiber cross-sectional area of triceps muscle. **B)** Mean cross-sectional area (CSA) of 28199 group triceps (975.8±53.3 μm2) showed a significant increase compared to PBS (836.4±47.3 μm2), (n≥3 mice per group). **C)** Anti-LTBP4 injections increased the number of large myofibers and reduced small sized myofibers compared to PBS. **D)** Triceps histology of both 28199 and 28200 antibody-injected mice had significantly more centralized nuclei compared to PBS via t-test (n≥3 per group, $P<0.05$). **E)** Both α-LTBP4 injections reduced F4/80 labeled macrophages on triceps compared to PBS, but only the 28199 group was found to have a significant decrease when compared via a one-way ANOVA (n≥3 per group, $P<0.05$).

(47.5±2.3%) via a t-test, while the 28200 group was also significant with a one-way ANOVA (**Figure 3.4D,** n≥3 mice per condition**,** P<0.05, ~ 125 fibers per mouse). These data suggest that α-LTBP4 antibody injections may promote myofiber regeneration and resistance to atrophic reduction.

Inflammation is a prominent feature in many forms of muscle disease and can be assayed by documenting macrophage infiltration (Kronqvist et al., 2002). Activated macrophages, marked by F4/80 staining were quantified in mid-belly quadriceps section and found to be lower in the group injected with the 28199 antibody (15.51±3.4 cells) compared to PBS (33.3±5.7 cells) and 28199 (20.31±4.3 cells) using a one-way ANOVA **(Figure 3.4E,** n≥3 mice per condition, P<0.05). These data combined suggest that the 28199 and 28200 antibodies increase the rate of myofiber regeneration compared to PBS, while 28199 has additional properties of reducing cross-sectional area and number of inflammatory cells per area compared to PBS.

EBD uptake is influenced by α neutralization.

Healthy myofibers with an intact sarcolemma exclude the vital tracer Evans blue dye (EBD) (Heydemann et al., 2009). In many forms of muscular dystrophy, decreased sarcolemmal integrity allows for uptake of this dye into the muscle (Swaggart et al., 2014). **Figure 3.5A** shows representative images of dye uptake (red) into the triceps muscle where myofibers were outlined with Alexa-488 conjugated wheat germ agglutinin (WGA) (green). When these images were processed for percent area of EBD, the 28199 injected group had significantly reduced area of EBD uptake

(2.1±1.0%) compared to PBS (6.7±3.4%) via t-test, while the 28200 injected group showed the most uptake (11.3±3.4%) (**Figure 3.5B,** n≥4 mice per condition, P<0.05).

EBD uptake was also measured via colorimetric assay of EBD from whole muscle lysate of the gluteus/hamstring, quadriceps, abdominal and gastrocnemius/soleus groups. This colorimetric method did not replicate the EBD reduction found with 28199 injection in triceps muscle by microscopy or show a reduction in any of the muscle groups measured including glut/ham and quadriceps (**Figure 3.5C and 3.5D,** n≥9 muscles per group). Muscle lysate from 28200 group showed significantly less EBD (0.33 ± 0.6 AU/g) than PBS (0.47 ± 0.8 AU/g) in the glut/ham as measured by t-test but did not reduce uptake in any other muscle group measured by ordinary one-way ANOVA or t-test **(Figure 3.5C and 3.5D,** n≥9 muscles per group, P<0.05**).**

In both mice and humans, elevated serum creatine kinase (CK) is a hallmark of muscle injury (De Luca, 2012). Raw and baseline normalized CK was analyzed at three time points for which serum was collected, day 0, day 20, and day 30. (**Figure 3.4E**, n≥10 mice per condition). No significant differences in serum CK levels were found between groups at any time point via ordinary one-way ANOVA or multiplicity adjusted t-test and all three groups had lower day 30 mean CK values than at baseline (day 1) although no significant differences were found within or between groups over time as tested by repeated-measures 2-way ANOVA (**Figure 3.5E,** n≥10 mice per condition). These data suggest that both 28199 and 28200 may reduce sarcolemmal leak but do so in different muscle groups.

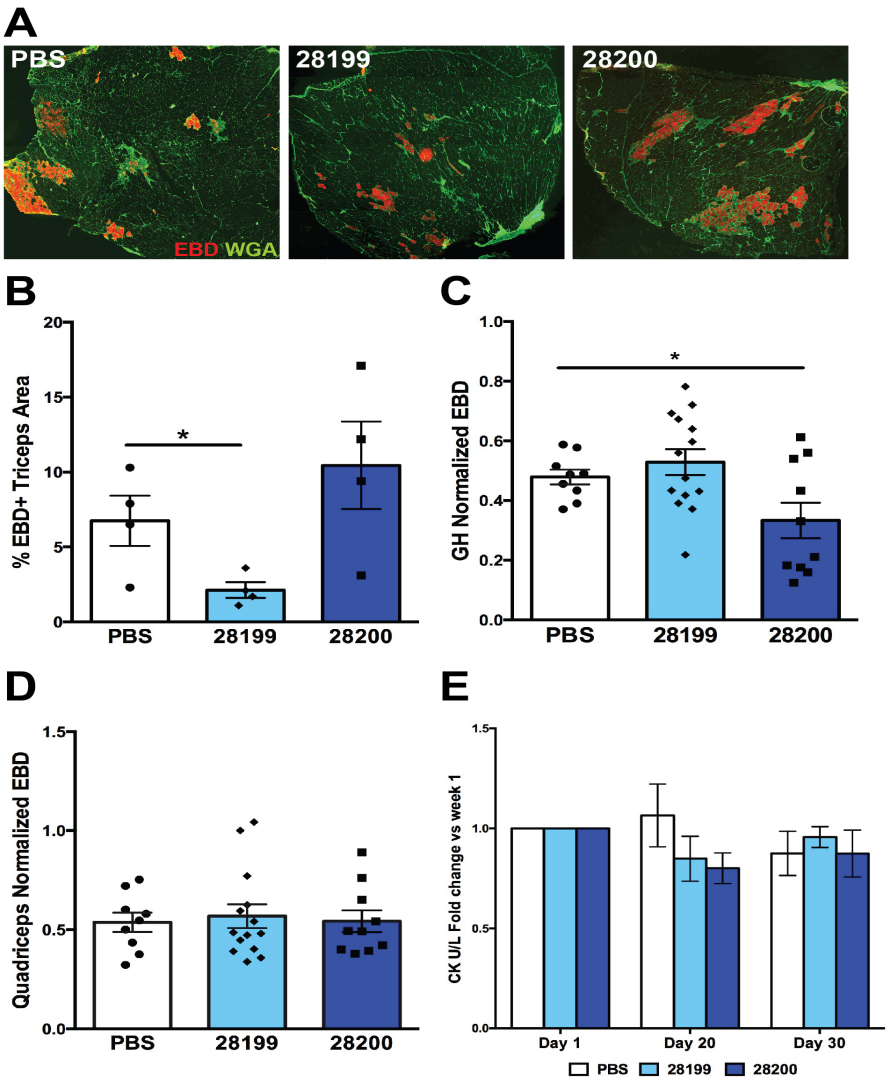

Figure 3.5 Anti-LTBP4 antibody injections reduce membrane damage and leak in two large muscle groups. A) Immunofluorescence microscopy of representative images of triceps muscle from animals that were injected with Evans blue dye (EBD) prior to sacrifice. Alexa-488 conjugated wheat germ agglutinin (WGA) was used to outline the boundaries of myofibers (green), while naturally fluorescent dye can be visualized as red cytoplasmic staining. **B)** Quantification of triceps dye uptake is significantly lower than PBS for the 28199 group when compared via t-test ($n \geq 3$ per condition, $P<0.05$). **C)** Colorimetric measurement of dye uptake in whole gluteus/hamstring muscle is significantly lower in the 28200 injected group ($P<0.05$, $n \geq 9$ muscles per condition). **D)** All three groups show a non-significant difference in colorimetric assay of EBD in the quadriceps. **E)** All groups experienced a slight decrease in serum creatine kinase (CK) over the 30-day trial period, however no group showed any statistically significant decreases and were not statistically different than one another at any time-point.

Both 28199 and 28200 injection reduced quadriceps fibrosis on histology.

Picrosirius red is a polyazo dye with high affinity for collagen used in histologic staining to highlight regions of extra-cellular matrix (ECM), connective tissue and fibrosis. The ECM is relatively thin in healthy muscle and therefore normally contains low levels of picrosirius red on histology. Mid-belly muscle sections of quadriceps muscle were stained with picrosirius red and imaged to determine the percent fibrotic area within each muscle **Figure 3.6A**. Significantly decreased levels of fibrosis were measured in 28199 (12.2±0.6%) and 28200 (9.3±0.98%) injected animals compared to PBS controls (15.5±1.2%) as measured by t-test, while the 28200 group was also significant via a one-way ANOVA (**Figure 3.6B,** $P<0.05$, $n\geq6$ mice per condition).

Hydroxyproline (HOP) is a modified amino acid found in collagen, and elevated HOP concentration is seen in dystrophic skeletal muscle (Heydemann et al., 2009). HOP content was quantified in the quadriceps, diaphragm and abdominal muscle groups. Neither 28199 nor 28200 showed any difference in fibrosis content using this assay in any of the three muscle groups measured. Additionally, HOP content in 28199 and 28200 injected quadriceps muscle did not replicate the decrease seen in picrosirius red analysis of the same organ when compared via t-test (**Figure 3.6C**). This discrepancy is not uncommon and is likely due to increased sensitivity of the picrosirius red imaging assay (Lohcharoenkal et al., 2014; Smith and Barton, 2014). These data combined suggest that 28199 and 28200 injections may reduce fibrosis within skeletal muscle over short-term trial periods.

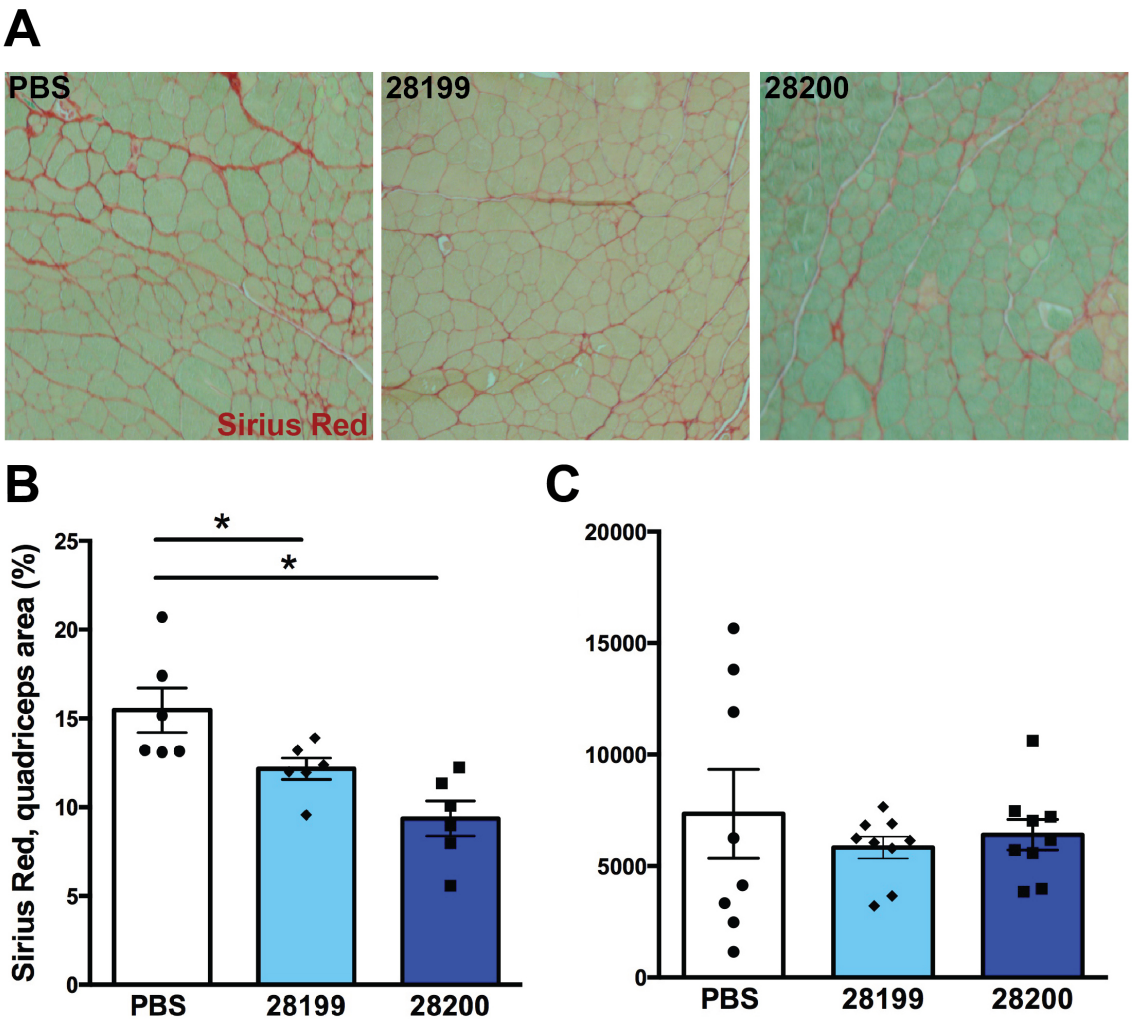

Figure 3.6 Anti-LTBP4 antibody therapy reduced fibrosis in the quadriceps muscle. A) Representative images of picrosirius red stained quadriceps muscle. **B)** Whole mid-belly quadriceps images were analyzed for percent area of picrosirius red staining per total quadriceps area. Both 28199 and 28200 injection significantly reduced the amount of picrosirius red compared to PBS when analyzed via t-test ($n \geq 6$ for each condition, $P<0.05$). **C)** Quadriceps fibrosis measured by the less sensitive HOP quantitation assay showed no difference between groups when measured by simple t-test.

Muscle strength and performance in α-LTBP4 injected mice

To investigate the effect α-LTBP4 antibody injections on muscle strength over time, *in vivo* grip strength was examined. Grip strength was measured on days 0, 7, 14, 21 and 28 of therapy and was observed to increase in all groups over time with respect to baseline (**Figure 3.7A**). The 28200 antibody injected group showed the greatest increase in strength over the trial period, with a nearly two-fold increase in mean grip-strength over 30 days over baseline (2.0±0.19 fold change over baseline). The 28199 and PBS showed modest improvement with a 30-day mean increase of (1.4±0.2 and 1.5±0.23 fold change over baseline, respectively). When baseline adjusted data is subjected to t-test between antibody groups and PBS within each time-point, the 28200 group showed significantly increased grip strength at day 7 and day 14 compared to PBS, but loses significance thereafter ($n \geq 9$ per condition, $P<0.05$). Since grip strength is a repeated measures test, maximum and minimum values can also be measured. We plotted and analyzed maximum (**Figure 3.7B**) and minimum (**Figure 3.7C**) grip strength values and found a similar trend between conditions independent of what value was analyzed.

Ex vivo muscle mechanics of the EDL muscle showed that 28200 antibody injection improved the percentage force decrease during eccentric contraction compared to PBS injection using a t-test and one-way ANOVA (31.5±5.0% compared to 64.1±4.2%, respectively) (**Figure 3.7D,** $P<0.05$, $n \geq 9$ muscles per condition). The 28199 antibody injections trended towards improved percentage force decrease while undergoing eccentric contraction compared to PBS (50.4±3.9%, $P<0.07$). Twitch and tetanic specific force, were not significantly improved with either α-LTBP4 injections

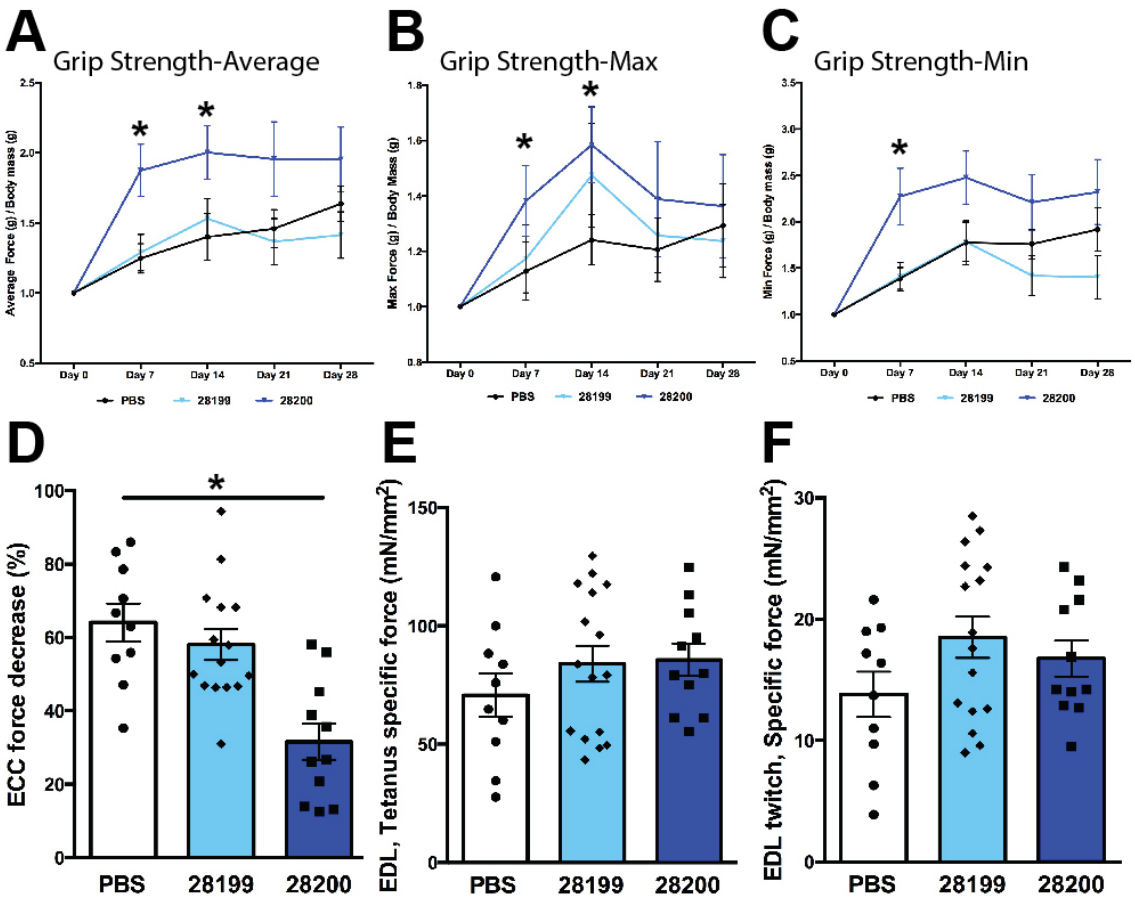

Figure 3.7 Injection of the 28200 antibody preserved grip strength and muscle function in response to eccentric contraction. A) Mean grip strength normalized to body mass over time reveals a general increase in strength over time across all conditions although the protocol. There were no significant differences via repeated measures 2-way ANOVA. When baseline normalized and raw values are analyzed via one-way ANOVA per each time point, only the 28200 group showed a significant difference compared to PBS and only at day 7 and 14 ($n \geq 10$ per group at each time-point, Day 7 $P<0.05$, Day 14 $P<0.05$). **B)** 28200 antibody injected mice showed a similar increase at day 7 and 14 when a similar analysis was conducted on the maximum grip force recorded on each day. **C)** When minimum grip-force for each mouse is analyzed, group 28200 loses significance at the day 14 measurement and only day 7 is significantly greater than PBS. **D)** *Ex vivo* muscle mechanics were analyzed on the extensor digitorum longus (EDL) muscle. The 28200 antibody injected group had a significantly smaller reduction in force compared to the PBS-injected group in response to repeated eccentric contractile injury ($n \geq 7$ muscles per group, $P<0.05$). **E and F)**. Anti-LTBP4 injected mice trended towards higher twitch (right) and tetanic (left) force than PBS injected animals, but this result was not significantly higher via ordinary one-way ANOVA or t-test.

(**Figure 3.7E and 3.7F)**. However, the α-LTBP4 28199 group trended towards an increase in twitch specific force when compared to the PBS group via a simple t-test (18.5±1.7 compared to 13.8±1.9, respectively) (**Figure 3.7F** $P<0.08$, $n\geq10$ muscles per group). These data suggest that 28200 injection protected myofibers against contraction-induced injury, preserving strength and performing better in both voluntary and involuntary assays of muscle strength.

Effect of α-LTBP4 antibody injection on cardiac function

Cardiac decline in muscular dystrophy has been characterized in both human disease and mouse models using imaging modalities (De Luca, 2012; Gardner et al., 2015). Echocardiography was performed at days 0, 14 and 28 and analyzed for measures of left-ventricular fractional shortening (LVFS), pulmonary artery flow, mitral valve function and quality of flow through the pulmonary artery.

Changes in mean LVFS at day 28 trended towards improvement in the 28199 group (25.9±2.0%) with a modest increase in 28200 (24.6±1.1%) compared to the PBS group (22.6±1.05%) (**Figure 3.8A**, $n\geq10$ for each condition). No significant differences in LVFS were found between any groups over time with repeated measures two-way ANOVA nor were any significant differences found at any single time-point between groups via ordinary one one-way ANOVA (**Table 3.3**). However, when an outlier in the 28199 group was removed on the basis of having an abnormal LVFS, then the 28199 group was significantly different at day 28 than PBS as compared via one-way ANOVA between groups ($n\geq10$ for all conditions, $p\leq0.05$).

The 28200 injected group trended towards a reduction in LVIDd on day 28 compared to the PBS injected group, with a mean value of 3.9 ± 0.05 mm compared to a 4.05±0.05mm (**Figure 3.8B,** n≥11 mice per condition). There was no significant difference in LVID;s with 28200 (3.04±0.08 mm) or 28199 (2.97±0.06mm) injection compared to the PBS (3.14±0.08mm) injected group (**Figure 3.8C,** n≥11 mice per condition). No significant differences in LVIDd or LVIDs were found between any groups at day 0 via a one-way ANOVA nor between any groups over time with repeated measures two-way ANOVA

Pulmonary artery velocity time integral (PA VTI) is a Doppler interrogation of blood flow in the pulmonary artery (PA) and is an indirect measure of right ventricular function (RV) and stroke volume. In both the 28199 and 28200 groups, PA VTI trended towards improvement at day 28 compared to the PBS group with final PA VTI values of 24.4±1.5cm^2, 24.5±1.7 cm^2, 20.7±1.2 cm^2, respectively (**Figure 3.8D,** P<0.08, n≥10 mice per condition). Despite this marked improvement, neither one-way nor repeated measures two-way ANOVA showed any significant differences between any conditions at any time-point. Decreased PAAT values have been positively correlated with higher PA pressures in mice as both values are affected by the compliance of the PA and its distal pulmonary circuitry (Thibault et al., 2010). In both the 28199 and 28200 groups, PAAT trended towards improvement at day 28 compared to the PBS group, with final PAAT values of 19.6±1.1ms, 19.1±1.1ms, 17.1±0.7ms, respectively (**Figure 3.8E,** n≥10 mice per condition). In the context of PBS showing progressive decrease of PAAT over time (day 28 PBS= -7.78% relative to baseline), these data suggest α-LTBP4 therapy

may stave off a characteristic increase in pulmonary artery pressure associated with elevate TGFβ signaling.

Flow through the mitral valve (MV) was measured and the ratio between maximum velocity during early passive ventricular filling (E) and maximum velocity during atrial kick (A) was calculated and analyzed for as many mice as time would permit ($n \geq 4$ for each group and time-point). A higher MV E/A is indicative of healthy passive ventricular diastolic filling (Jearawiriyapaisarn et al., 2010). MV E/A declined progressively in PBS group over time, with a final mean value of 1.3±0.25. The 28199 group trended towards an increase in MV E/A, 1.8±0.14, however, no differences were found between 28199 and PBS at any time point when values were compared via ordinary one-way ANOVA or t-test (**Figure 3.8F,** $P<0.08$, $n \geq 4$ mice per condition). In contrast, 28200 saw a marked improvement in MV E/A, 2.1±0.5, compared to the PBS group using a one-way ANOVA (**Figure 3.8F,** $P<0.58$, $n \geq 4$ mice per condition). In the context of all echocardiographic data combined, 28199 appeared to have a more prominent effect in the heart.

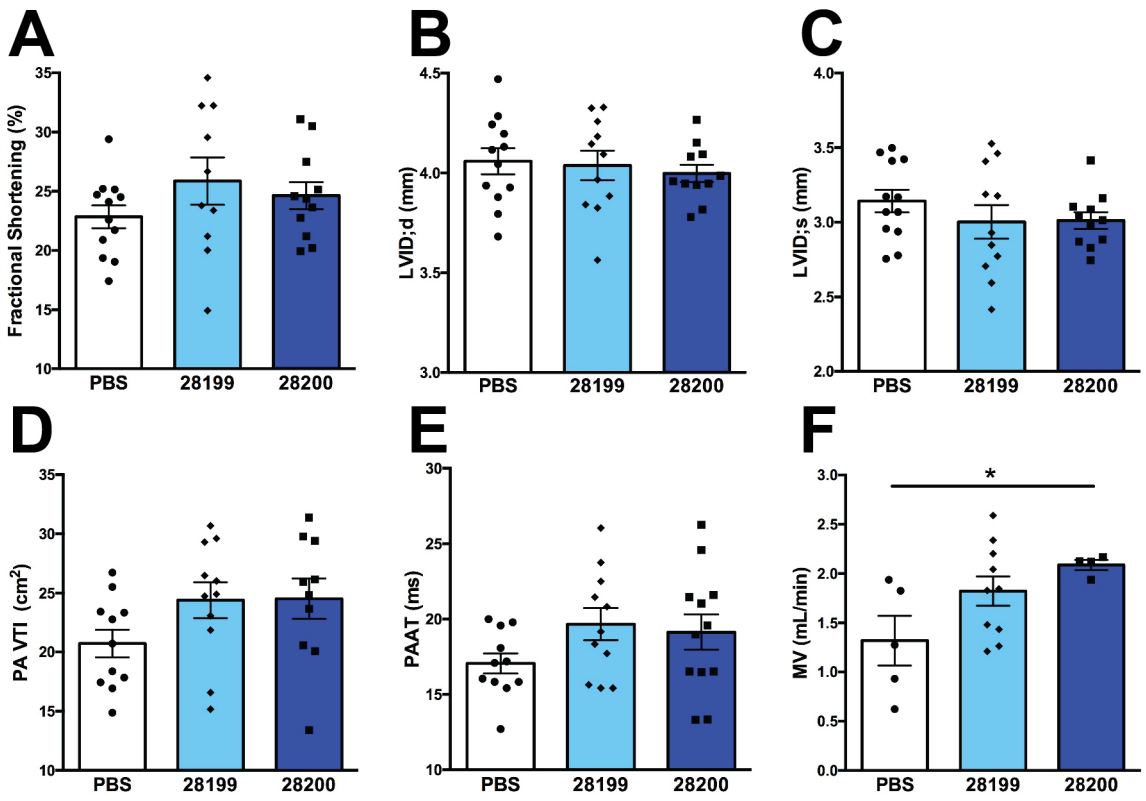

Figure 3.8 Anti-LTBP4 antibody effect on cardiac function. A) Mean Fractional shortening (FS) trended towards improvement with 28199 injection compared to PBS, however, no significant differences were found between groups (n≥10 mice per condition). **B & C)** LVIDd and LVIDs trended towards reduction compared to PBS although this was non-significant (n≥11 mice per condition. **D)** Pulmonary artery velocity time integral (PA VTI) increased in 28199 and 28200 groups, but this was not statistically significant compared to the PBS group (n≥10 mice per condition, P<0.08). **E)** Pulmonary artery acceleration time (PAAT) increased in 28199 and 28200 groups, but this was not statistically significant compared to the PBS group (n≥10 mice per condition, P<0.08). **F)** Mitral valve E/A ratio increased in both the 28199 and 28200 groups compared to the PBS group, but was only significantly different for 28200 group compared to the PBS group (n≥4 mice per condition, P<0.05).

Table 3.3 Anti-LTBP4 antibody effect on cardiac function.

	PBS-1		28199		28200	
Echo parameter	Day 0	Day 28	Day 0	Day 28	Day 0	Day 28
FS (%)						
Mean ± SEM	26.7 ± 1.45	22.6 ± 1.05	21.5 ± 1.74	25.9 ± 1.99	25.6 ± 0.91	24.6 ± 1.11
N=	9	12	11	10	10	11
LVID;d (mm)						
Mean ± SEM	3.98 ± 0.1	4.1 ± 0.06	3.78 ± 0.09	4.04 ± 0.07	4.05 ± 0.05	4.0 ± 0.04
N=	9	12	11	11	10	11
LVID;s (mm)						
Mean ± SEM	2.91 ± 0.1	3.14 ± 0.08	2.96 ± 0.1	3.00 ± 0.19	3.02 ± 0.06	3.01 ± 0.06
N=	9	12	11	11	10	11
PA VTI (cm^2)						
Mean ± SEM	25.6 ± 1.6	20.7 ± 1.2	20.6 ± 0.9	24.4 ± 1.5	24.9± 1.7	24.5 ± 1.7
N=	6	11	12	11	10	10
PAAT (ms)						
Mean ± SEM	18.5 ± 1.6	17.1 ± 0.7	20.0 ± 0.8	19.6 ± 1.1	18.4 ± 0.6	19.1 ± 1.1
N=	6	11	12	11	10	12
M/V (cm^2/cm^2)						
Mean ± SEM	2.0 ± 0.22	1.3 ± 0.25	1.0 ± 0.2	1.8 ± 0.14	2.0 ± 0.23	2.1 ± 0.05
N=	8	5	4	10	5	4

DISCUSSION

The LTBP4 hinge region is important in TGFβ availability and activation.

Although receptors for TGFβ are broadly expressed and found on nearly all cell types, TGFβ activation is limited to sites where TGFβ has been released from latency. TGFβ's active domain is secreted in the extracellular matrix (ECM) non-covalently bound by a large amino-terminal pro-domain, commonly referred to as the latency-associated peptide (LAP) to form the small latent complex. The small latent complex is secreted with and binds to scaffolding proteins like LTBPs forming the large latent complex (LAP) and its TGFβ dimer are secreted bound to scaffolding proteins such as LTBP or similar fibrillin-like family members (Todorovic and Rifkin, 2012). There are four LTBPs, and LTBP4 is expressed highly in muscle although other LTBPs are also present. TGFβ is liberated from the large latent complex by at least two, independent mechanisms: 1) enzymatic cleavage by activated matrix metalloproteinase (MMP), or by 2) the physical unfolding of LAP dimer by cellular traction force applied through integrins and/or shearing forces. (Maeda et al., 2011). Universal to both activating modes is a requisite/resultant cleavage in LTBP family members at a proline-rich molecular "hinge" region adjacent to the TGFβ binding motif, separating the protein in two fragments that can be independently identified on western-blot post-activation (Ceco et al., 2014).

We now tested antibodies against the LTBP4 hinge region for their ability to alter the phenotype of muscular dystrophy in a mouse model. We tested two antibodies raised to identical polypeptide fragments within the hinge region. These antibodies were raised in rabbits as polyclonal species and therefore can be expected to differ from each other in epitope and affinity. Moreover, the rabbit species of origin limited the use

of these antibodies in mice because of potential recognition by the mouse host as a foreign protein. Therefore, these studies were carried out for a limited interval in order to determine whether any benefit could be seen. The two different antibodies, 28199 and 28200, showed trends in the same general direction for many measures, but by most measures the 28199 antibody performed better. Neither antibody appeared toxic.

The 28199 antibody showed an increase in quadriceps and gluteus/hamstring muscle mass, increased triceps myofiber cross sectional area, increased internalized nuclei and a reduction in macrophage infiltration. These features support an increase in regeneration prompted by the 28199 antibody. The 28199 antibody also showed a decrease in Evans blue dye positive fibers in the triceps muscle and a reduction in the percentage of the quadriceps muscle that was fibrotic. The 29200 antibody generally performed less well with only trends towards these same effects and generally failing to reach significance. By functional measures, including grip strength and ex vivo muscle mechanics, the 29200 antibody did suggest improvement in performance while the 29200 antibody did not show this same effect. These measurements notably assess different muscle groups (the forelimbs and EDL muscles, respectively), and it is possible that antibody access to these muscles may differ based on animal activity or inherent properties of different muscle groups. We did not assess the effect of antibody injection on the animals' performance such as ambulation and climbing and these features may change measurements like serum creatine kinase and Evans blue dye uptake.

LTBP4 binds both myostatin and TGFβ and antibody blockade may affect the bioavailability of both.

In vitro, LTBP4 binds all three TGFβ isoforms (Lamar et al., 2016b). Moreover in separate experiments, we found that LTBP4 also binds myostatin (Lamar et al., 2016a). Myostatin is a negative regulator of muscle mass (McPherron et al., 1997). Antibodies that neutralize myostatin or block its receptor can stimulate muscle growth and in the setting of muscular dystrophy, reduce fibrosis (Bogdanovich et al., 2002; Bogdanovich et al., 2008; Latres et al., 2015). It is possible that the effects of growth seen with anti-LTBP4 antibodies are, in part, mediated by enhancing LTBP4's ability to sequester myostatin.

The short term nature of anti-LTBP4 antibody exposure and lack of documentation of dose efficacy limit conclusions.

The relative affinity of the 28199 and 28200 polyclonal rabbit antibodies is not known. Dosing of antibody therapy is often largely based on affinity as measured in quantitative ELISA or similar methods and was not available prior to our study. An additional limitation of our study was the fact that these antibodies were raised in rabbits, and therefore may be recognized as foreign and neutralized by the murine hosts. For this reason, long term dosing was not carried out. Indeed, the loss of efficacy seen in the grip strength over the week assessment may relate to neutralization. Many measures included in this study were only collected after four week dosing, limiting the ability to document efficacy or changes over the four week dosing. Nonetheless, several features were observed to improve suggesting that additional studies with species matched antibodies are worthwhile to conduct.

Chapter 4

Cardiac function in muscular dystrophy associates with abdominal muscle pathology

ABSTRACT

The muscular dystrophies target muscle groups differentially. In mouse models of muscular dystrophy, notably the *mdx* model of Duchenne Muscular Dystrophy, the diaphragm muscle shows marked fibrosis and at an earlier age than other muscle groups, more reflective of the histopathology seen in human muscular dystrophy. Using a mouse model of limb girdle muscular dystrophy, the *Sgcg* mouse, we compared muscle pathology across different muscle groups and heart. A cohort of nearly 200 *Sgcg* mice were studied using multiple measures of pathology including echocardiography, Evans blue dye uptake and hydroxyproline content in multiple muscle groups. Spearman rank correlations were determined among echocardiographic and pathological parameters. The abdominal muscles were found to have more fibrosis than other muscle groups, including the diaphragm muscle. The abdominal muscles also had more Evans blue dye uptake than other muscle groups. The amount of diaphragm fibrosis was found to correlate positively with fibrosis in the left ventricle, and abdominal muscle fibrosis correlated with impaired left ventricular

function. Fibrosis in the abdominal muscles negatively correlated with fibrosis in the diaphragm and right ventricles. Together these data reflect the recruitment of abdominal muscles as respiratory muscles in muscular dystrophy, a finding consistent with data from human patients.

RESPECTIVE CONTRIBUTIONS

This work was published as Gardner BB, Swaggart KA, Kim G, Watson S, **McNally EM.** Cardiac function in muscular dystrophy associates with abdominal muscle pathology. (2015) J. Neuromusc Dis. 2(1):39-49. PMCID: PMC4447317. Dr. Kayleigh Swaggart conducted the breeding and analyzed hydroxyproline content in multiple muscle groups. Dr. Gene Kim helped perform the echocardiographic studies. I analyzed the data and drafted the manuscript. Dr. Sydeaka Watson helped with the statistical analysis. Dr. Elizabeth McNally conceived the study, analyzed the data and edited the manuscript.

INTRODUCTION

The muscular dystrophies (MD) are a heterogeneous set of muscular disorders often linked to mutations in proteins within the dystrophin-glycoprotein complex (DGC). The DGC is a large protein complex localized to the sarcolemma of skeletal, smooth, and cardiac muscle fibers. The dystrophin glycoprotein complex physically links the extracellular matrix to intracellular cytoskeletal elements. Dystrophin and its associated proteins prevent sarcolemmal damage by mechanically stabilizing the lipid membrane, while additionally localizing important membrane repair mechanisms to their site of action (Rybakova et al., 2000). Mouse models of muscular dystrophy are highly useful

as preclinical models because they are small, reproduce easily, and can be genetically manipulated. The most studied mouse model of muscular dystrophy, the *mdx* mouse, recapitulates many of the pathologic hallmarks seen in Duchenne Muscular Dystrophy (DMD), and the *mdx* diaphragm muscle displays profound features of disease with severe replacement fibrosis that can be seen grossly on inspection (Hack et al., 1998; Ishizaki et al., 2008; Stedman et al., 1991). Mouse models of sarcoglycan gene mutations similarly reflect the pathology seen in humans with Limb Girdle Muscular Dystrophies (LGMDs), and like the *mdx* mouse have marked pathology in the diaphragm muscle compared to other muscle groups (Vainzof et al., 2008).

In heart failure, diaphragm muscle and cardiac function are interdependent (Habedank et al., 2013; van Hees et al., 2010). This interdependence is especially evident in muscular dystrophy, where primary deficits in respiratory muscles and the myocardium may accelerate pathology and dysfunction. Deletion of the skeletal muscle specific transcription factor *MyoD* in the *mdx* mouse, which specifically impairs skeletal muscle regeneration, accelerates cardiomyopathy (Megeney et al., 1999). Correspondingly, rescue of diaphragm muscle with utrophin overexpression in the *mdx/utrophin* double null mice improved right-ventricular (RV) and left-ventricular (LV) ejection fraction (EF) (Crisp et al., 2011). In another study, cardiomyopathy was evident in older *mdx* mice whose skeletal muscle, including diaphragm muscle, had been rescued by micro-dystrophin transgene expression (Wasala et al., 2013). These findings emphasize the importance of correcting multiple muscle groups, including the respiratory and cardiac muscles.

The diaphragm muscle is responsible for approximately 50% of respiratory force in humans, but this contribution varies with body position and exercise demands (Sant'Ambrogio et al., 1966; Wang and Josenhans, 1971). Other muscle groups contribute significantly to respiration, especially when the primary breathing muscle is diseased, as it is in muscular dystrophy. The abdominal muscle group is considered an accessory of respiration, aiding mostly in expiration (Kaneko and Horie, 2012). Increasing evidence suggests that the abdominal muscles adapt for additional function in patients with muscular dystrophy by contributing to both expiration and inspiration (Mauro et al., 2009; Romei et al., 2012; Ugalde et al., 2001). The progression of disease in the abdominal musculature is not as well characterized as the diaphragm muscle in human patients or animal models of MD, and it still remains largely unknown what relationship, if any, the abdominal muscles have with *in vivo* measures of cardiopulmonary function. We now used a mouse model of muscular dystrophy to assess the relationship between markers of abdominal muscle pathology and measures of cardiopulmonary dysfunction. We took advantage of a large well characterized cohort of mice lacking the dystrophin associated protein γ-sarcoglycan, as these mice are a model for severe childhood autosomal recessive muscular dystrophy, also known as LGMD 2C (Azibi et al., 1993). This subtype of muscular dystrophy is notable for its similar phenotype to DMD, and this model was selected since it displays an earlier cardiac phenotype more reminiscent of what is seen in human DMD and LGMD 2C. The rectus abdominus muscle is the primary abdominal muscle, and abdominal muscles are important in maintaining posture for proper respiration, in addition to being the primary muscle of expiration. We studied mice at an early time-point in disease, 8

weeks, and found that abdominal muscle pathology correlated with *in vivo* and postmortem markers of cardiopulmonary dysfunction. These findings demonstrate that the abdominal muscles are useful and accessible muscles to study in preclinical models and reflect cardiopulmonary pathology.

MATERIALS AND METHODS

Animals. Sgcg mice, a model for limb girdle muscular dystrophy, were described previously (Hack et al., 1998; Heydemann et al., 2005). *Sgcg* on the DBA/2J (D2) background and the 129T2/SvEmsJ (129) background were intercrossed to create homozygous *Sgcg* mice on a mixed D2/129 genetic background. Male (n=95) and female (n=101) $Sgcg^{D2/129}$ mice were studied (total cohort 196). Animals were housed in a single pathogen-free barrier facility under the approval of the University of Chicago Animal Care and Use Committee. At 8 weeks of age, animals were sacrificed and muscle groups removed and isolated for further processing. Hydroxyproline (HOP) content was measured in the whole diaphragm, the right ventricular free wall (right ventricle), left ventricular free wall and septum (left ventricle), abdominal muscle, and one half of each quadriceps muscle. The abdominal muscle was taken from two 1cm square dissections adjacent to, but not including, the non-muscular *linea alba*. The abdominal muscle taken did not include lateral portions of the abdominal wall, and therefore, the abdominal rectus muscle is likely most represented in our dissection. Evans blue dye (EBD) content was measured in whole triceps, gluteus group/hamstrings, gastrocnemius/soleus and abdominal muscles, and one half of each quadriceps muscle. Together, this generated 35 different data points measured for

each animal, and all 35 measurements were available from 126 animals. The remaining 70 animals had more than 30 data points available. The measurements of HOP and EBD utilized the entire muscle groups. Histopathology was performed on separate animals.

Echocardiography. Echocardiographic studies were conducted on animals following standard protocols (Spurney et al., 2009) and as described previously (Wheeler et al., 2004). Animals were anesthetized using isoflurane, 2% in O_2, and then placed on a heated pad. Imaging studies were typically completed in less than 15 minutes of total anesthesia time. During imaging, isoflurane was titrated to avoid heart rates less than 350 bpm. Imaging utilized a Vevo 770 (Visualsonics, Toronto, Ontario, Canada) ultrasound machine with 30Mhz probe to acquire all measurements and images. Left-ventricular fractional shortening was acquired by collecting M-mode images in both the parasternal long-axis and parasternal short-axis views.

Hydroxyproline measurement. Hydroxyproline (HOP) assay was performed as described previously (Heydemann et al., 2005). Muscles were removed, minced, weighed and hydrolyzed in 2ml of 6 M hydrochloric acid at 110°C overnight. After incubation, Ehrlich's reagent was added and absorbance was measured at 558 nm. Heart ventricles were assayed after removal of atria and great vessels. Results were reported per milligram of tissue. HOP measurements were performed on half the abdominal and quadriceps muscles, and on the entire diaphragm and cardiac ventricles where the right and left ventricle were assayed separately.

Dye uptake. Evans blue dye (EBD) uptake into muscle was measured as described previously (Heydemann et al., 2005; Thurston et al., 1999). Forty hours prior to sacrifice, animals were injected intraperitoneally with 5 μl/g body mass EBD (Sigma, E-2129) in phosphate-buffered saline at 10 mg/ml. The entire gastrocnemius/soleus, gluteus/hamstrings, and triceps muscles were harvested for the dye uptake assay. Half of each abdominal and quadriceps muscle was used, while the other half was used for HOP measurement (see above). Muscles were removed, minced, weighed and incubated in 1 ml of formamide for 2 h at 55°C. Absorbance was measured at 620 nm, and results reported as the Z score of absorbance per milligram of tissue.

Histology. Hematoxylin and eosin staining or Mason Trichrome was performed on *Sgcg* (DBA/2J) mice or *mdx* (C57Bl10) mice as described (Hack et al., 1998) (n= 2-5 mice of each genotype).

Statistical Analysis. Statistical analysis was performed using Prism 6 software (GraphPad Software, San Diego California, USA, www.graphpad.com) and R (R Foundation for Statistical Computing, Vienna, Austria). For 3 images (LV fibrosis vs abdominal fibrosis, LV fibrosis vs diaphragm fibrosis, and RV fibrosis vs diaphragm fibrosis), 3 data points were removed for the purposes of presentation. The 3 data points were removed only from the visual depiction of the data because these points were so elevated as to compress the remaining data visualization. All data were included for statistical calculations, including those three points that were removed from

each of the three above referenced images. All parameters were evaluated for the normality of their distribution using a D'Agostino and Pearson omnibus test. Non-parametric Spearman rank correlation coefficients were used to examine pairwise relationships among muscle groups due to the non-normal distribution of multiple parameters. Additionally, non-parametric methods (Dunn's multiple comparison test and Mann-Whitney U test) were used to test for significant differences in parameters across muscle groups. P values < 0.05 were accepted as significant.

RESULTS

A large, genetically heterogeneous cohort of mice reflects variability seen in human muscular dystrophy.

Sgcg mice lack the dystrophin-associated protein, γ-sarcoglycan, and are a model for limb girdle muscular dystrophy (LGMD) type 2C (Hack et al., 1998). Like LGMD 2C and DMD patients, *Sgcg* mice characteristically develop a progressive muscle disease marked by inflammation, necrosis and muscle weakness (Griffin et al., 2005). LGMD 2C is phenotypically heterogeneous, even with an identical primary gene mutation (Kefi et al., 2003). To model this phenotypic variability in mice, we generated a cohort of *Sgcg* mice on a mixed genetic background taking advantage of the observation that the muscular dystrophy phenotype is enhanced in the DBA/2J (D2) background and repressed in the 129T2/SvEmsJ (129) background (Heydemann et al., 2005). The D2 strain background harbors a number of genetic loci that enhance muscular dystrophy, and the genetic locus that contributes is the chromosome 7 encoded latent TGFβ binding protein 4 (*Ltbp4*) gene (Swaggart et al., 2011). A cohort of 196 *Sgcg* mice was

assessed for cardiac function at 8 weeks of age using echocardiography followed by post mortem measurements of fibrosis and muscle damage. Although increased fibrosis can be detected in the heart at this stage, severe cardiac dysfunction is not yet present. This cohort showed a range of disease severity affecting multiple muscle groups and the heart (**Figure 4.1**).

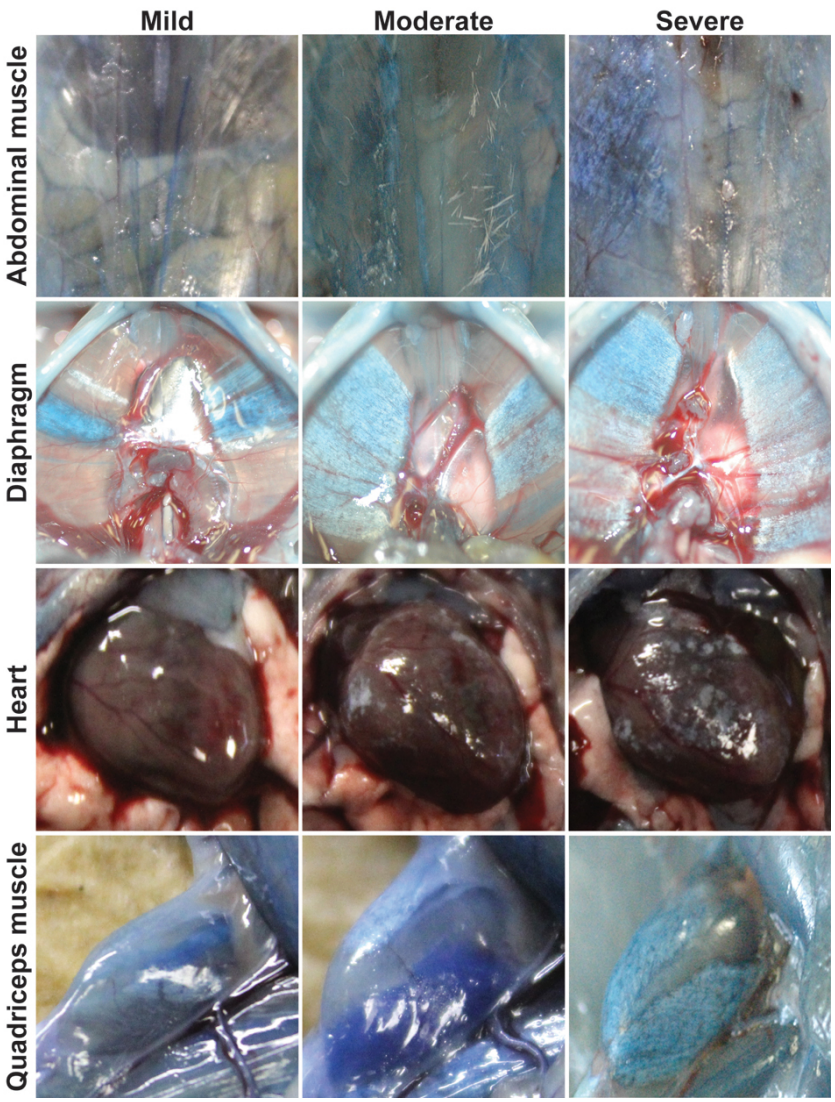

Figure 4.1 *Sgcg*$^{D2/129}$ mice replicate a range of severity and muscle group involvement similar to human muscular dystrophy. *Sgcg* mice, a model for limb girdle muscular dystrophy, were studied on a mixed genetic background. At eight weeks of age, a relatively early time point in disease, *Sgcg*$^{D2/129}$ mice displayed significant variability in severity of membrane leak and fibrosis. Gross images are shown from the abdominal, diaphragm and quadriceps muscles, as well as the heart. Animals were injected with Evans blue dye to mark muscle damage, and this is seen as blue areas of muscles. Fibrosis appears as white patches or streaks, and turns otherwise translucent muscle opaque. Dye uptake and fibrosis often occur together, and individual animals can vary in how severely individual muscle groups are affected.

The abdominal muscle group experiences the most severe membrane leak.

Evans blue dye (EBD) is an azol dye with high binding affinity for serum albumin. EBD does not accumulate in healthy muscle tissue; rather, it characteristically accumulates in muscles where the sarcolemma has been disrupted. Dye uptake, as a reflection of abnormal muscle membrane permeability, can be quantified as a temporal marker of tissue damage present at the time of analysis (Hamer et al., 2002; Wooddell et al., 2010). Dye uptake was determined for the abdominal, triceps, quadriceps, gastrocnemius/soleus and gluteus/hamstring muscle groups (n=124 mice) that are subject to heavy use, even in cage-bound animals. Compared to the limb skeletal muscles, the abdominal muscle group had a significantly higher mean dye uptake (6.67 ± 2.59 OD/mg) (**Figure 4.2A**). This mean was 34.9% higher than mean for gluteus/hamstring, the second most affected muscle group. Mean abdominal muscle dye uptake was significantly higher than all other muscle groups assayed ($p<0.0001$ for all pairwise comparisons with the abdominal muscle). No significant differences were found when considering dye uptake between other muscles groups. The distributions of values for dye uptake in the abdominal muscles and gastrocnemius/soleus muscles were non-normal ($p=0.003$ for abdominal, and $p<0.0001$ for gastrocnemius/soleus) (**Figure 4.2B).** No other significant departures from normality were observed in any of the other muscles assayed for dye uptake.

It has previously been reported that *mdx* mice may display an asymmetry that was observed to affect both the quadriceps muscle and gastrocnemius muscles (Kobayashi et al., 2012). The lateral preference was seen to affect performance on a treadmill and correlate with increased muscle damage on the side bearing more of the

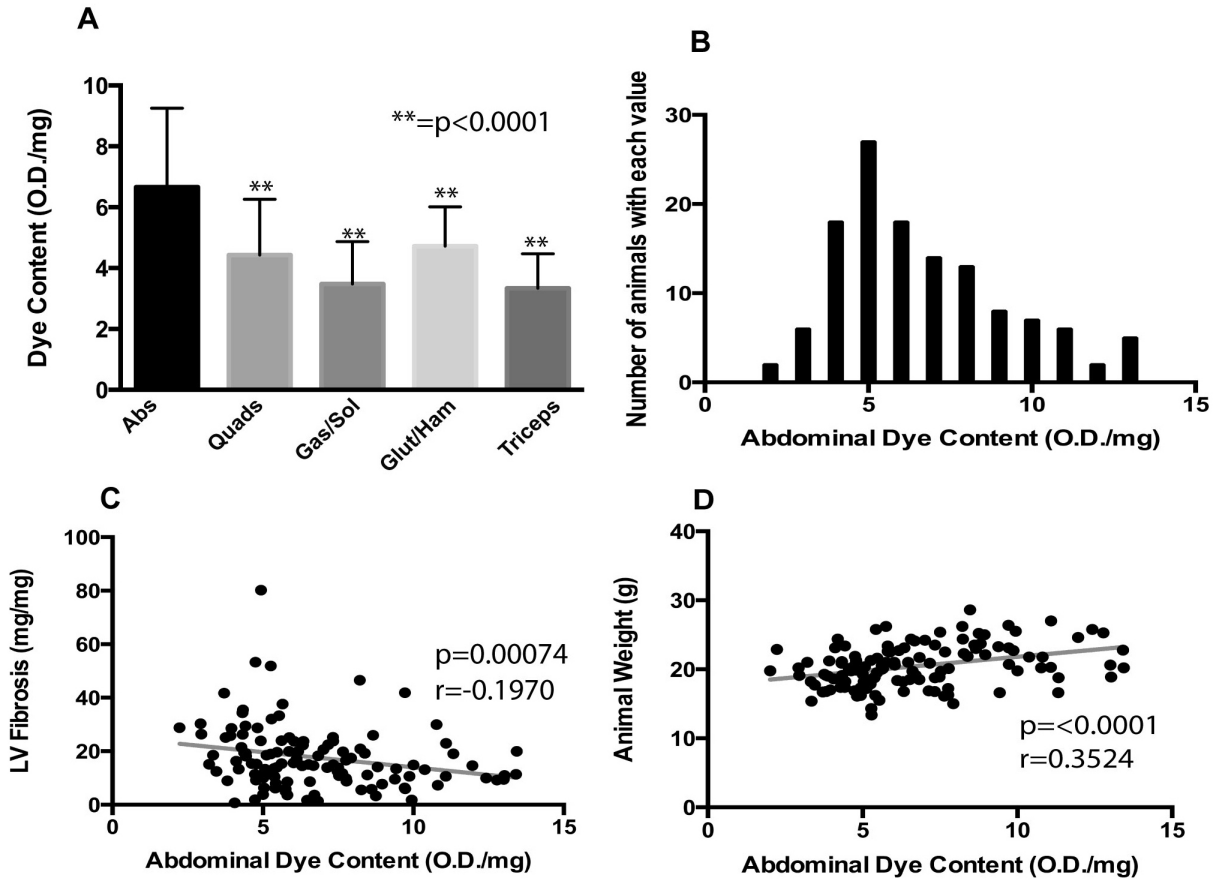

Figure 4.2 Mean dye uptake, as marker of muscle damage, was highest in the abdominal muscles. A large cohort (n=196) of *Sgcg*$^{D2/129}$ mice was assayed for dye uptake in multiple muscle groups. **A)** Mean dye uptake was found to be highest in the abdominal muscles (m=6.67 ± 2.59 OD/mg), This value was found to be significantly higher than other muscles assayed for EBD when compared by Dunn's multiple comparison tests (p<0.0001). Error bars represent standard deviation. **B**) A histogram representing the distribution of abdominal muscle dye uptake. This distribution was found to be non-normal, and right-skewed. **C**) Abdominal dye uptake was significantly, negatively correlated with fibrosis in the left ventricle of the heart. **D**) Furthermore, abdominal dye uptake was significantly, positively correlated with animal weight. Taken together, these data support a model in which abdominal muscles are recruited to support cardiopulmonary output.

load. The *Sgcg* model similarly displayed asymmetry in two muscle groups: the gastrocnemius/soleus muscle groups and the quadriceps muscles. A Wilcoxon signed rank test found that mean dye uptake was significantly higher in the left gastrocnemius/soleus ($p=0.0495$), while mean fibrosis, measured as hydroxyproline content, was significantly higher in the left quadriceps ($p<0.0001$). Additionally, we found two traits to exhibit sexual dimorphism. As expected, male mice had greater body mass than female mice (male: 21.96 g ± 2.95, female: 19.50 g ± 2.58, $p<0.007$). Male mice were also found to have significantly higher dye uptake in the abdominal muscles than female mice (male: 7.63 ± 2.49, female: 5.86 ± 2.33, $p<0.0001$). However, these sex-based differences did not alter any of the reported correlations.

Abdominal muscle dye uptake correlates with reduced left ventricular fibrosis and increased animal mass.

Spearman based correlations were used to analyze relationships between abdominal dye uptake and all other functional and pathologic markers. Abdominal dye content correlated negatively with left-ventricular fibrosis, as measured by hydroxyproline (HOP) content (**Figure 4.2C**). Abdominal muscle dye uptake was found to correlate significantly and positively with animal weight (**Figure 4.2D**). No other studied muscle group was found to correlate significantly with animal weight. Interestingly, abdominal muscle dye uptake showed a weak correlation with the measurement of mean velocity of blood across the pulmonary artery ($r=0.1898$, $p=0.0502$), which is a reflection of right ventricular function. Taken together, these data suggest that increased dye uptake in the abdominal muscles was seen in larger animals with less left ventricular fibrosis. An

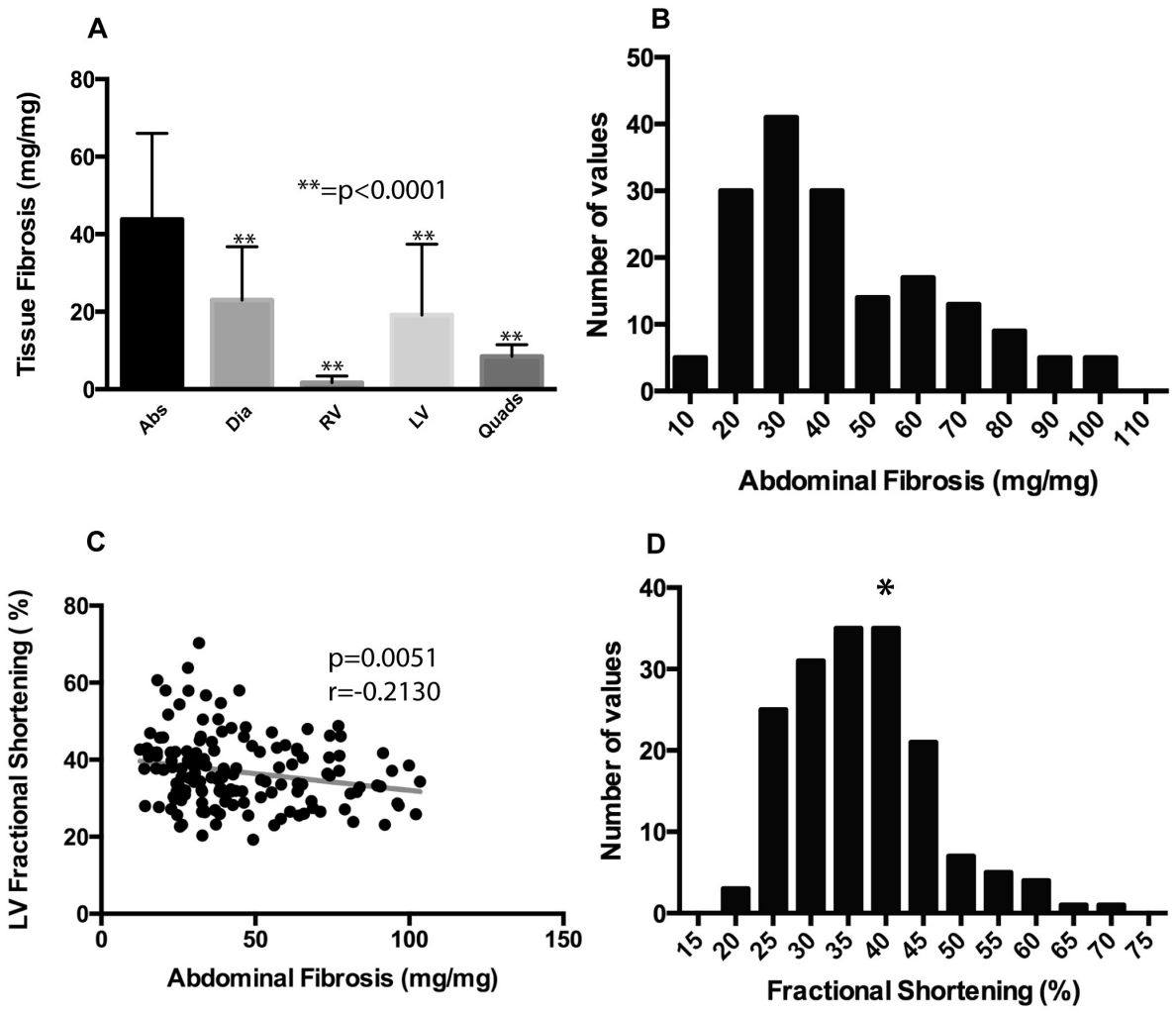

Figure 4.3 Mean tissue fibrosis was highest in the abdominal muscles. *Sgcg*$^{D2/129}$ mice from the same cohort (n=196) were assayed for hydroxyproline (HOP) content as a direct measure of fibrosis. **A**) Mean fibrosis, measured by HOP content, was highest in the abdominal muscles (43.79 ± 22.16 mg/mg). This value was found to be significantly higher than other muscles when compared by Dunn's multiple comparison tests ($p<0.0001$). Error bars represent standard deviation. **B**) A histogram representing the distribution of abdominal muscle fibrosis (HOP content.) This is a non-normal distribution and is right-skewed. **C**) Abdominal muscle fibrosis was significantly negatively correlated with left-ventricular fractional shortening (LVFS) using Spearman based calculations**. D)** Distribution of LVFS in the *Sgcg* cohort. The asterisk indicates normal LVFS.

animal's mass may be large in part due to edema, which would be reflected as dye uptake. We infer the increased abdominal muscle damage is consistent with these muscles being recruited as accessory muscles of respiration, which in the shorter term, may be protective for the heart by improving oxygenation.

The abdominal muscles have more fibrosis than other muscles.

Hydroxyproline (HOP) content was used as reflection of fibrosis because this modified amino acid is found in matrix deposited collagen. The abdominal muscles had a mean HOP measurement of 43.79 ± 22.16 mg/mg, which was 47.5% higher than the diaphragm muscle and 131% higher than what was seen in the left ventricle. Fibrosis in the abdominal muscles was significantly higher than all other groups assayed (**Figure 4.3A**). Much like abdominal dye uptake, the distribution of values was right-skewed ($p=0.0002$). Total body mass was found to correlate negatively with abdominal muscle fibrosis ($r = -0.206$, $p=0.0071$), which could be influenced by sexual dimorphic differences in body mass.

Left ventricular fractional shortening (LVFS) is a commonly used measure of heart function applicable to both human and murine hearts. A normal LVFS for mice under isoflurane anesthesia, as used here, is 39% (Gao et al., 2011). The mean LVFS for *Sgcg* mice was 36.93% (SD ± 9.1), and more than 30 animals had LVFS < 30% reflecting cardiomyopathy. Those animals with the least abdominal muscle fibrosis had the best cardiac function measured by LVFS (**Figure 4.3C**). The distribution of LVFS in the cohort is shown in **Figure 4.3D**. Abdominal muscle fibrosis did not correlate with LV fibrosis ($r = -0.0975$, $p=0.2124$). However, cardiac function measured by LVFS also did

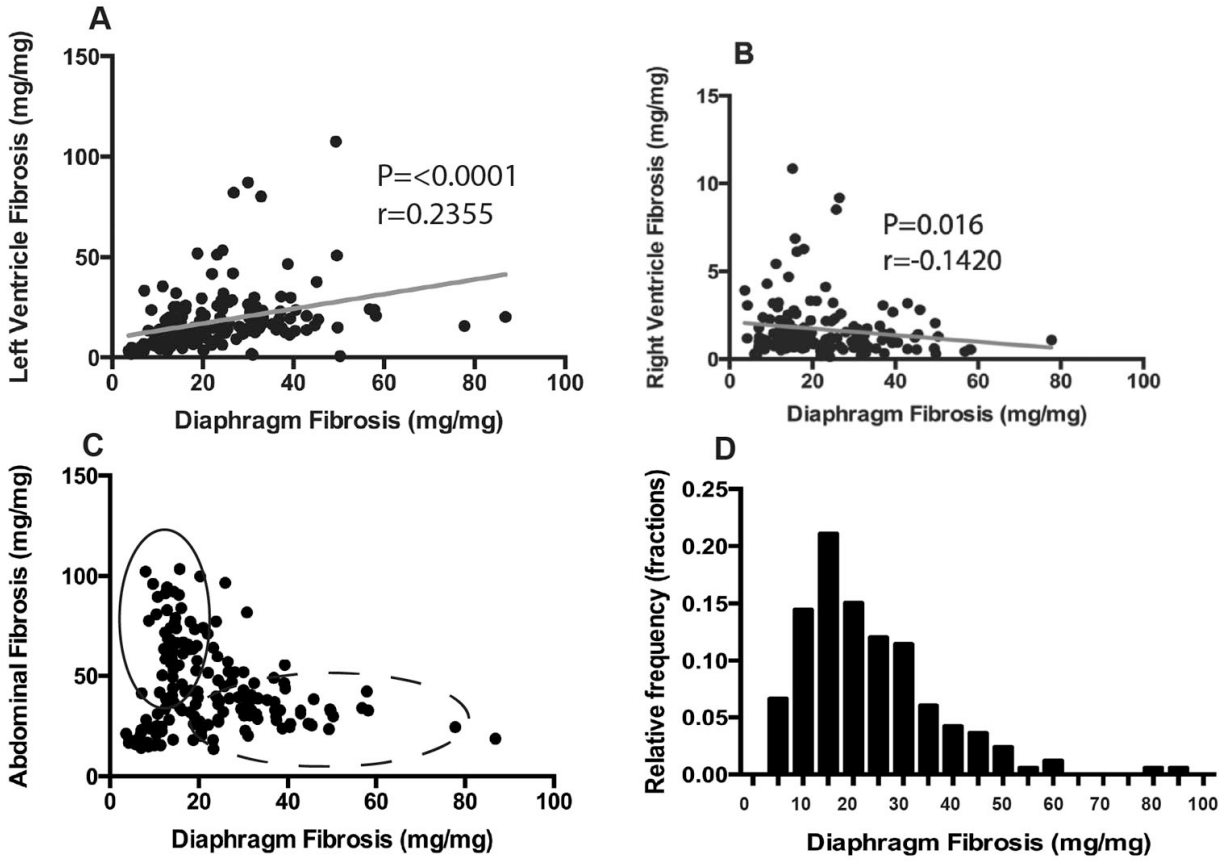

Figure 4.4. Diaphragm fibrosis associates with fibrosis in the heart. A) Diaphragm fibrosis correlated positively with LV fibrosis using Spearman based methods, further supporting the concept that scarring in the respiratory muscles may predict scarring in the LV. **B)** Interestingly, diaphragm fibrosis correlated negatively with RV fibrosis, indicating that the diaphragm correlation with LV fibrosis is independent of RV pathology. **C)** Scatter plot representing abdominal and diaphragm fibrosis for each animal. Although abdominal fibrosis correlates negatively with diaphragm fibrosis, the distribution suggests a more complex relationship between the two organs. Specifically, there are very few animals with high level abdominal *and* diaphragm fibrosis (intersection point). Rather, the cohort can be divided into two virtual populations: those that preferentially developed diaphragm fibrosis with little abdominal fibrosis, and those that preferentially developed abdominal fibrosis with little diaphragm fibrosis. **D)** Frequency distribution of fibrosis found within the diaphragm of the full cohort.

not correlate significantly with LV fibrosis (r = -0.1300, p=0.1165), indicating that cardiac dysfunction at this stage is not arising from fibrotic infiltration of the heart. These findings are consistent with the view that respiratory dysfunction contributes to cardiac dysfunction.

Diaphragm fibrosis correlates positively with left-ventricular fibrosis, and negatively with right-ventricular fibrosis.

The diaphragm, in both large and small animals, is thought to be the major respiratory muscle and is known to be particularly affected in muscle dystrophy in humans and mouse models (Stedman et al., 1991). Diaphragm muscle fibrosis, as measured by HOP content, was found to correlate positively with left-ventricular fibrosis (**Figure 54.4A**). These data suggest that the left-ventricle and diaphragm become fibrotic relatively early in this model of muscular dystrophy. Conversely, diaphragm muscle fibrosis correlated negatively with right-ventricular fibrosis (**Figure 4.4B**, r=0.1420, p=0.016). It is important to note that, on average, the right-ventricle experienced the least fibrosis of all muscles sampled by the HOP assay (1.771 ± 1.72 OD/mg). This was 79% lower than the next most fibrotic organ, the quadriceps muscle (mean quadriceps HOP 8.48 ± 3.03 OD/mg).

***Very few animals have severe diaphragm fibrosis and abdominal fibrosis*.**

Figure 4.4C is a paired scatter plot correlating diaphragm muscle fibrosis and abdominal muscle fibrosis. These data are plotted without transformation and without a

best-fit line in order to better visualize the data. Although there are independent populations of mice that have severe diaphragm fibrosis (dashed line) or abdominal fibrosis (solid line), there are few to no animals that have both severely scarred abdominal and diaphragm muscles. The distribution for diaphragm HOP content is right skewed (p=<0.0001) (**Figure 4.4D**).

Comparable histopathology between abdominal muscles and diaphragm muscles in mouse models of MD.

To correlate the quantitative measures of pathology used above, histological sections were examined from *Sgcg* mice to evaluate abdominal and diaphragm muscle pathology (**Figure 4.5**). The abdominal muscle displayed the same range of pathology seen in the diaphragm muscle with notable calcification, necrosis, and inflammation in both muscles. Mason Trichrome staining highlighted significant fibrosis in the abdominal muscles, consistent with the measurements made using hydroxyproline. Abdominal muscles from *mdx* mice were examined and were similarly found to display qualitatively comparably dystrophic features as the diaphragm muscle. Together these data complement the findings in the large *Sgcg* cohort.

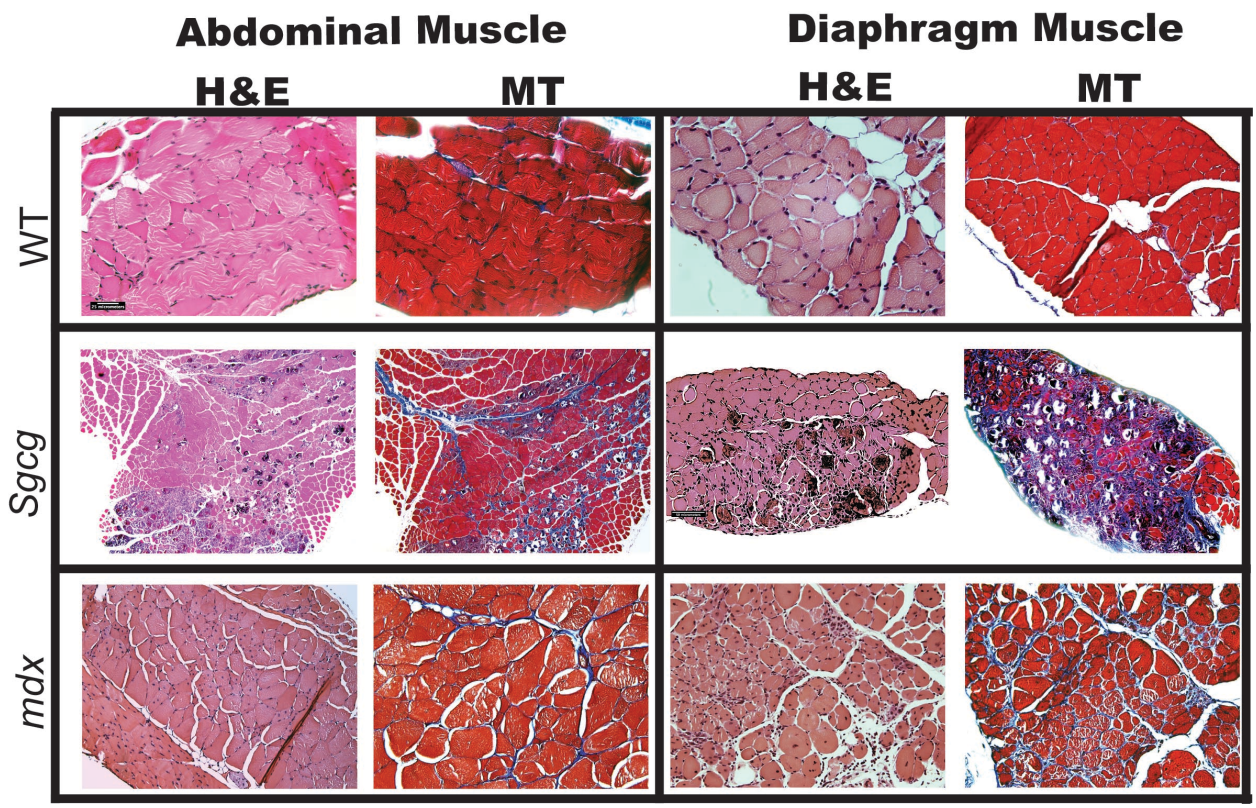

Figure 4.5 Abdominal muscle and diaphragm muscle histopathology is comparable in mouse models of MD. Representative histopathologic sections taken from the diaphragm and abdominal muscles of normal wild-type (WT), *Sgcg*, and *mdx* and *Sgcg* mice at an early time point in disease. All mice were less than 12 weeks old. Hematoxylin and eosin (HE) staining highlights necrosis, calcification, and inflammation. Mason's trichrome (MT) stained sections from *Sgcg* and *mdx* mice both revealed a more dense intercellular fibrosis throughout the abdominal and diaphragm muscles. This degree of histopathology is greater than what is seen in limb-based skeletal muscles (not shown).

DISCUSSION

Abdominal muscles are severely affected in a mouse model of muscular dystrophy.

At 8 weeks of age, a time-point that reflects established muscle pathology and emerging cardiac dysfunction, we found the abdominal muscles had significantly elevated Evans blue dye uptake as well as fibrosis. Evans blue dye is a measure of sarcolemmal disruption and directly reflects myofiber injury and damage (Matsuda et al., 1995; Straub et al., 1997). What triggers such notable pathology in the abdominal muscles at such an early time point is not known, but it is likely that these muscles are being recruited to participate in respiratory function. In this model of muscular dystrophy, like the *mdx* model of muscular dystrophy, the diaphragm muscle displays profound histopathological changes. At 8 weeks of age, the diaphragm muscle is nearly completely replaced by fibrosis, which is visible both grossly and histologically, which is anticipated to alter compliance. With the loss of the diaphragm muscle, other muscle groups are expected to contribute to the work of breathing. The pathological findings in the abdominal muscles in *Sgcg* mice are consistent with these muscles being recruited for respiration.

The lack of correlation between diaphragm muscle and abdominal muscle fibrosis is striking. Specifically, there were virtually no animals that displayed high levels of fibrosis in both the diaphragm muscle and abdominal muscle. Many of the animals collected at this time point had severe diaphragm fibrosis or severe abdominal fibrosis, but rarely both. From this, we infer that animals with severe fibrosis in both muscle groups may have a survival disadvantage. For example, if breathing were severely

compromised in the first four weeks of life, such animals may not survive weaning and would not be included in our analysis. The animals in this study were evaluated at 8 weeks of age, post puberty, and an equivalent age of the late second decade of human life.

Respiratory muscle pathology correlates with cardiac measures of pathology and dysfunction.

Markers of abdominal and diaphragm muscle pathology correlated significantly with cardiac functional measures in this mouse model of muscular dystrophy. The strongest correlates were between abdominal muscle damage and the mean velocity of blood across the aortic valve, a measure of heart function. Fibrosis in the abdominal muscles also correlated negatively with fractional shortening in the LV. Those animals with the greatest abdominal muscle fibrosis had the most preserved LV function. We interpret these findings as consistent with a model whereby cardiac function can be maintained at the cost of increased breathing, reflected in the use and damage in the abdominal muscles. It is notable that diaphragm muscle fibrosis and LV fibrosis were correlated. This progression is supported by the correlation between diaphragm muscle fibrosis and left ventricular fibrosis, furthering the notion that respiratory muscle fibrosis has a negative impact on cardiac fibrosis (**Figure 4.6**).

Implications for human muscular dystrophy

The diaphragm and abdominal muscles oppose one another biomechanically, the former serving as the primary muscle of inspiration while the latter serves as the

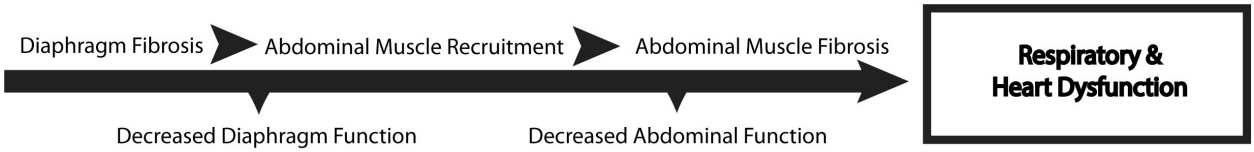

Figure 4.6 The abdominal muscle group may compensate for early diaphragm failure in the *Sgcg* model of MD. Above is a simplified timeline representing a progression for respiratory and heart dysfunction in muscular dystrophy based on data taken at 8 weeks of age in mouse model of muscular dystrophy. This model parallels studies in human DMD and myotonic dystrophy suggesting that the abdominal muscles are "paradoxically" recruited during inspiration to compensate for diaphragm paralysis and maintain function (Smith et al., 1989; Ugalde et al., 2001). Mice with poor heart function had higher levels of fibrosis in the abdominal muscles, suggesting a relationship between abdominal muscle health and heart function. Furthermore, animals with the highest levels of abdominal fibrosis had relatively low levels of diaphragm fibrosis, and vice versa. This relationship is supportive of a model in which these two organs are compensatory to one another.

primary muscle of expiration (Ugalde et al., 2001). Advanced plethsymography methods have been used to characterize respiratory mechanics in DMD patients (D'Angelo et al., 2011; Lo Mauro et al., 2010; Lomauro et al., 2013; Mauro et al., 2009; Romei et al., 2012). With disease progression, DMD patients demonstrated less abdominal wall distention during normal inspiration in the supine position. It was suggested that these low abdominal volume changes during inspiration correlate strongly with nocturnal hypoxemia, serving as a predictor of nocturnal desaturation. These data are congruent with other observations that the paradoxical activation of the abdominal muscles during inspiration may help expand the chest wall and thoracic cavity during inspiration (Ugalde et al., 2001). Abdominal muscle activation may also enhance venous return to the heart by further lowering thoracic pressures. Clinically, supporting the abdominal muscles may increase both heart and lung function. Indeed, abdominal binding has been shown to improve cardiac function in a handful of patients with spinal cord injury (West et al., 2012).

Supporting and maintaining proper cardiopulmonary function in neuromuscular disease is a mainstay of therapy. Sufficient ventilation is important for preventing hypoxia and acidosis; two conditions that exacerbate cardiomyocyte dysfunction (Portal et al., 2013; Tanaka et al., 1994). Maintaining diaphragm health has been the focus of many studies in both humans and mice with muscular dystrophy, but few studies have focused on supporting and evaluating the accessory muscles of respiration such as the abdominal muscles. Therapies that spare the muscles of respiration in muscular dystrophy have been shown to slow down overall disease progression and prolong life (Kohler et al., 2009; Smith et al., 1989). The effects of nocturnal noninvasive ventilation

on the accessory muscles of respiration are relatively unknown. The accessory muscles of respiration, whether in human patients or animal models, may prove a viable target especially for therapy directed at specific muscle groups. The abdominal muscles are easily accessible and dissectible in mice, making them readily available for study.

Chapter 5

Discussion

Portions of this text derive from a Chapter entitled “Abnormal Muscle Physiology” appearing in Cardioskeletal Myopathies in Children and Young Adults by EM McNally, BB Gardner, S. Bogdanovich. (eds. Towbin, Jefferies, Blaxall, Robbins, Elsevier)

Summary

In this dissertation I discuss two main lines of experiments. The first line of experiments assesses the effect of neutralizing or limiting the activation of TGFβ isoforms in a mouse model of muscular dystrophy. The results of these studies potentially pave the path towards a biological therapy for patients with muscular dystrophy. The second line of experiments examined the differential disease involvement of muscle groups, including the heart muscle, in a separate but related mouse model of muscular dystrophy. The findings from this work provide important insight into potential endpoints for clinical trials and also yield clues as to the inter-relationship between heart function and breathing muscles. These two areas are tied together in that the breathing muscles, the diaphragm and as I have shown the abdominal muscles, demonstrate the most profound pathological changes in animal models of muscular dystrophy and therefore these muscles are critical to assessing new and developing therapies. In this Chapter, I will discuss the repercussions from both lines of experimentation.

Approaches and Implications of blocking TGFβ in Muscular Dystrophy

Several different biologic, genetic, and non-biologic approaches have been taken to assess whether inhibiting the TGFβ pathway is useful in mouse models of muscular dystrophy. An early approach to inhibiting TGFβ, albeit indirectly and nonspecifically, relied on using losartan, an angiotension receptor blocker (Cohn et al., 2007b). In this same study, a pan-TGFβ neutralizing antibody was tested for its effects on regeneration after cardiotoxin injury. The losartan studies were carried out on a longer timeframe with clear reduction in fibrosis and promotion of regeneration in skeletal muscle in the mdx mouse model. These and other data suggested that this approach can have some use and indeed, it has now become a recommendation to treat Duchenne Muscular Dystrophy with compounds in this pathway, as these drugs are approved by the Food and Drug Administration for the treatment of heart failure (Allen et al., 2013; Bish et al., 2011; Fakhfakh et al., 2012; Spurney et al., 2011). A more direct approach to inhibiting TGFβ was examined using the pan-TGFβ 1D11 antibody (Nelson et al., 2011b), although the results by some were felt to be rather disappointing. The Nelson study did show improvement in the diaphragm muscle and in respiratory function, but did not see as much improvement in other skeletal muscles. One potential explanation for this limited effect could be the use of the *mdx* mouse model in the traditional C57Bl10 background. This model has less evident fibrosis and therefore it may be difficult to see an effect where the pathological process is so much less than what occurs in the human setting. Since the *mdx* diaphragm muscle is thought to more closely replicate the human DMD process (Stedman et al., 1991), it is possible that the diaphragm results are actually most important. Another interpretation is that the therapeutic window for

blocking TGFβ itself is limited by TGFβ widespread expression. More potent means of blocking TGFβ throughout the body may actually be associated with unacceptable side effects. It was for this reason that isoform specific TGFβ antibodies were tested and anti-LTBP4 antibodies were developed. Understanding the mechanism and forces required for TGFβ activation from LAP is key to the development of small molecule based therapies aimed at disrupting TGFβ activation.

Anti-TGFβ antibodies in pre-clinical models of muscular dystrophy

Increased TGFβ signaling is a hallmark of muscular dystrophy and anti-TGFβ antibodies have been shown to increase muscle function and reduce fibrosis in the *mdx* mouse model of muscular dystrophy (Nelson et al., 2011a). The data presented in Chapter 2 are generally in agreement with these findings, although the shorter duration of testing is a key difference. In Chapter 2, we found that anti-TGFβ2 antibodies and anti-TGFβ3 antibodies elicited some of the same effects as pan-TGFβ neutralization, suggesting that each isoform may contribute to the same pathways of injury repair and regeneration, including effects on fibrosis. It was recently suggested that TGFβ2 was most critical for muscle regeneration (Biressi et al., 2014) with a direct effect on myoblast differentiation. It is possible that TGFβ3 alters distinct aspects of the repair rather than the regeneration process. While each TGFβ isoform may have different direct functions in muscle injury, repair, and regeneration, indirect effects may account for the general trends. For example, partially inhibiting regeneration in the situation where fibrosis is present may actually have beneficial effects. Long term pre-clinical

investigation of TGFβ neutralization is needed to address these effects especially in the setting of a chronic disease like muscular dystrophy.

TGFβ Receptor Type 1 Blockade

TGFβ homodimers are secreted in the extracellular matrix (ECM) bound non-covalently by a pro-domain that is in turn bound to latent binding proteins, typically LTBP1, LTBP2 or LTBP4. TGFβ remains inactive in the ECM until activating events physically decouple TGFβ from its pro-domain, also referred to as the latency associated peptide (LAP). The LAP itself appears to sterically hinder TGFβ-homodimers from binding the TGFβ type 1 receptor, but can be unbound from LAP with high heat, pH, proteolysis or physical force and then activated to a bound state. The LAP monomer contains an αvβ6 integrin binding Arginine-Glycine-Aspartic Acid (RGD) sequence important in TGFβ activation for many cell types, including myofibroblasts. Interestingly, the RGD sequence contained within the LAP can only activate TGFβ when LAP is bound to LTBP family members specifically (Kantola et al., 2008). Deletion of the αvβ6 integrin from mice recapitulates a phenotype consistent with a TGFβ null mouse (Yang et al., 2007). Buscemi et al. observed activation of TGFβ signaling only if the LAP was tethered to ECM via its adaptor protein, LTBP-1. When LAP was tethered to mica and tugged, TGFβ activation was not significantly increased above background (Buscemi et al., 2011). Although not directly visualized, they predicted that TGFβ release should occur at 40 pN of force applied to LAP dimers bound to ECM. They propose an “all-or-nothing” snap mechanism for TGFβ release, in which the LAP dimer becomes

denatured to a new stable confirmation when force is applied beyond a given threshold, thereby releasing TGFβ. Identifying the force required to liberate TGFβ activation would help validate this model of mechanical release. Additionally, it is possible that less force is required for activation, which would favor the application of small molecular therapies aimed at disrupting TGFβ activation. Therapies aimed at keeping LAP "closed" have been proposed, but the force required to keep LAP inactivated is unknown (Rifkin, 2005).

Inhibition of the SMAD pathway

Intracellular TGFβ signaling occurs through the canonical (SMAD) pathway as well as non-canonical pathways. SMAD signaling can be targeted directly and indirectly, although lacks specificity to muscle since this pathway is ubiquitously present and activated in response to TGFβ. In a Drosophila model of muscular dystrophy, genetic reduction of SMAD by use of heterozygous co-SMAD mutations was observed to improve walking function and heart tube contractility (Goldstein et al., 2011). Because "dystrophic flies" do not demonstrate fibrosis, this finding suggests that partial inhibition of SMAD activity in the muscle cells themselves is actually beneficial. A similar finding was documented using heterozygous deletion of SMAD4 in a mouse model of muscular dystrophy where improved cardiac function and skeletal muscle pathology was seen (Goldstein et al., 2014). Together these data suggest that muscle intrinsic features of pathology may be improved by decreasing intracellular TGFβ signaling.

LTBP4 antibody design, optimization and assessment

Antibodies directed against LTBP4 were developed and tested as a means of reducing TGFβ liberation and activation in Chapter 3. This anti-LTBP4 approach is unique from the prior methods of TGFβ neutralization in that it has the added theoretical benefit of 1) blocking TGFβ at an upstream part of the pathway prior to release from latency and 2) neutralizing multiple TGFβ isoforms at once in a stoichiometry relative to the expressional levels of the TGFβ isoforms in the underlying tissue. Some basal level of paracrine-induced TGFβ activation is needed for regular function in nearly all cell types and may be why many pre-clinical trials have experienced diminished affects of long-term anti-TGFβ therapy (De Luca, 2012; Nelson et al., 2011a). TGFβ is highly expressed and known to be important in the lungs, spleen, liver, testes in addition to muscle and direct ablation of TGFβ likely disrupts function in other more acutely vital organs (Robertson et al., 2015). In this way, the upstream nature of anti-LTBP4 stabilization would have a different tissue specific affect than direct neutralizing of TGFβ would. LTBP4 is not as widely expressed as TGFβ, and has secondary functions as a matrix scaffolding protein, similar to fibrillin. Its role as a scaffolding protein binding elastin and fibrillin-layered microfibrils is important to consider in discerning its role in muscle and how this may modify disease. It is possible that LTBP4 serves as a signal of elastic fiber damage. How LTBP4 changes the matrix stiffness compared to other "fibrillin-like" proteins is unknown. In Chapter 3, we found that anti-LTBP4 antibodies showed reductions in pathologic markers such as fibrosis and inflammation suggesting that this approach is feasible. A comparison of the two antibody mediated approaches is shown in **Figure 5.1**.

A key to refining this approach will be a better understanding of how LTBP4 is activated and specifically how this is coupled to TGFβ activation. The structure of LTBP4 has not been well characterized but important domains, such as the 8-cysteine TGFβ region as well as TGFβ itself seated within its latency associated peptide (LAP) is known. LTBP4 likely confers latency to the TGFβ LAP domain by steric hindrance of the proline rich arm that prevents access to TGFβ. The TGFβ LAP domain itself contains a uniquely placed RGD sequence that binds cellular integrins, and when under traction can apply forces that unbind TGFβ. This may be one major method of activation in normal healthy muscle that is misaligned in muscular dystrophy in addition to other pathology that includes increased levels of thromobospondin, a TGFβ activating serum protein. There is strong correlative evidence that suggest myofibroblasts activate TGFβ primarily through cellular traction forces applied through integrins (Aluwihare et al., 2009). Further work is needed to elucidate the role of LTBP4 in muscle and what population of cells produce the two seemingly different pools of TGFβ. One pool of LTBP4 was observed to be enriched between myofibers in a similar location to laminin (Lamar et al., 2016a). A second pool of LTBP4 was seen in a striated, costameric pattern that is very closely apposed to the sarcolemma. It is likely that this pool is made by myofibers themselves due to its close proximity to myofiber membrane. The more distal pool is of unknown cellular origin, but looks similar to many large collagen fibrils observed recently and may be of fibroblastic origin. The LTBP4 that is adherent to the sarcolemma may be particularly important for signaling within the myofibers.

Animal models of muscular dystrophy and cardiopulmonary findings.

In Chapter 4, I outlined findings in a large cohort of Sgcg animals that were characterized for cardiac and muscle pathology at 8 weeks of age. This represents a relatively early timepoint in mouse muscular dystrophy pathology, but one that proved useful for making correlations between cardiac function and specific muscle pathology. Both human patients and animals with muscular dystrophy experience early and severe impairment of the respiratory muscles. The diaphragm of the *mdx* mouse recapitulates many of the histological changes the DMD human diaphragm undergoes including pseudohypertrophy, varying fiber size, necrosis and inflammatory infiltrate (Stedman et al., 1991). Remarkably, the abnormal histopathology in the *mdx* mouse diaphragm can be detected using whole body plethysmography (WBP) (Gayraud et al., 2007; Ishizaki et al., 2008; Nelson et al., 2011a). Ex vivo muscle mechanical experiments on the *mdx* diaphragm revealed functional changes in force that are reflected by reduced twitch and contraction properties. In older *mdx* mice, collagen content is increased 7 to 10 times compared to wildtype mice in both the diaphragm and leg muscles. Diaphragm dysfunction has been characterized in other animal models as well. Respiratory insufficiency as a cause of death in DMD was studied in the golden retriever muscular dystrophy model. The authors noted diaphragm remodeling and compensatory mechanics that grew worse over time based on plethysmography in the living animal and correlating this with histology post mortem. The failing late-stage diaphragm became a passive organ and the work of breathing was transmitted to the abdominal muscles among other accessory muscles of respiration (DeVanna et al., 2014; Mead et al., 2014). It appears that the diaphragm is particularly sensitive to Ca^{2+} mishandling,

and overexpression of the sarcoplasmic reticulum calcium pump in diaphragm alone reduced centrally nucleated fibers and rescued dysfunction measured as resistance to injury after lengthening contractions in *mdx* mice (Avitabile et al., 2014; Morine et al., 2010).

Most mouse models of muscular dystrophy do not develop a cardiac phenotype as severe as human patients, and therefore, double knockouts and transgenic mice have been created to amplify cardiomyopathy and better model human disease. One such model is the *mdx* allele combined with a null allele for the myogenic regulatory transcription factor MyoD (*mdx/Myod*$^{-/-}$) (Megeney et al., 1999). This unique model lacks both dystrophin and MyoD, a muscle specific transcription factor important for stem cell differentiation into muscle cells during development and regeneration. Despite no role for MyoD in cardiac muscle, *mdx/Myod*$^{-/-}$ mice developed cardiomyopathy, which likely reflects the degree to which accelerated skeletal muscle pathology induces cardiac pathology. Histologically, these mice have apical foci, with both necrosis and fibrosis in the left ventricle. This phenotype characteristically develops over time as a failed compensatory mechanism to initial left ventricle overload and hypertrophy.

Cardiorespiratory decline in Muscular Dystrophy

Boys with DMD aged from 6-14 years old show a steady decline in some but not all respiratory parameters, and it is during this same interval that early phase cardiomyopathy becomes clinically evident along with sinus tachycardia. Sensitive measures of pulmonary dysfunction include sniff nasal inspiratory pressure (SNIP), forced vital capacity, and diaphragmatic tension-time index (TTdi) (Anderson et al.,

2012; Connolly et al., 2015). The first two values are related to a patient's ability to produce cough, while the last is a measure of the diaphragm's resistance to fatigue.

Another muscle disease with preferential diaphragm involvement is Pompe disease, a glycogen storage disease caused by a mutation in the acid α-glucosidase gene. In mice, certain pharmacological agents provide additional phrenic and hypoglossal nerve stimulus and increase respiratory drive and reduce respiratory variation (ElMallah et al., 2015). In human Pompe, gene therapy restoration of enzyme deficiency in the diaphragm muscle has been used to reduce ventilatory time (Smith et al., 2013). A 14 year longitudinal study in DMD observed a correlation between respiratory functional decline and overall measures of disease progression as monitored by echocardiography (Khirani et al., 2014b). They also observed that early respiratory functional decline was noted in groups of patients who lost their ambulation at the age of 8 more often than those who lost it at a mean age of 16.

As severe skeletal muscle disease, particularly as it affects the respiratory muscle, can impair cardiac muscle function, it is possible that in heart failure and congenital heart disease, there may be concomitant skeletal muscle dysfunction (Alonso-Gonzalez et al., 2013; Buber and Rhodes, 2014; Middlekauff, 2010). The diaphragm muscle is a highly oxidative organ making it particularly susceptible to hypoxia, and therefore the diaphragm may more readily exhibit a secondary response to compensatory recruitment of the diaphragm and respiratory muscles in response to heart failure. Diaphragm dysfunction may be monitored in heart failure as reduced dynamic lung volumes measured as forced expiratory volume/1 second and forced vital capacity.

Inspiratory Muscles in Muscular Dystrophy.

The primary muscles active during inspiration are the diaphragm, scalenes, parasternals, external intercostals and the transverse abdominis. During inspiration, the respiratory muscles expand the thoracic cavity in as efficient a manner as possible, thereby reducing the relative pressure of this compartment in accordance with Boyle's law. The diaphragm is the most important muscle in this process, and is closely related to the lungs through its superior surface, attaching to the inferior parietal-pleura. During inspiration, the diaphragm is displaced caudally and anteriorly, displacing abdominal contents and raising the pressure of the abdominal compartment. As the abdomen is displaced, the rectus abdominis relaxes while the transverse abdominis contracts slightly, helping to flatten the diaphragm as it draws the inferior parietal pleura caudally as well.

The diaphragm is a complex muscle with unique anatomy, developmental origins and biomechanical insertion points. In development, the diaphragm appears during the fourth week and is a fusion of two distinct structures, the septum transversum from lumbar mesoderm and pleuroperitoneal folds (Merrell and Kardon, 2013). In adult humans, the diaphragm is dome shaped and mostly muscular, with the exception of the central tendon that is connective and non-contractile. Its proximal insertion points span the T8-12 vertebrae, serving as a fairly immobile anchoring point. Distally, the diaphragm inserts on the inferior costal surface of the thoracic ribs. These anchoring points, combined with the fan like array of myofiber organization best suits the

diaphragm for compressing abdominal contents infero-anteriorly, especially when the rectus abdominis muscles are relaxed.

The diaphragm is the most well characterized respiratory organ in animal models of muscular dystrophy. Correlating diaphragm fibrosis to respiratory function in humans has been difficult but has been accomplished with moderate success in the *mdx* mouse (Ishizaki et al., 2008). Notably, another study found that correction of the gene deletion in the *mdx* mouse under a diaphragm specific promoter increased cardiac function in addition to pulmonary function (Crisp et al., 2011). Most animal and human forms of muscular dystrophy have diaphragm involvement, and preserving diaphragm function is a therapeutic goal. It is notable that the diaphragm muscle, because of its discrete position and limited mass and thickness, is a highly tractable target for gene therapy and other targeted correction methods (Ishizaki et al., 2011).

The primary muscles of expiration are the rectus abdominis, internal intercostals and triangularis sterni. Of these, the rectus abdominis are the most important, although little activation of expiratory muscle is necessary during quiet respiration in healthy subjects. Alveolar elasticity combined with diaphragm relaxation at the end of inspiration provides most of the force needed for tidal expiration. However, when healthy subjects are stressed by exercise, or under duress, the abdominal muscles are recruited heavily during expiration and, in muscular dystrophy patients, the abdominal muscles are similarly recruited for respiration. In muscular dystrophy, the abdominal muscles are recruited more than expected during expiration, and sometimes, during inspiration as well (Lo Mauro et al., 2010; LoMauro et al., 2014).

Generating a productive cough is key to preventing respiratory tract infection, and maintenance of cough or use of cough assist devices is critical with muscle disease. Forced vital capacity, sniff inspiratory pressure, and peak expiratory velocity are three important pulmonary function measurements that are measures of expiratory muscle functional decline. An understanding of the compensatory mechanisms used to compensate for respiratory muscle failure in end-stage muscle disease is important. As respiratory muscles fail in end-stage DMD, some patients will develop paradoxical chest-wall mechanics, while others will not, suggesting that individuals with similar underlying mutations can develop unique compensatory mechanisms (Khirani et al., 2014a). Posture plays a large role in determining respiratory muscles. Therefore, the posture of patients and animals is important to take into account when comparing physiologic studies of respiration in muscular dystrophy. To this end, supine measurements of forced vital capacity may provide one of the early and sensitive measures of respiratory muscle decline in DMD (Mayer et al., 2015; Seferian et al., 2015; Yasuma et al., 2001). A normal seated forced vital capacity in the face of an abnormal supine forced vital capacity is attributed to the fact that the diaphragm operates more efficiently on its length-tension curve in the seated position.

In Chapter 4, we showed that the abdominal and diaphragm muscle pathology correlated strongly with cardiac outcomes in the Sgcg mouse model. Extrapolating these findings to what is known about human muscular dystrophy, cardiomyopathy and physiology, suggests strongly that the abdominal muscles are being recruited as accessory muscles of respiration. The finding of profound pathological changes in this muscle group provides another useful muscle group for monitoring pre-clinical testing

and better understanding the molecular defects that lead to disease. It remains a significant problem for the field that mouse models do not fully recapitulate the severity of skeletal and cardiac phenotypes as their human counterpart diseases. The findings in this thesis provide new approaches to reduce the hyper-TGFβ state that accompanies muscular dystrophy and importantly novel pre-clinical measures to document the utility of this inhibition.

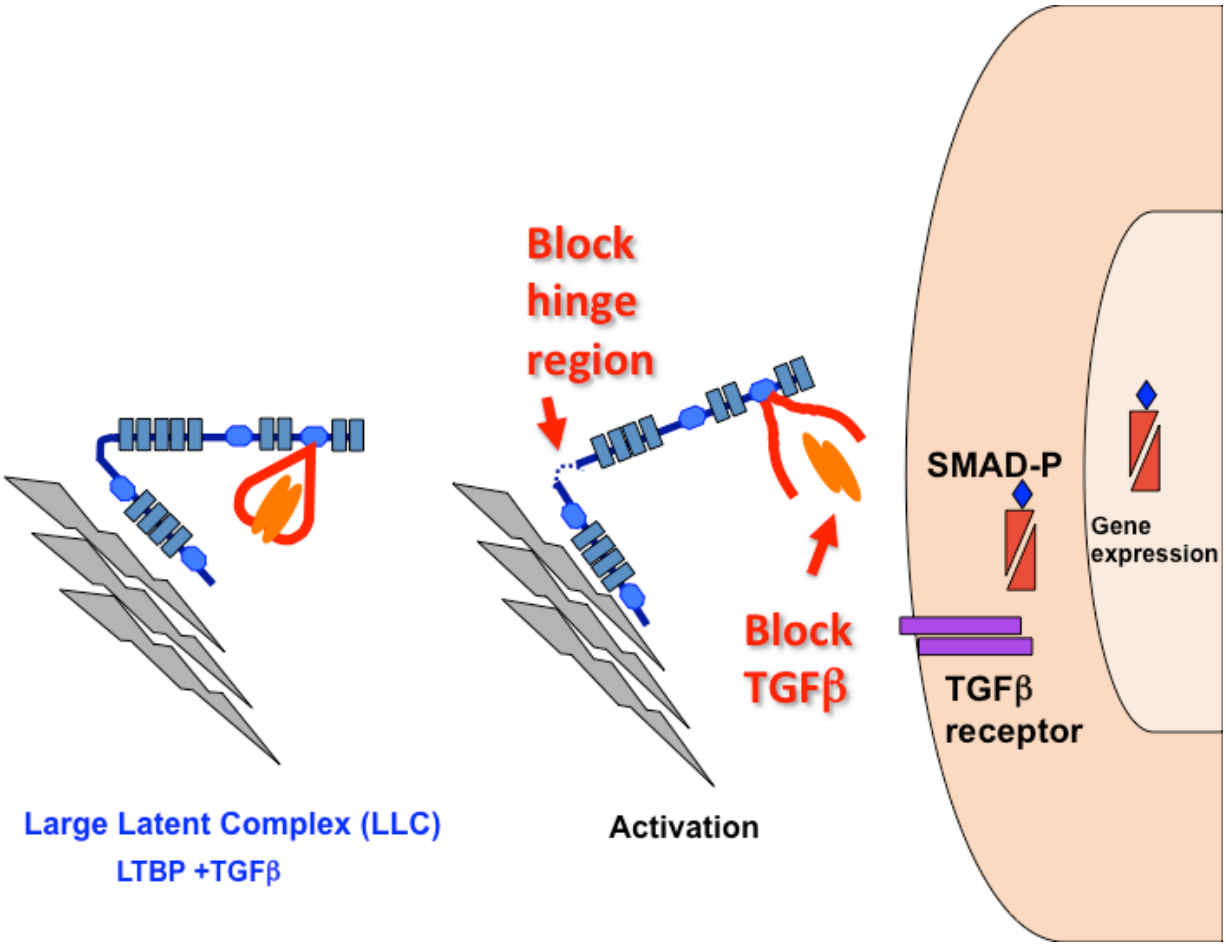

Figure 5.1 A schematic of the approaches used to block TGFβ activity or release is shown. Our anti-LTBP-4 antibodies were generated against the proline rich "hinge" region of the protein. This unique region has been shown to be critical in confering a latency to TGFβ family members. Via mechanisms that are still poorly understood, this specialized region must be cleaved and disjointed in order to release TGFβ. We hope to stabilizing this proline rich "hinge" region against enzymatic attack, thereby preventing release of TGFβ.

LITERATURE CITED

Alexander, J.M., and B.G. Bruneau. 2010. Lessons for cardiac regeneration and repair through development. *Trends in molecular medicine*. 16:426-434.

Allen, D.G., and N.P. Whitehead. 2011. Duchenne muscular dystrophy--what causes the increased membrane permeability in skeletal muscle? *The international journal of biochemistry & cell biology*. 43:290-294.

Allen, H.D., K.M. Flanigan, P.T. Thrush, I. Dvorchik, H. Yin, C. Canter, A.M. Connolly, M. Parrish, C.M. McDonald, E. Braunlin, S.D. Colan, J. Day, B. Darras, and J.R. Mendell. 2013. A randomized, double-blind trial of lisinopril and losartan for the treatment of cardiomyopathy in duchenne muscular dystrophy. *PLoS currents*. 5.

Alonso-Gonzalez, R., F. Borgia, G.P. Diller, R. Inuzuka, A. Kempny, A. Martinez-Naharro, O. Tutarel, P. Marino, K. Wustmann, M. Charalambides, M. Silva, L. Swan, K. Dimopoulos, and M.A. Gatzoulis. 2013. Abnormal lung function in adults with congenital heart disease: prevalence, relation to cardiac anatomy, and association with survival. *Circulation*. 127:882-890.

Aluwihare, P., Z. Mu, Z. Zhao, D. Yu, P.H. Weinreb, G.S. Horan, S.M. Violette, and J.S. Munger. 2009. Mice that lack activity of alphavbeta6- and alphavbeta8-integrins reproduce the abnormalities of Tgfb1- and Tgfb3-null mice. *Journal of cell science*. 122:227-232.

Ameen, V., and L.G. Robson. 2010. Experimental models of duchenne muscular dystrophy: relationship with cardiovascular disease. *The open cardiovascular medicine journal*. 4:265-277.

Amenta, A.R., A. Yilmaz, S. Bogdanovich, B.A. McKechnie, M. Abedi, T.S. Khurana, and J.R. Fallon. 2011. Biglycan recruits utrophin to the sarcolemma and counters dystrophic pathology in mdx mice. *Proc Natl Acad Sci U S A*. 108:762-767.

Anderson, V.B., J.A. McKenzie, C. Seton, D.A. Fitzgerald, R.I. Webster, K.N. North, D.A. Joffe, and H.K. Young. 2012. Sniff nasal inspiratory pressure and sleep disordered breathing in childhood neuromuscular disorders. *Neuromuscul Disord*. 22:528-533.

Avitabile, C.M., M.B. Leonard, B.S. Zemel, J.L. Brodsky, D. Lee, K. Dodds, C. Hayden-Rush, K.K. Whitehead, E. Goldmuntz, S.M. Paridon, J. Rychik, and D.J. Goldberg. 2014. Lean mass deficits, vitamin D status and exercise capacity in children and young adults after Fontan palliation. *Heart*. 100:1702-1707.

Azibi, K., L. Bachner, J.S. Beckmann, K. Matsumura, E. Hamouda, M. Chaouch, A. Chaouch, R. Ait-Ouarab, A. Vignal, J. Weissenbach, and et al. 1993. Severe childhood autosomal recessive muscular dystrophy with the deficiency of the 50 kDa dystrophin-associated glycoprotein maps to chromosome 13q12. *Hum Mol Genet*. 2:1423-1428.

Beggs, A.H., E.P. Hoffman, J.R. Snyder, K. Arahata, L. Specht, F. Shapiro, C. Angelini, H. Sugita, and L.M. Kunkel. 1991. Exploring the molecular basis for variability among patients with Becker muscular dystrophy: dystrophin gene and protein studies. *Am J Hum Genet*. 49:54-67.

Bello, L., A. Kesari, H. Gordish-Dressman, A. Cnaan, L.P. Morgenroth, J. Punetha, T. Duong, E.K. Henricson, E. Pegoraro, C.M. McDonald, and E.P. Hoffman. 2015. Genetic modifiers of ambulation in the Cooperative International Neuromuscular Research Group Duchenne Natural History Study. *Ann Neurol*. 77:684-696.

Bernasconi, P., E. Torchiana, P. Confalonieri, R. Brugnoni, R. Barresi, M. Mora, F. Cornelio, L. Morandi, and R. Mantegazza. 1995. Expression of transforming growth factor-beta 1 in dystrophic patient muscles correlates with fibrosis. Pathogenetic role of a fibrogenic cytokine. *The Journal of clinical investigation*. 96:1137-1144.

Bies, R.D., C.T. Caskey, and R. Fenwick. 1992. An intact cysteine-rich domain is required for dystrophin function. *The Journal of clinical investigation*. 90:666-672.

Biressi, S., E.H. Miyabara, S.D. Gopinath, P.M. Carlig, and T.A. Rando. 2014. A Wnt-TGFbeta2 axis induces a fibrogenic program in muscle stem cells from dystrophic mice. *Science translational medicine*. 6:267ra176.

Bish, L.T., M. Yarchoan, M.M. Sleeper, J.A. Gazzara, K.J. Morine, P. Acosta, E.R. Barton, and H.L. Sweeney. 2011. Chronic losartan administration reduces mortality and preserves cardiac but not skeletal muscle function in dystrophic mice. *PloS one*. 6:e20856.

Bladen, C.L., D. Salgado, S. Monges, M.E. Foncuberta, K. Kekou, K. Kosma, H. Dawkins, L. Lamont, A.J. Roy, T. Chamova, V. Guergueltcheva, S. Chan, L. Korngut, C. Campbell, Y. Dai, J. Wang, N. Barisic, P. Brabec, J. Lahdetie, M.C. Walter, O. Schreiber-Katz, V. Karcagi, M. Garami, V. Viswanathan, F. Bayat, F. Buccella, E. Kimura, Z. Koeks, J.C. van den Bergen, M. Rodrigues, R. Roxburgh, A. Lusakowska, A. Kostera-Pruszczyk, J. Zimowski, R. Santos, E. Neagu, S. Artemieva, V.M. Rasic, D. Vojinovic, M. Posada, C. Bloetzer, P.Y. Jeannet, F. Joncourt, J. Diaz-Manera, E. Gallardo, A.A. Karaduman, H. Topaloglu, R. El

Sherif, A. Stringer, A.V. Shatillo, A.S. Martin, H.L. Peay, M.I. Bellgard, J. Kirschner, K.M. Flanigan, V. Straub, K. Bushby, J. Verschuuren, A. Aartsma-Rus, C. Beroud, and H. Lochmuller. 2015. The TREAT-NMD DMD Global Database: Analysis of More than 7,000 Duchenne Muscular Dystrophy Mutations. *Human mutation*.

Bogdanovich, S., T.O. Krag, E.R. Barton, L.D. Morris, L.A. Whittemore, R.S. Ahima, and T.S. Khurana. 2002. Functional improvement of dystrophic muscle by myostatin blockade. *Nature*. 420:418-421.

Bogdanovich, S., E.M. McNally, and T.S. Khurana. 2008. Myostatin blockade improves function but not histopathology in a murine model of limb-girdle muscular dystrophy 2C. *Muscle Nerve*. 37:308-316.

Border, W.A., and N.A. Noble. 1994. Transforming growth factor beta in tissue fibrosis. *N Engl J Med*. 331:1286-1292.

Bostick, B., Y. Yue, C. Long, and D. Duan. 2008. Prevention of dystrophin-deficient cardiomyopathy in twenty-one-month-old carrier mice by mosaic dystrophin expression or complementary dystrophin/utrophin expression. *Circ Res*. 102:121-130.

Brown, S.C.a.L., J.L. 1997. Dystrophin: Gene, Protein and Cell Biology. Cambridge University Press, Cambridge.

Buber, J., and J. Rhodes. 2014. Exercise physiology and testing in adult patients with congenital heart disease. *Heart failure clinics*. 10:23-33.

Bulfield, G., W.G. Siller, P.A. Wight, and K.J. Moore. 1984. X chromosome-linked muscular dystrophy (mdx) in the mouse. *Proc Natl Acad Sci U S A*. 81:1189-1192.

Burks, T.N., and R.D. Cohn. 2011. Role of TGF-beta signaling in inherited and acquired myopathies. *Skelet Muscle*. 1:19.

Buscemi, L., D. Ramonet, F. Klingberg, A. Formey, J. Smith-Clerc, J.J. Meister, and B. Hinz. 2011. The single-molecule mechanics of the latent TGF-beta1 complex. *Current biology : CB*. 21:2046-2054.

Carlson, B.M., and J.A. Faulkner. 1983. The regeneration of skeletal muscle fibers following injury: a review. *Medicine and science in sports and exercise*. 15:187-198.

Carter, G.T., M.A. Wineinger, S.A. Walsh, S.J. Horasek, R.T. Abresch, and W.M. Fowler, Jr. 1995. Effect of voluntary wheel-running exercise on muscles of the mdx mouse. *Neuromuscul Disord*. 5:323-332.

Ceco, E., S. Bogdanovich, B. Gardner, T. Miller, A. DeJesus, J.U. Earley, M. Hadhazy, L.R. Smith, E.R. Barton, J.D. Molkentin, and E.M. McNally. 2014. Targeting latent TGFbeta release in muscular dystrophy. *Science translational medicine*. 6:259ra144.

Chang, N.C., and M.A. Rudnicki. 2014. Satellite cells: the architects of skeletal muscle. *Curr Top Dev Biol*. 107:161-181.

Chapman, V.M., D.R. Miller, D. Armstrong, and C.T. Caskey. 1989. Recovery of induced mutations for X chromosome-linked muscular dystrophy in mice. *Proc Natl Acad Sci U S A*. 86:1292-1296.

Charge, S.B., and M.A. Rudnicki. 2004. Cellular and molecular regulation of muscle regeneration. *Physiological reviews*. 84:209-238.

Chen, Y.W., K. Nagaraju, M. Bakay, O. McIntyre, R. Rawat, R. Shi, and E.P. Hoffman. 2005. Early onset of inflammation and later involvement of TGFbeta in Duchenne muscular dystrophy. *Neurology*. 65:826-834.

Cheung, T.H., and T.A. Rando. 2013. Molecular regulation of stem cell quiescence. *Nature reviews. Molecular cell biology*. 14:329-340.

Chin, G.S., W. Liu, Z. Peled, T.Y. Lee, D.S. Steinbrech, M. Hsu, and M.T. Longaker. 2001. Differential expression of transforming growth factor-beta receptors I and II and activation of Smad 3 in keloid fibroblasts. *Plast Reconstr Surg*. 108:423-429.

Coffey, A.J., R.G. Roberts, E.D. Green, C.G. Cole, R. Butler, R. Anand, F. Giannelli, and D.R. Bentley. 1992. Construction of a 2.6-Mb contig in yeast artificial chromosomes spanning the human dystrophin gene using an STS-based approach. *Genomics*. 12:474-484.

Cohn, R.D., C. van Erp, J.P. Habashi, A.A. Soleimani, E.C. Klein, M.T. Lisi, M. Gamradt, C.M. ap Rhys, T.M. Holm, and B.L. Loeys. 2007a. Angiotensin II type 1

receptor blockade attenuates TGF-β–induced failure of muscle regeneration in multiple myopathic states. *Nature medicine*. 13:204-210.

Cohn, R.D., C. van Erp, J.P. Habashi, A.A. Soleimani, E.C. Klein, M.T. Lisi, M. Gamradt, C.M. ap Rhys, T.M. Holm, B.L. Loeys, F. Ramirez, D.P. Judge, C.W. Ward, and H.C. Dietz. 2007b. Angiotensin II type 1 receptor blockade attenuates TGF-beta-induced failure of muscle regeneration in multiple myopathic states. *Nat Med*. 13:204-210.

Connolly, A.M., E.C. Malkus, J.R. Mendell, K.M. Flanigan, J.P. Miller, J.R. Schierbecker, C.A. Siener, P.T. Golumbek, C.M. Zaidman, C.M. McDonald, L. Johnson, A. Nicorici, P.I. Karachunski, J.W. Day, J.M. Kelecic, L.P. Lowes, L.N. Alfano, B.T. Darras, P.B. Kang, J. Quigley, A.E. Pasternak, J.M. Florence, and M.D.C.R. Network. 2015. Outcome reliability in non-Ambulatory Boys/Men with duchenne muscular dystrophy. *Muscle Nerve*. 51:522-532.

Cooper, B.J., N.J. Winand, H. Stedman, B.A. Valentine, E.P. Hoffman, L.M. Kunkel, M.O. Scott, K.H. Fischbeck, J.N. Kornegay, R.J. Avery, and et al. 1988. The homologue of the Duchenne locus is defective in X-linked muscular dystrophy of dogs. *Nature*. 334:154-156.

Costamagna, D., M. Quattrocelli, R. Duelen, V. Sahakyan, I. Perini, G. Palazzolo, and M. Sampaolesi. 2014. Fate choice of post-natal mesoderm progenitors: skeletal versus cardiac muscle plasticity. *Cellular and molecular life sciences : CMLS*. 71:615-627.

Coulton, G.R., J.E. Morgan, T.A. Partridge, and J.C. Sloper. 1988. The mdx mouse skeletal muscle myopathy: I. A histological, morphometric and biochemical investigation. *Neuropathol Appl Neurobiol*. 14:53-70.

Cox, G.A., S.F. Phelps, V.M. Chapman, and J.S. Chamberlain. 1993. New mdx mutation disrupts expression of muscle and nonmuscle isoforms of dystrophin. *Nat Genet*. 4:87-93.

Crisp, A., H. Yin, A. Goyenvalle, C. Betts, H.M. Moulton, Y. Seow, A. Babbs, T. Merritt, A.F. Saleh, M.J. Gait, D.J. Stuckey, K. Clarke, K.E. Davies, and M.J. Wood. 2011. Diaphragm rescue alone prevents heart dysfunction in dystrophic mice. *Hum Mol Genet*. 20:413-421.

Crosbie, R.H., L.E. Lim, S.A. Moore, M. Hirano, A.P. Hays, S.W. Maybaum, H. Collin, S.A. Dovico, C.A. Stolle, M. Fardeau, F.M. Tome, and K.P. Campbell. 2000.

Molecular and genetic characterization of sarcospan: insights into sarcoglycan-sarcospan interactions. *Hum Mol Genet*. 9:2019-2027.

D'Angelo, M.G., M. Romei, A. Lo Mauro, E. Marchi, S. Gandossini, S. Bonato, G.P. Comi, F. Magri, A.C. Turconi, A. Pedotti, N. Bresolin, and A. Aliverti. 2011. Respiratory pattern in an adult population of dystrophic patients. *Journal of the Neurological Sciences*. 306:54-61.

Dadgar, S., Z. Wang, H. Johnston, A. Kesari, K. Nagaraju, Y.W. Chen, D.A. Hill, T.A. Partridge, M. Giri, R.J. Freishtat, J. Nazarian, J. Xuan, Y. Wang, and E.P. Hoffman. 2014. Asynchronous remodeling is a driver of failed regeneration in Duchenne muscular dystrophy. *J Cell Biol*. 207:139-158.

Dahlqvist, J.R., L.G. Voss, T. Lauridsen, T.O. Krag, and J. Vissing. 2014. A pilot study of muscle plasma protein changes after exercise. *Muscle Nerve*. 49:261-266.

Dallas, S.L., J.L. Rosser, G.R. Mundy, and L.F. Bonewald. 2002. Proteolysis of latent transforming growth factor-beta (TGF-beta)-binding protein-1 by osteoclasts. A cellular mechanism for release of TGF-beta from bone matrix. *The Journal of biological chemistry*. 277:21352-21360.

Dasch, J.R., D.R. Pace, W. Waegell, D. Inenaga, and L. Ellingsworth. 1989. Monoclonal antibodies recognizing transforming growth factor-beta. Bioactivity neutralization and transforming growth factor beta 2 affinity purification. *J Immunol*. 142:1536-1541.

De Luca, A. 2012. Pre-clinical drug tests in the mdx mouse as a model of dystrophinopathies: an overview. *Acta myologica : myopathies and cardiomyopathies : official journal of the Mediterranean Society of Myology / edited by the Gaetano Conte Academy for the study of striated muscle diseases*. 31:40-47.

De Luca, A., S. Pierno, A. Liantonio, M. Cetrone, C. Camerino, B. Fraysse, M. Mirabella, S. Servidei, U.T. Ruegg, and D. Conte Camerino. 2003. Enhanced dystrophic progression in mdx mice by exercise and beneficial effects of taurine and insulin-like growth factor-1. *J Pharmacol Exp Ther*. 304:453-463.

Deconinck, A.E., J.A. Rafael, J.A. Skinner, S.C. Brown, A.C. Potter, L. Metzinger, D.J. Watt, J.G. Dickson, J.M. Tinsley, and K.E. Davies. 1997. Utrophin-dystrophin-deficient mice as a model for Duchenne muscular dystrophy. *Cell*. 90:717-727.

Deconinck, N., J.A. Rafael, G. Beckers-Bleukx, D. Kahn, A.E. Deconinck, K.E. Davies, and J.M. Gillis. 1998. Consequences of the combined deficiency in dystrophin and utrophin on the mechanical properties and myosin composition of some limb and respiratory muscles of the mouse. *Neuromuscul Disord*. 8:362-370.

Demonbreun, A.R., K.E. Swanson, A.E. Rossi, H.K. Deveaux, J.U. Earley, M.V. Allen, P. Arya, S. Bhattacharyya, H. Band, P. Pytel, and E.M. McNally. 2015. Eps 15 Homology Domain (EHD)-1 Remodels Transverse Tubules in Skeletal Muscle. *PloS one*. 10:e0136679.

DeVanna, J.C., J.N. Kornegay, D.J. Bogan, J.R. Bogan, J.L. Dow, and E.C. Hawkins. 2014. Respiratory dysfunction in unsedated dogs with golden retriever muscular dystrophy. *Neuromuscul Disord*. 24:63-73.

Dubowitz, V. 1975. Neuromuscular disorders in childhood. Old dogmas, new concepts. *Arch Dis Child*. 50:335-346.

ElMallah, M.K., S. Pagliardini, S.M. Turner, A.J. Cerreta, D.J. Falk, B.J. Byrne, J.J. Greer, and D.D. Fuller. 2015. Ampakines Stimulate Respiratory Motor Output and Ventilation in a Murine Model of Pompe Disease. *American journal of respiratory cell and molecular biology*.

Fakhfakh, R., Y. Lamarre, D. Skuk, and J.P. Tremblay. 2012. Losartan enhances the success of myoblast transplantation. *Cell transplantation*. 21:139-152.

Fayssoil, A., O. Nardi, D. Orlikowski, and D. Annane. 2010. Cardiomyopathy in Duchenne muscular dystrophy: pathogenesis and therapeutics. *Heart Fail Rev*. 15:103-107.

Feng, X.H., and R. Derynck. 2005. Specificity and versatility in tgf-beta signaling through Smads. *Annu Rev Cell Dev Biol*. 21:659-693.

Finsterer, J., and C. Stollberger. 2003. The heart in human dystrophinopathies. *Cardiology*. 99:1-19.

Finsterer, J., and C. Stollberger. 2008. Cardiac involvement in Becker muscular dystrophy. *Can J Cardiol*. 24:786-792.

Flanigan, K.M., E. Ceco, K.M. Lamar, Y. Kaminoh, D.M. Dunn, J.R. Mendell, W.M. King, A. Pestronk, J.M. Florence, K.D. Mathews, R.S. Finkel, K.J. Swoboda, E. Gappmaier, M.T. Howard, J.W. Day, C. McDonald, E.M. McNally, R.B. Weiss, and P. United Dystrophinopathy. 2013. LTBP4 genotype predicts age of ambulatory loss in Duchenne muscular dystrophy. *Ann Neurol*. 73:481-488.

Flanigan, K.M., D.M. Dunn, A. von Niederhausern, P. Soltanzadeh, E. Gappmaier, M.T. Howard, J.B. Sampson, J.R. Mendell, C. Wall, W.M. King, A. Pestronk, J.M. Florence, A.M. Connolly, K.D. Mathews, C.M. Stephan, K.S. Laubenthal, B.L. Wong, P.J. Morehart, A. Meyer, R.S. Finkel, C.G. Bonnemann, L. Medne, J.W. Day, J.C. Dalton, M.K. Margolis, V.J. Hinton, and R.B. Weiss. 2009. Mutational spectrum of DMD mutations in dystrophinopathy patients: application of modern diagnostic techniques to a large cohort. *Human mutation*. 30:1657-1666.

Flanigan, K.M., D.M. Dunn, A. von Niederhausern, P. Soltanzadeh, M.T. Howard, J.B. Sampson, K.J. Swoboda, M.B. Bromberg, J.R. Mendell, L.E. Taylor, C.B. Anderson, A. Pestronk, J.M. Florence, A.M. Connolly, K.D. Mathews, B. Wong, R.S. Finkel, C.G. Bonnemann, J.W. Day, C. McDonald, C. United Dystrophinopathy Project, and R.B. Weiss. 2011. Nonsense mutation-associated Becker muscular dystrophy: interplay between exon definition and splicing regulatory elements within the DMD gene. *Human mutation*. 32:299-308.

Flaumenhaft, R., M. Abe, Y. Sato, K. Miyazono, J. Harpel, C.H. Heldin, and D.B. Rifkin. 1993. Role of the latent TGF-beta binding protein in the activation of latent TGF-beta by co-cultures of endothelial and smooth muscle cells. *J Cell Biol*. 120:995-1002.

Flesch, M., F. Schiffer, O. Zolk, Y. Pinto, S. Rosenkranz, C. Hirth-Dietrich, G. Arnold, M. Paul, and M. Böhm. 1997. Contractile systolic and diastolic dysfunction in renin-induced hypertensive cardiomyopathy. *Hypertension*. 30:383-391.

Fontana, L., Y. Chen, P. Prijatelj, T. Sakai, R. Fassler, L.Y. Sakai, and D.B. Rifkin. 2005. Fibronectin is required for integrin alphavbeta6-mediated activation of latent TGF-beta complexes containing LTBP-1. *FASEB journal : official publication of the Federation of American Societies for Experimental Biology*. 19:1798-1808.

Fraysse, B., A. Liantonio, M. Cetrone, R. Burdi, S. Pierno, A. Frigeri, M. Pisoni, C. Camerino, and A. De Luca. 2004. The alteration of calcium homeostasis in adult dystrophic mdx muscle fibers is worsened by a chronic exercise in vivo. *Neurobiology of disease*. 17:144-154.

Gaengel, K., G. Genove, A. Armulik, and C. Betsholtz. 2009. Endothelial-mural cell signaling in vascular development and angiogenesis. *Arterioscler Thromb Vasc Biol*. 29:630-638.

Gao, S., D. Ho, D.E. Vatner, and S.F. Vatner. 2011. Echocardiography in Mice. *Curr Protoc Mouse Biol*. 1:71-83.

Gardner, B.B., K.A. Swaggart, G. Kim, S. Watson, and E.M. McNally. 2015. Cardiac function in muscular dystrophy associates with abdominal muscle pathology. *J Neuromuscul Dis*. 2:39-49.

Gayraud, J., S. Matecki, K. Hnia, D. Mornet, C. Prefaut, J. Mercier, A. Michel, and M. Ramonatxo. 2007. Ventilation during air breathing and in response to hypercapnia in 5 and 16 month-old mdx and C57 mice. *J Muscle Res Cell Motil*. 28:29-37.

Ge, G., and D.S. Greenspan. 2006. BMP1 controls TGFbeta1 activation via cleavage of latent TGFbeta-binding protein. *J Cell Biol*. 175:111-120.

Goldstein, J.A., S. Bogdanovich, A. Beiriger, L.M. Wren, A.E. Rossi, Q.Q. Gao, B.B. Gardner, J.U. Earley, J.D. Molkentin, and E.M. McNally. 2014. Excess SMAD signaling contributes to heart and muscle dysfunction in muscular dystrophy. *Human molecular genetics*.

Goldstein, J.A., S.M. Kelly, P.P. LoPresti, A. Heydemann, J.U. Earley, E.L. Ferguson, M.J. Wolf, and E.M. McNally. 2011. SMAD signaling drives heart and muscle dysfunction in a Drosophila model of muscular dystrophy. *Hum Mol Genet*. 20:894-904.

Gosselin, L.E., J.E. Williams, M. Deering, D. Brazeau, S. Koury, and D.A. Martinez. 2004. Localization and early time course of TGF-beta 1 mRNA expression in dystrophic muscle. *Muscle Nerve*. 30:645-653.

Goumans, M.-J., Z. Liu, and P. ten Dijke. 2009. TGF-β signaling in vascular biology and dysfunction. *Cell research*. 19:116-127.

Grady, R.M., H. Teng, M.C. Nichol, J.C. Cunningham, R.S. Wilkinson, and J.R. Sanes. 1997. Skeletal and cardiac myopathies in mice lacking utrophin and dystrophin: a model for Duchenne muscular dystrophy. *Cell*. 90:729-738.

Griffin, M.A., H. Feng, M. Tewari, P. Acosta, M. Kawana, H.L. Sweeney, and D.E. Discher. 2005. γ-Sarcoglycan deficiency increases cell contractility, apoptosis and MAPK pathway activation but does not affect adhesion. *Journal of cell science*. 118:1405-1416.

Guo, X., and X.F. Wang. 2009. Signaling cross-talk between TGF-beta/BMP and other pathways. *Cell Res*. 19:71-88.

Habedank, D., F.J. Meyer, R. Hetzer, S.D. Anker, and R. Ewert. 2013. Relation of respiratory muscle strength, cachexia and survival in severe chronic heart failure. *J Cachexia Sarcopenia Muscle*.

Hack, A.A., C.T. Ly, F. Jiang, C.J. Clendenin, K.S. Sigrist, R.L. Wollmann, and E.M. McNally. 1998. γ-Sarcoglycan deficiency leads to muscle membrane defects and apoptosis independent of dystrophin. *The Journal of cell biology*. 142:1279-1287.

Hamer, P.W., J.M. McGeachie, M.J. Davies, and M.D. Grounds. 2002. Evans Blue Dye as an in vivo marker of myofibre damage: optimising parameters for detecting initial myofibre membrane permeability. *J Anat*. 200:69-79.

Hathout, Y., R.L. Marathi, S. Rayavarapu, A. Zhang, K.J. Brown, H. Seol, H. Gordish-Dressman, S. Cirak, L. Bello, K. Nagaraju, T. Partridge, E.P. Hoffman, S. Takeda, J.K. Mah, E. Henricson, and C. McDonald. 2014. Discovery of serum protein biomarkers in the mdx mouse model and cross-species comparison to Duchenne muscular dystrophy patients. *Hum Mol Genet*. 23:6458-6469.

Heydemann, A., E. Ceco, J.E. Lim, M. Hadhazy, P. Ryder, J.L. Moran, D.R. Beier, A.A. Palmer, and E.M. McNally. 2009. Latent TGF-beta-binding protein 4 modifies muscular dystrophy in mice. *The Journal of clinical investigation*. 119:3703-3712.

Heydemann, A., J.M. Huber, A. Demonbreun, M. Hadhazy, and E.M. McNally. 2005. Genetic background influences muscular dystrophy. *Neuromuscul Disord*. 15:601-609.

Heydemann, A., and E.M. McNally. 2007. Consequences of disrupting the dystrophin-sarcoglycan complex in cardiac and skeletal myopathy. *Trends in cardiovascular medicine*. 17:55-59.

Hoffman, E.P., R.H. Brown, Jr., and L.M. Kunkel. 1987. Dystrophin: the protein product of the Duchenne muscular dystrophy locus. *Cell*. 51:919-928.

Holt, K.H., and K.P. Campbell. 1998. Assembly of the sarcoglycan complex. Insights for muscular dystrophy. *The Journal of biological chemistry*. 273:34667-34670.

Hor, K.N., J. Wansapura, L.W. Markham, W. Mazur, L.H. Cripe, R. Fleck, D.W. Benson, and W.M. Gottliebson. 2009. Circumferential strain analysis identifies strata of cardiomyopathy in Duchenne muscular dystrophy: a cardiac magnetic resonance tagging study. *J Am Coll Cardiol*. 53:1204-1210.

Hyytiainen, M., J. Taipale, C.H. Heldin, and J. Keski-Oja. 1998. Recombinant latent transforming growth factor beta-binding protein 2 assembles to fibroblast extracellular matrix and is susceptible to proteolytic processing and release. *The Journal of biological chemistry*. 273:20669-20676.

Iannaccone, S., A. Quattrini, S. Smirne, M. Sessa, F. de Rino, L. Ferini-Strambi, and R. Nemni. 1995. Connective tissue proliferation and growth factors in animal models of Duchenne muscular dystrophy. *J Neurol Sci*. 128:36-44.

Im, W.B., S.F. Phelps, E.H. Copen, E.G. Adams, J.L. Slightom, and J.S. Chamberlain. 1996. Differential expression of dystrophin isoforms in strains of mdx mice with different mutations. *Hum Mol Genet*. 5:1149-1153.

Ishizaki, M., Y. Maeda, R. Kawano, T. Suga, Y. Uchida, K. Uchino, S. Yamashita, E. Kimura, and M. Uchino. 2011. Rescue from respiratory dysfunction by transduction of full-length dystrophin to diaphragm via the peritoneal cavity in utrophin/dystrophin double knockout mice. *Molecular therapy : the journal of the American Society of Gene Therapy*. 19:1230-1235.

Ishizaki, M., T. Suga, E. Kimura, T. Shiota, R. Kawano, Y. Uchida, K. Uchino, S. Yamashita, Y. Maeda, and M. Uchino. 2008. Mdx respiratory impairment following fibrosis of the diaphragm. *Neuromuscul Disord*. 18:342-348.

Jackson, K.A., S.M. Majka, H. Wang, J. Pocius, C.J. Hartley, M.W. Majesky, M.L. Entman, L.H. Michael, K.K. Hirschi, and M.A. Goodell. 2001. Regeneration of ischemic cardiac muscle and vascular endothelium by adult stem cells. *The Journal of clinical investigation*. 107:1395-1402.

Jearawiriyapaisarn, N., H.M. Moulton, P. Sazani, R. Kole, and M.S. Willis. 2010. Long-term improvement in mdx cardiomyopathy after therapy with peptide-conjugated morpholino oligomers. *Cardiovascular research*. 85:444-453.

Jennekens, F.G., L.P. ten Kate, M. de Visser, and A.R. Wintzen. 1991. Diagnostic criteria for Duchenne and Becker muscular dystrophy and myotonic dystrophy. *Neuromuscul Disord*. 1:389-391.

Jung, C., A.S. Martins, E. Niggli, and N. Shirokova. 2008. Dystrophic cardiomyopathy: amplification of cellular damage by Ca2+ signalling and reactive oxygen species-generating pathways. *Cardiovascular research*. 77:766-773.

Kalluri, R., and E.G. Neilson. 2003. Epithelial-mesenchymal transition and its implications for fibrosis. *The Journal of clinical investigation*. 112:1776-1784.

Kamogawa, Y., S. Biro, M. Maeda, M. Setoguchi, T. Hirakawa, H. Yoshida, and C. Tei. 2001. Dystrophin-deficient myocardium is vulnerable to pressure overload in vivo. *Cardiovascular research*. 50:509-515.

Kane, C.J., P.A. Hebda, J.N. Mansbridge, and P.C. Hanawalt. 1991. Direct evidence for spatial and temporal regulation of transforming growth factor beta 1 expression during cutaneous wound healing. *J Cell Physiol*. 148:157-173.

Kaneko, H., and J. Horie. 2012. Breathing Movements of the Chest and Abdominal Wall in Healthy Subjects. *Respiratory Care*. 57:1442-1451.

Kantola, A.K., J. Keski-Oja, and K. Koli. 2008. Fibronectin and heparin binding domains of latent TGF-beta binding protein (LTBP)-4 mediate matrix targeting and cell adhesion. *Exp Cell Res*. 314:2488-2500.

Karonen, T., L. Jeskanen, and J. Keski-Oja. 1997. Transforming growth factor beta 1 and its latent form binding protein-1 associate with elastic fibres in human dermis: accumulation in actinic damage and absence in anetoderma. *Br J Dermatol*. 137:51-58.

Kefi, M., R. Amouri, A. Driss, C. Ben Hamida, M. Ben Hamida, L.M. Kunkel, and F. Hentati. 2003. Phenotype and sarcoglycan expression in Tunisian LGMD 2C patients sharing the same del521-T mutation. *Neuromuscul Disord*. 13:779-787.

Kharraz, Y., J. Guerra, C.J. Mann, A.L. Serrano, and P. Munoz-Canoves. 2013. Macrophage plasticity and the role of inflammation in skeletal muscle repair. *Mediators Inflamm*. 2013:491497.

Khirani, S., I. Dabaj, A. Amaddeo, A. Ramirez, S. Quijano-Roy, and B. Fauroux. 2014a. The value of respiratory muscle testing in a child with congenital muscular dystrophy. *Respirol Case Rep*. 2:95-98.

Khirani, S., A. Ramirez, G. Aubertin, M. Boule, C. Chemouny, V. Forin, and B. Fauroux. 2014b. Respiratory muscle decline in duchenne muscular dystrophy. *Pediatr Pulmonol*. 49:473-481.

Khurana, T.S., E.P. Hoffman, and L.M. Kunkel. 1990. Identification of a chromosome 6-encoded dystrophin-related protein. *The Journal of biological chemistry*. 265:16717-16720.

Kobayashi, Y.M., E.P. Rader, R.W. Crawford, and K.P. Campbell. 2012. Endpoint measures in the mdx mouse relevant for muscular dystrophy pre-clinical studies. *Neuromuscul Disord*. 22:34-42.

Koenig, M., A.H. Beggs, M. Moyer, S. Scherpf, K. Heindrich, T. Bettecken, G. Meng, C.R. Muller, M. Lindlof, H. Kaariainen, and et al. 1989. The molecular basis for Duchenne versus Becker muscular dystrophy: correlation of severity with type of deletion. *Am J Hum Genet*. 45:498-506.

Koenig, M., A.P. Monaco, and L.M. Kunkel. 1988. The complete sequence of dystrophin predicts a rod-shaped cytoskeletal protein. *Cell*. 53:219-228.

Kohler, M., C.F. Clarenbach, C. Bahler, T. Brack, E.W. Russi, and K.E. Bloch. 2009. Disability and survival in Duchenne muscular dystrophy. *Journal of neurology, neurosurgery, and psychiatry*. 80:320-325.

Koli, K., J. Saharinen, M. Hyytiainen, C. Penttinen, and J. Keski-Oja. 2001. Latency, activation, and binding proteins of TGF-beta. *Microscopy research and technique*. 52:354-362.

Krag, T.O., S. Bogdanovich, C.J. Jensen, M.D. Fischer, J. Hansen-Schwartz, E.H. Javazon, A.W. Flake, L. Edvinsson, and T.S. Khurana. 2004. Heregulin ameliorates the dystrophic phenotype in mdx mice. *Proc Natl Acad Sci U S A*. 101:13856-13860.

Kronqvist, P., N. Kawaguchi, R. Albrechtsen, X. Xu, H.D. Schrøder, B. Moghadaszadeh, F.C. Nielsen, C. Fröhlich, E. Engvall, and U.M. Wewer. 2002. ADAM12 alleviates the skeletal muscle pathology in mdx dystrophic mice. *The American journal of pathology*. 161:1535-1540.

Lamar, K.M., S. Bogdanovich, B.B. Gardner, Q.Q. Gao, T. Miller, J.U. Earley, M. Hadhazy, A.H. Vo, L. Wren, J.D. Molkentin, and E.M. McNally. 2016a. Overexpression of latent TGFbeta binding protein 4 in muscle ameliorates muscular dystrophy through myostatin and TGFbeta. *PLoS Genetics*. in press.

Lamar, K.M., T. Miller, L. Dellefave-Castillo, and E.M. McNally. 2016b. Genotype-Specific Interaction of Latent TGFbeta Binding Protein 4 with TGFbeta. *PloS one*. 11:e0150358.

Latres, E., J. Pangilinan, L. Miloscio, R. Bauerlein, E. Na, T.B. Potocky, Y. Huang, M. Eckersdorff, A. Rafique, J. Mastaitis, C. Lin, A.J. Murphy, G.D. Yancopoulos, J. Gromada, and T. Stitt. 2015. Myostatin blockade with a fully human monoclonal antibody induces muscle hypertrophy and reverses muscle atrophy in young and aged mice. *Skelet Muscle*. 5:34.

Leask, A., and D.J. Abraham. 2004. TGF-beta signaling and the fibrotic response. *FASEB journal : official publication of the Federation of American Societies for Experimental Biology*. 18:816-827.

Lieber, R.L., S. Shah, and J. Friden. 2002. Cytoskeletal disruption after eccentric contraction-induced muscle injury. *Clinical orthopaedics and related research*:S90-99.

Lin, R.Y., K.M. Sullivan, P.A. Argenta, M. Meuli, H.P. Lorenz, and N.S. Adzick. 1995. Exogenous transforming growth factor-beta amplifies its own expression and induces scar formation in a model of human fetal skin repair. *Ann Surg*. 222:146-154.

Lo Mauro, A., M.G. D'Angelo, M. Romei, F. Motta, D. Colombo, G.P. Comi, A. Pedotti, E. Marchi, A.C. Turconi, N. Bresolin, and A. Aliverti. 2010. Abdominal volume contribution to tidal volume as an early indicator of respiratory impairment in Duchenne muscular dystrophy. *Eur Respir J*. 35:1118-1125.

Lohcharoenkal, W., Y. Liu, L. Wang, Y. Yang, and Y. Rojanasakul. 2014. Luciferase reporter cells as a platform to detect SMAD-dependent collagen production. *Journal of bioscience and bioengineering*. 118:732-735.

Lomauro, A., M. Romei, M.G. D'Angelo, and A. Aliverti. 2013. Determinants of cough efficiency in Duchenne muscular dystrophy. *Pediatr Pulmonol*.

LoMauro, A., M. Romei, M.G. D'Angelo, and A. Aliverti. 2014. Determinants of cough efficiency in Duchenne muscular dystrophy. *Pediatr Pulmonol*. 49:357-365.

MacDonald, E.M., and R.D. Cohn. 2012. TGFβ signaling: its role in fibrosis formation and myopathies. *Current opinion in rheumatology*. 24:628-634.

Maeda, T., T. Sakabe, A. Sunaga, K. Sakai, A.L. Rivera, D.R. Keene, T. Sasaki, E. Stavnezer, J. Iannotti, R. Schweitzer, D. Ilic, H. Baskaran, and T. Sakai. 2011. Conversion of mechanical force into TGF-beta-mediated biochemical signals. *Current biology : CB*. 21:933-941.

Matsuda, R., A. Nishikawa, and H. Tanaka. 1995. Visualization of dystrophic muscle fibers in mdx mouse by vital staining with Evans blue: evidence of apoptosis in dystrophin-deficient muscle. *J Biochem (Tokyo)*. 118:959-964.

Matsumura, T., T. Saito, H. Fujimura, and S. Shinno. 2007. Cardiac troponin I for accurate evaluation of cardiac status in myopathic patients. *Brain & development*. 29:496-501.

Mauro, A.L., M.G. D'Angelo, M. Romei, F. Motta, D. Colombo, G.P. Comi, A. Pedotti, E. Marchi, A. Turconi, and N. Bresolin. 2009. Abdominal volume contribution to tidal volume as an early indicator of respiratory impairment in Duchenne Muscular Dystrophy. *European respiratory journal*. 35:1118-1125.

Mayer, O.H., R.S. Finkel, C. Rummey, M.J. Benton, A.M. Glanzman, J. Flickinger, B.M. Lindstrom, and T. Meier. 2015. Characterization of pulmonary function in Duchenne Muscular Dystrophy. *Pediatr Pulmonol*.

McAdam, L.C., A.L. Mayo, B.A. Alman, and W.D. Biggar. 2012. The Canadian experience with long-term deflazacort treatment in Duchenne muscular dystrophy. *Acta myologica : myopathies and cardiomyopathies : official journal of the Mediterranean Society of Myology / edited by the Gaetano Conte Academy for the study of striated muscle diseases*. 31:16-20.

McCully, K.K., and J.A. Faulkner. 1986. Characteristics of lengthening contractions associated with injury to skeletal muscle fibers. *Journal of applied physiology (Bethesda, Md. : 1985)*. 61:293-299.

McPherron, A.C., A.M. Lawler, and S.J. Lee. 1997. Regulation of skeletal muscle mass in mice by a new TGF-beta superfamily member. *Nature*. 387:83-90.

Mead, A.F., M. Petrov, A.S. Malik, M.A. Mitchell, M.K. Childers, J.R. Bogan, G. Seidner, J.N. Kornegay, and H.H. Stedman. 2014. Diaphragm remodeling and compensatory respiratory mechanics in a canine model of Duchenne muscular dystrophy. *Journal of applied physiology (Bethesda, Md. : 1985)*. 116:807-815.

Megeney, L.A., B. Kablar, R.L. Perry, C. Ying, L. May, and M.A. Rudnicki. 1999. Severe cardiomyopathy in mice lacking dystrophin and MyoD. *Proc Natl Acad Sci U S A*. 96:220-225.

Melacini, P., M. Fanin, D.J. Duggan, M.P. Freda, A. Berardinelli, G.A. Danieli, A. Barchitta, E.P. Hoffman, S. Dalla Volta, and C. Angelini. 1999. Heart involvement in muscular dystrophies due to sarcoglycan gene mutations. *Muscle Nerve*. 22:473-479.

Mercola, M., P. Ruiz-Lozano, and M.D. Schneider. 2011. Cardiac muscle regeneration: lessons from development. *Genes & development*. 25:299-309.

Merrell, A.J., and G. Kardon. 2013. Development of the diaphragm -- a skeletal muscle essential for mammalian respiration. *The FEBS journal*. 280:4026-4035.

Middlekauff, H.R. 2010. Making the case for skeletal myopathy as the major limitation of exercise capacity in heart failure. *Circulation. Heart failure*. 3:537-546.

Mitrpant, C., S. Fletcher, and S.D. Wilton. 2009. Personalised genetic intervention for Duchenne muscular dystrophy: antisense oligomers and exon skipping. *Current molecular pharmacology*. 2:110-121.

Moens, P., P.H. Baatsen, and G. Marechal. 1993. Increased susceptibility of EDL muscles from mdx mice to damage induced by contractions with stretch. *J Muscle Res Cell Motil*. 14:446-451.

Monaco, A.P., C.J. Bertelson, S. Liechti-Gallati, H. Moser, and L.M. Kunkel. 1988. An explanation for the phenotypic differences between patients bearing partial deletions of the DMD locus. *Genomics*. 2:90-95.

Monaco, A.P., R.L. Neve, C. Colletti-Feener, C.J. Bertelson, D.M. Kurnit, and L.M. Kunkel. 1986. Isolation of candidate cDNAs for portions of the Duchenne muscular dystrophy gene. *Nature*. 323:646-650.

Morine, K.J., M.M. Sleeper, E.R. Barton, and H.L. Sweeney. 2010. Overexpression of SERCA1a in the mdx diaphragm reduces susceptibility to contraction-induced damage. *Hum Gene Ther*. 21:1735-1739.

Moxley, R.T., 3rd, S. Pandya, E. Ciafaloni, D.J. Fox, and K. Campbell. 2010. Change in natural history of Duchenne muscular dystrophy with long-term corticosteroid treatment: implications for management. *Journal of child neurology*. 25:1116-1129.

Nelson, C.A., R.B. Hunter, L.A. Quigley, S. Girgenrath, W.D. Weber, J.A. McCullough, C.J. Dinardo, K.A. Keefe, L. Ceci, and N.P. Clayton. 2011a. Inhibiting TGF-β activity improves respiratory function in mdx mice. *The American journal of pathology*. 178:2611-2621.

Nelson, C.A., R.B. Hunter, L.A. Quigley, S. Girgenrath, W.D. Weber, J.A. McCullough, C.J. Dinardo, K.A. Keefe, L. Ceci, N.P. Clayton, A. McVie-Wylie, S.H. Cheng, J.P. Leonard, and B.M. Wentworth. 2011b. Inhibiting TGF-beta activity improves respiratory function in mdx mice. *Am J Pathol*. 178:2611-2621.

Partridge, T.A. 2013. The mdx mouse model as a surrogate for Duchenne muscular dystrophy. *The FEBS journal*. 280:4177-4186.

Penn, J.W., A.O. Grobbelaar, and K.J. Rolfe. 2012. The role of the TGF-beta family in wound healing, burns and scarring: a review. *Int J Burns Trauma*. 2:18-28.

Petrof, B.J., J.B. Shrager, H.H. Stedman, A.M. Kelly, and H.L. Sweeney. 1993. Dystrophin protects the sarcolemma from stresses developed during muscle contraction. *Proc Natl Acad Sci U S A*. 90:3710-3714.

Politano, L., V. Nigro, L. Passamano, V. Petretta, L.I. Comi, S. Papparella, G. Nigro, P.F. Rambaldi, P. Raia, A. Pini, M. Mora, M.A. Giugliano, and M.G. Esposito. 2001. Evaluation of cardiac and respiratory involvement in sarcoglycanopathies. *Neuromuscul Disord*. 11:178-185.

Portal, L., V. Martin, R. Assaly, A. d'Anglemont de Tassigny, S. Michineau, A. Berdeaux, B. Ghaleb, and S. Pons. 2013. A model of hypoxia-reoxygenation on isolated adult mouse cardiomyocytes: characterization, comparison with ischemia-reperfusion, and application to the cardioprotective effect of regular treadmill exercise. *Journal of cardiovascular pharmacology and therapeutics*. 18:367-375.

Rafael, J.A., Y. Nitta, J. Peters, and K.E. Davies. 2000. Testing of SHIRPA, a mouse phenotypic assessment protocol, on Dmd(mdx) and Dmd(mdx3cv) dystrophin-deficient mice. *Mamm Genome*. 11:725-728.

Relaix, F., and P.S. Zammit. 2012. Satellite cells are essential for skeletal muscle regeneration: the cell on the edge returns centre stage. *Development*. 139:2845-2856.

Rifkin, D.B. 2005. Latent transforming growth factor-beta (TGF-beta) binding proteins: orchestrators of TGF-beta availability. *The Journal of biological chemistry*. 280:7409-7412.

Roberts, N.W., J. Holley-Cuthrell, M. Gonzalez-Vega, A.J. Mull, and A. Heydemann. 2015. Biochemical and Functional Comparisons of mdx and Sgcg(-/-) Muscular Dystrophy Mouse Models. *BioMed research international*. 2015:131436.

Robertson, I.B., M. Horiguchi, L. Zilberberg, B. Dabovic, K. Hadjiolova, and D.B. Rifkin. 2015. Latent TGF-beta-binding proteins. *Matrix biology : journal of the International Society for Matrix Biology*. 47:44-53.

Romei, M., M.G. D'Angelo, A. LoMauro, S. Gandossini, S. Bonato, E. Brighina, E. Marchi, G.P. Comi, A.C. Turconi, and A. Pedotti. 2012. Low abdominal contribution to breathing as daytime predictor of nocturnal desaturation in adolescents and young adults with Duchenne Muscular Dystrophy. *Respiratory medicine*. 106:276-283.

Rouillon, J., A. Zocevic, T. Leger, C. Garcia, J.M. Camadro, B. Udd, B. Wong, L. Servais, T. Voit, and F. Svinartchouk. 2014. Proteomics profiling of urine reveals specific titin fragments as biomarkers of Duchenne muscular dystrophy. *Neuromuscul Disord*. 24:563-573.

Rybakova, I.N., J.R. Patel, and J.M. Ervasti. 2000. The dystrophin complex forms a mechanically strong link between the sarcolemma and costameric actin. *J Cell Biol*. 150:1209-1214.

Sacco, P., and D.A. Jones. 1992. The protective effect of damaging eccentric exercise against repeated bouts of exercise in the mouse tibialis anterior muscle. *Experimental physiology*. 77:757-760.

Saharinen, J., M. Hyytiainen, J. Taipale, and J. Keski-Oja. 1999. Latent transforming growth factor-beta binding proteins (LTBPs)--structural extracellular matrix proteins for targeting TGF-beta action. *Cytokine & growth factor reviews*. 10:99-117.

Saharinen, J., and J. Keski-Oja. 2000. Specific sequence motif of 8-Cys repeats of TGF-beta binding proteins, LTBPs, creates a hydrophobic interaction surface for binding of small latent TGF-beta. *Mol Biol Cell*. 11:2691-2704.

Saharinen, J., J. Taipale, O. Monni, and J. Keski-Oja. 1998. Identification and characterization of a new latent transforming growth factor-beta-binding protein, LTBP-4. *The Journal of biological chemistry*. 273:18459-18469.

Sant'Ambrogio, G., M. Decandia, and L. Provini. 1966. Diaphragmatic contribution to respiration in the rabbit. *J Appl Physiol*. 21:843-847.

Sawnani, H., L. Thampratankul, R.D. Szczesniak, M.C. Fenchel, and N. Simakajornboon. 2015. Sleep disordered breathing in young boys with duchenne muscular dystrophy. *J Pediatr*. 166:640-645 e641.

Schatzberg, S.J., N.J. Olby, M. Breen, L.V. Anderson, C.F. Langford, H.F. Dickens, S.D. Wilton, C.J. Zeiss, M.M. Binns, J.N. Kornegay, G.E. Morris, and N.J. Sharp. 1999. Molecular analysis of a spontaneous dystrophin 'knockout' dog. *Neuromuscul Disord*. 9:289-295.

Schiller, M., D. Javelaud, and A. Mauviel. 2004. TGF-beta-induced SMAD signaling and gene regulation: consequences for extracellular matrix remodeling and wound healing. *J Dermatol Sci*. 35:83-92.

Schmierer, B., and C.S. Hill. 2007. TGFbeta-SMAD signal transduction: molecular specificity and functional flexibility. *Nature reviews. Molecular cell biology*. 8:970-982.

Seferian, A.M., A. Moraux, M. Annoussamy, A. Canal, V. Decostre, O. Diebate, A.G. Le Moing, T. Gidaro, N. Deconinck, F. Van Parys, W. Vereecke, S. Wittevrongel, M. Mayer, K. Maincent, I. Desguerre, C. Themar-Noel, J.M. Cuisset, V. Tiffreau, S. Denis, V. Jousten, S. Quijano-Roy, T. Voit, J.Y. Hogrel, and L. Servais. 2015. Upper limb strength and function changes during a one-year follow-up in non-ambulant patients with Duchenne Muscular Dystrophy: an observational multicenter trial. *PloS one*. 10:e0113999.

Sharp, N.J., J.N. Kornegay, S.D. Van Camp, M.H. Herbstreith, S.L. Secore, S. Kettle, W.Y. Hung, C.D. Constantinou, M.J. Dykstra, A.D. Roses, and et al. 1992. An error in dystrophin mRNA processing in golden retriever muscular dystrophy, an animal homologue of Duchenne muscular dystrophy. *Genomics*. 13:115-121.

Sinha, S., C. Nevett, C.A. Shuttleworth, and C.M. Kielty. 1998. Cellular and extracellular biology of the latent transforming growth factor-beta binding proteins. *Matrix biology : journal of the International Society for Matrix Biology*. 17:529-545.

Smith, B.K., S.W. Collins, T.J. Conlon, C.S. Mah, L.A. Lawson, A.D. Martin, D.D. Fuller, B.D. Cleaver, N. Clement, D. Phillips, S. Islam, N. Dobjia, and B.J. Byrne. 2013. Phase I/II trial of adeno-associated virus-mediated alpha-glucosidase gene therapy to the diaphragm for chronic respiratory failure in Pompe disease: initial safety and ventilatory outcomes. *Hum Gene Ther*. 24:630-640.

Smith, L.R., and E.R. Barton. 2014. Collagen content does not alter the passive mechanical properties of fibrotic skeletal muscle in mdx mice. *Am J Physiol Cell Physiol*. 306:C889-898.

Smith, P.E., R.H. Edwards, and P.M. Calverley. 1989. Ventilation and breathing pattern during sleep in Duchenne muscular dystrophy. *Chest*. 96:1346-1351.

Spurney, C.F., H. Gordish-Dressman, A.D. Guerron, A. Sali, G.S. Pandey, R. Rawat, J.H. Van Der Meulen, H.J. Cha, E.E. Pistilli, T.A. Partridge, E.P. Hoffman, and K. Nagaraju. 2009. Preclinical drug trials in the mdx mouse: assessment of reliable and sensitive outcome measures. *Muscle Nerve*. 39:591-602.

Spurney, C.F., S. Knoblach, E.E. Pistilli, K. Nagaraju, G.R. Martin, and E.P. Hoffman. 2008. Dystrophin-deficient cardiomyopathy in mouse: expression of Nox4 and Lox are associated with fibrosis and altered functional parameters in the heart. *Neuromuscul Disord*. 18:371-381.

Spurney, C.F., A. Sali, A.D. Guerron, M. Iantorno, Q. Yu, H. Gordish-Dressman, S. Rayavarapu, J. van der Meulen, E.P. Hoffman, and K. Nagaraju. 2011. Losartan decreases cardiac muscle fibrosis and improves cardiac function in dystrophin-deficient mdx mice. *Journal of cardiovascular pharmacology and therapeutics*. 16:87-95.

Stedman, H.H., H.L. Sweeney, J.B. Shrager, H.C. Maguire, R.A. Panettieri, B. Petrof, M. Narusawa, J.M. Leferovich, J.T. Sladky, and A.M. Kelly. 1991. The mdx mouse diaphragm reproduces the degenerative changes of Duchenne muscular dystrophy. *Nature*. 352:536-539.

Sterner-Kock, A., I.S. Thorey, K. Koli, F. Wempe, J. Otte, T. Bangsow, K. Kuhlmeier, T. Kirchner, S. Jin, J. Keski-Oja, and H. von Melchner. 2002. Disruption of the gene encoding the latent transforming growth factor-beta binding protein 4 (LTBP-4) causes abnormal lung development, cardiomyopathy, and colorectal cancer. *Genes & development*. 16:2264-2273.

Straub, V., J.A. Rafael, J.S. Chamberlain, and K.P. Campbell. 1997. Animal models for muscular dystrophy show different patterns of sarcolemmal disruption. *J Cell Biol*. 139:375-385.

Swaggart, K.A., A.R. Demonbreun, A.H. Vo, K.E. Swanson, E.Y. Kim, J.P. Fahrenbach, J. Holley-Cuthrell, A. Eskin, Z. Chen, K. Squire, A. Heydemann, A.A. Palmer, S.F. Nelson, and E.M. McNally. 2014. Annexin A6 modifies muscular dystrophy by mediating sarcolemmal repair. *Proc Natl Acad Sci U S A*. 111:6004-6009.

Swaggart, K.A., A. Heydemann, A.A. Palmer, and E.M. McNally. 2011. Distinct genetic regions modify specific muscle groups in muscular dystrophy. *Physiol Genomics*. 43:24-31.

Taipale, J., K. Koli, and J. Keski-Oja. 1992. Release of transforming growth factor-beta 1 from the pericellular matrix of cultured fibroblasts and fibrosarcoma cells by plasmin and thrombin. *The Journal of biological chemistry*. 267:25378-25384.

Tanaka, M., H. Ito, S. Adachi, H. Akimoto, T. Nishikawa, T. Kasajima, F. Marumo, and M. Hiroe. 1994. Hypoxia induces apoptosis with enhanced expression of Fas antigen messenger RNA in cultured neonatal rat cardiomyocytes. *Circ Res*. 75:426-433.

Tandon, A., J.L. Jefferies, C.R. Villa, K.N. Hor, B.L. Wong, S.M. Ware, Z. Gao, J.A. Towbin, W. Mazur, R.J. Fleck, J.J. Sticka, D.W. Benson, and M.D. Taylor. 2015a. Dystrophin genotype-cardiac phenotype correlations in duchenne and becker muscular dystrophies using cardiac magnetic resonance imaging. *The American journal of cardiology*. 115:967-971.

Tandon, A., C.R. Villa, K.N. Hor, J.L. Jefferies, Z. Gao, J.A. Towbin, B.L. Wong, W. Mazur, R.J. Fleck, J.J. Sticka, D.W. Benson, and M.D. Taylor. 2015b. Myocardial Fibrosis Burden Predicts Left Ventricular Ejection Fraction and Is Associated With Age and Steroid Treatment Duration in Duchenne Muscular Dystrophy. *Journal of the American Heart Association*. 4.

ten Dijke, P., and H.M. Arthur. 2007. Extracellular control of TGFβ signalling in vascular development and disease. *Nature reviews Molecular cell biology*. 8:857-869.

Thibault, H.B., B. Kurtz, M.J. Raher, R.S. Shaik, A. Waxman, G. Derumeaux, E.F. Halpern, K.D. Bloch, and M. Scherrer-Crosbie. 2010. Noninvasive Assessment of Murine Pulmonary Arterial Pressure Validation and Application to Models of Pulmonary Hypertension. *Circulation: Cardiovascular Imaging*. 3:157-163.

Thomas, T.O., T.M. Morgan, W.B. Burnette, and L.W. Markham. 2012. Correlation of heart rate and cardiac dysfunction in Duchenne muscular dystrophy. *Pediatr Cardiol*. 33:1175-1179.

Thurston, G., C. Suri, K. Smith, J. McClain, T.N. Sato, G.D. Yancopoulos, and D.M. McDonald. 1999. Leakage-resistant blood vessels in mice transgenically overexpressing angiopoietin-1. *Science*. 286:2511-2514.

Tidball, J.G., and S.A. Villalta. 2010. Regulatory interactions between muscle and the immune system during muscle regeneration. *Am J Physiol Regul Integr Comp Physiol*. 298:R1173-1187.

Todorovic, V., and D.B. Rifkin. 2012. LTBPs, more than just an escort service. *J Cell Biochem*. 113:410-418.

Ugalde, V., S. Walsh, R.T. Abresch, H.W. Bonekat, and E. Breslin. 2001. Respiratory abdominal muscle recruitment and chest wall motion in myotonic muscular dystrophy. *Journal of Applied Physiology*. 91:395-407.

Vainzof, M., D. Ayub-Guerrieri, P.C. Onofre, P.C. Martins, V.F. Lopes, D. Zilberztajn, L.S. Maia, K. Sell, and L.U. Yamamoto. 2008. Animal models for genetic neuromuscular diseases. *Journal of molecular neuroscience : MN*. 34:241-248.

van den Bergen, J.C., M. Hiller, S. Bohringer, L. Vijfhuizen, H.B. Ginjaar, A. Chaouch, K. Bushby, V. Straub, M. Scoto, S. Cirak, V. Humbertclaude, M. Claustres, C. Scotton, C. Passarelli, H. Lochmuller, F. Muntoni, S. Tuffery-Giraud, A. Ferlini, A.M. Aartsma-Rus, J.J. Verschuuren, P.A. t Hoen, and P. Spitali. 2015. Validation of genetic modifiers for Duchenne muscular dystrophy: a multicentre study assessing SPP1 and LTBP4 variants. *Journal of neurology, neurosurgery, and psychiatry*. 86:1060-1065.

van Hees, H.W., C.A. Ottenheijm, H.L. Granzier, P.N. Dekhuijzen, and L.M. Heunks. 2010. Heart failure decreases passive tension generation of rat diaphragm fibers. *International journal of cardiology*. 141:275-283.

Vulin, A., N. Wein, D.M. Strandjord, E.K. Johnson, A.R. Findlay, B. Maiti, M.T. Howard, Y.J. Kaminoh, L.E. Taylor, T.R. Simmons, W.C. Ray, F. Montanaro, J.M. Ervasti, and K.M. Flanigan. 2014. The ZZ domain of dystrophin in DMD: making sense of missense mutations. *Human mutation*. 35:257-264.

Wagner, K.R., A.C. McPherron, N. Winik, and S.J. Lee. 2002. Loss of myostatin attenuates severity of muscular dystrophy in mdx mice. *Annals of neurology*. 52:832-836.

Wang, C.S., and W.T. Josenhans. 1971. Contribution of diaphragmatic-abdominal displacement to ventilation in supine man. *J Appl Physiol*. 31:576-580.

Wasala, N.B., B. Bostick, Y. Yue, and D. Duan. 2013. Exclusive skeletal muscle correction does not modulate dystrophic heart disease in the aged mdx model of Duchenne cardiomyopathy. *Hum Mol Genet*. 22:2634-2641.

West, C.R., I.G. Campbell, R.E. Shave, and L.M. Romer. 2012. Effects of abdominal binding on cardiorespiratory function in cervical spinal cord injury. *Respiratory physiology & neurobiology*. 180:275-282.

Wheeler, M.T., C.E. Korcarz, K.A. Collins, K.A. Lapidos, A.A. Hack, M.R. Lyons, S. Zarnegar, J.U. Earley, R.M. Lang, and E.M. McNally. 2004. Secondary coronary artery vasospasm promotes cardiomyopathy progression. *Am J Pathol*. 164:1063-1071.

Wooddell, C.I., G. Zhang, J.B. Griffin, J.O. Hegge, T. Huss, and J.A. Wolff. 2010. Use of Evans blue dye to compare limb muscles in exercised young and old mdx mice. *Muscle Nerve*. 41:487-499.

Worton, R.G., P.N. Ray, S. Bodrug, A.H. Burghes, X. Hu, and M.W. Thompson. 1988. The problem of Duchenne muscular dystrophy. *Philos Trans R Soc Lond B Biol Sci*. 319:275-284.

Yasuda, S., D. Townsend, D.E. Michele, E.G. Favre, S.M. Day, and J.M. Metzger. 2005. Dystrophic heart failure blocked by membrane sealant poloxamer. *Nature*. 436:1025-1029.

Yasuma, F., T. Kato, Y. Matsuoka, and M. Konagaya. 2001. Row-a-boat phenomenon: respiratory compensation in advanced Duchenne muscular dystrophy. *Chest*. 119:1836-1839.

Yuan, X., A.K. Downing, V. Knott, and P.A. Handford. 1997. Solution structure of the transforming growth factor beta-binding protein-like module, a domain associated with matrix fibrils. *The EMBO journal*. 16:6659-6666.

Zammit, P.S., T.A. Partridge, and Z. Yablonka-Reuveni. 2006. The skeletal muscle satellite cell: the stem cell that came in from the cold. *The journal of*

histochemistry and cytochemistry : official journal of the Histochemistry Society. 54:1177-1191.

Zavadil, J., and E.P. Böttinger. 2005. TGF-β and epithelial-to-mesenchymal transitions. *Oncogene*. 24:5764-5774.

Zwaagstra, J.C., T. Sulea, J. Baardsnes, A.E. Lenferink, C. Collins, C. Cantin, B. Paul-Roc, S. Grothe, S. Hossain, L.P. Richer, D. L'Abbe, R. Tom, B. Cass, Y. Durocher, and M.D. O'Connor-McCourt. 2012. Engineering and therapeutic application of single-chain bivalent TGF-beta family traps. *Mol Cancer Ther*. 11:1477-1487.